QATAR UNIVERSITY

COLLEGE OF ENGINEERING

INFLUENCE OF METAL OXIDE COATINGS ON THE PERFORMANCE OF HIGH-VOLTAGE $LiNi_{0.5}Mn_{1.5}O_4$ (LNMO) CATHODE MATERIALS FOR RECHARGEABLE LITHIUM-ION BATTERIES (LIBS)

BY

ZAWAR ALAM QURESHI

A Thesis Submitted to

the College of Engineering

in Partial Fulfillment of the Requirements for the Degree of

Master of Science in Environmental Engineering

January 2023

COMMITTEE PAGE

The members of the Committee approve the Thesis of
Zawar Alam Qureshi defended on 29/12/2022.

Professor Ramazan Kahraman
Thesis Supervisor

Dr. Abdul Shakoor
Thesis Co-Supervisor

Professor Shaheen Al-Muhtaseb
Committee Member

Approved:

Khalid Kamal Naji, Dean, College of Engineering

ABSTRACT

QURESHI, ZAWAR A., Masters : January : 2023:,

Masters of Science in Environmental Engineering

Title: Influence of Metal Oxide Coatings on the Performance of High-Voltage LiNi0.5Mn1.5O4 (LNMO) Cathode Materials for Rechargeable Lithium-Ion Batteries

Supervisor of Thesis: Professor Ramazan Kahraman.

Lithium-ion batteries (LIBs) have been publicized as suitable candidates for their utilization in portable electronics and electric vehicles (EVs). This move has been made in the past decade to address global warming and climate change concerns. The cathode materials utilized in the rechargeable lithium-ion batteries are vital as they primarily donate lithium-ions in the system. Spinel $LiNi_{0.5}Mn_{1.5}O_4$ (Lithium Nickel Manganese Oxide; LNMO) has attracted much attention as a cathode material due to its high voltage of 4.7 V vs. Li, high specific energy of 700 Wh/kg, lower cost, and environmental friendliness. However, LNMO cathodes are currently suffering from poor cyclability and capacity degradation, hindering commercialization. Many strategies have been suggested in the literature to address the challenges associated with spinel cathode materials. Among those, surface modification techniques like surface coatings have proven to be promising and may enhance the electrochemical performance of LNMO. Towards this direction, during the proposed research work, LNMO will be synthesized by microwave-assisted chemical co-precipitation technique and then coated with graphene wrapped ceramic materials (Al_2O_3 and CeO_2). A comparison of structural, thermal, and electrochemical performance of pristine material with the coated LNMO will be accomplished. The novelty of the proposed research work resides in the fact that synthesis of LNMO by the proposed method and its surface modification through graphene wrapped ceramic materials has not yet been reported.

DEDICATION

"*Sometimes the wrong choices bring us to the right places.*"

This work is dedicated to my parents and siblings, who sacrificed so much to provide me the chance at further education.

ACKNOWLEDGMENTS

I would like to acknowledge the support of my thesis supervisor Professor Ramazan Kahraman for being a source of knowledge, inspiration and for being utmost patient with my progress. The benefit of his perspective is a privilege, and I am blessed to have had that level of wisdom at my disposal.

I would also like to sincerely thank my co-supervisor Dr. Abdul Shakoor. It was under his mentorship and guidance, that I truly prospered. It has been an honor to be under his tutelage and I praise his expertise on both scientific and worldly knowledge. Furthermore, I would also like to thank my friends and mentors, Umair Nisar, Hanan Abdurehman Tariq and Jeffin James Abraham for their constant guidance and assistance towards my thesis.

The thesis was supported by the Qatar National Research Fund's NPRP Grant # NPRP11S-1225-170128 (a member of the Qatar Foundation). This work was also sponsored via an internal grant from Qatar University (QUCG-CENG-20/21-2).

Moreover, I would like to express a great deal of gratitude to the Center of Advanced Materials (CAM) and the Central Laboratory Unit (CLU) at Qatar University, for conducting microstructural, thermal and spectrometry investigations for this work.

TABLE OF CONTENTS

LIST OF TABLES

LIST OF FIGURES

Chapter 1: Introduction

From a technological perspective, a two-pronged solution must be developed to tackle the energy crisis and the increasing intensity of climate change. Hence, a new generation of Energy Storage Systems (ESS) must be utilized to assist in the global transition to renewable energy; by storing energy generated from solar, wind, and other renewable sources. The ESS has to be functional enough to have sufficient capacity to fuel our ever-increasing demand for energy. At the same time, the ESS should also be scalable to allow for portability and expansion, enabling their applications in Hybrid Electrical Vehicles (HEVs), Electric Vehicles (EVs), grid storage, or portable electronic devices[1]. Current battery technologies like the lead-acid (LA) or nickel-metal hydride (NiMH) cannot be utilized as ESS for sustainable development as they offer low energy density, low operating voltage, and lack environmental friendliness[2]. In that respect, the development and optimization of Lithium-ion battery (LIB) technology could prove to be fruitful in future-proofing our energy needs while protecting the environment. It is reported that LIBs offer higher power and energy density compared to other types of battery technologies, as shown in Figure 1a[2]. LIBs have dominated consumer electronics, communication, and computer

products in the preceding two decades[3]. However, further improvement in energy and power density is required to drive down costs and increase the adaption of LIBs towards large-scale applications.

Figure 1b illustrates a LIB that contains the cathode active material supported by an aluminum current collector forming the positive electrode and anode material on a copper current collector forming the negative electrode[4]. When an external voltage is applied to the cell, lithium ions migrate from the cathode through the electrolyte and intercalate inside the anode compound, which typically has a layered structure. The

electrolyte should be an excellent ionic conductor for lithium-ions but a poor electronic conductor to avoid shorting the circuit. When a load is attached to the cell, discharging occurs, and the lithium-ions intercalate back within the cathode structure. Thus, the significant components of LIBs are the anode, electrolyte, and cathode. The anode utilized in commercial LIBs is graphite because it is inexpensive and safe. The electrolyte used is $LiPF_6$ dissolved in a binary mixture of ethylene carbonate (EC) and dimethyl carbonate (DMC), offering high ionic conductivity for lithium; while being stable towards the anode and cathode by forming a solid-electrolyte-interface (SEI)[5,6]. The cathode, however, has been of primary research interest as it forms a significant part of the cell, contributing 30% towards the cost related to the battery[7,8]. Moreover, the energy density of the battery is associated with the operating voltage output the battery provides over its capacity. As such, increasing the working voltage of the battery can result in significant improvements to the energy density. Hence, the improvement in overall energy density relies on improving cathode materials as anode materials already operate at a voltage close to metallic lithium[7].

An ideal cathode material should have several essential characteristics: a high amount of energy per unit mass and volume (energy density), high rate of energy delivery (power density), structural integrity during cycling and high-temperature operations, longer life (high cyclability), low fabrication cost and environmental friendliness[9]. Conventional cathode materials used in LIBs differ in structure and composition; the most commonly utilized cathode materials are layered structure compounds: like $LiCoO_2$ (LCO), olivine structure compounds: $LiFePO_4$ (LFP), spinel structure compounds: like $LiMn_2O_4$ (LMO)[10,11]. The commercial LCO suffers from safety issues resulting from structural instability and also environmental concerns, limiting its progress for adoption in large-scale applications[12]. Hence, polyanionic

cathode compounds were developed like olivine $LiMPO_4$, fluorophosphates $LiMPO_4F$, borates $LiMBO_3$, monoclinic $Li_3M_2(PO_4)_3$, fluorosulfates $LiMSO_4F$ and orthosilicates Li_2MSiO_4, where M stands for any transition metal (Fe, Mn, Ni, Co, etc.)[4,13]. However, these compounds also fail to provide high energy density, as they operate at a voltage below 4.2 V vs Li/Li^{+}[14]. Moreover, nickel-rich cathode materials like NMC (Lithium Nickel Manganese Cobalt Oxide) and NCA (Lithium Nickel Cobalt Aluminum Oxide) have been widely adopted in electric vehicles over the past decade, but their cost is sensitive to nickel and cobalt availability[15]. To increase the energy density of the battery, high voltage cathode materials need to be utilized in the battery, such as $LiCoPO_4$ (LCP;518 $Whkg^{-1}$), $LiFePO_4$ (LFP;495 $Whkg^{-1}$), $LiNi_{1/3}Co_{1/3}Mn_{1/3}O_2$ (NMC;576 $Whkg^{-1}$) and LNMO, that could operate above 4.5 V vs Li/Li^{+}[3,16].

The spinel compound $LiNi_{0.5}Mn_{1.5}O_4$ (LNMO) has been gaining traction as a high-voltage cathode material due to its high working voltage of 4.7 V vs Li and a high theoretical capacity of 147 $mAhg^{-1}$ resulting in a specific density of 700 $Whkg^{-1}$ [17]. The high operating voltage makes it an attractive alternative when compared to highly commercial $LiCoO_2$ and $LiFePO_4$ by offering an increase in the energy density of 20% and 30%, respectively[12]. Moreover, LNMO does not contain any expensive cobalt and excessive lithium, making it suitable and cost-effective for large-scale ESSs and EVs. Spinel LNMO can be synthesized in two different cubic structures according to the metal-ions ordering within the structure. The ordered P-type ($P4_332$) LNMO undergoes two phase transitions and a disordered F-type (Fd3m) cubic structure that undergoes a single-phase transition, making the disordered structure superior in terms of structural reversibility during lithiation/de-lithiation[18]. However, the F-type material suffers limitations due to its poor cyclability as the cathode structure is compromised owing to the Jahn-Teller (JTE) distortion of Mn^{3+} to Mn^{2+}. This phenomenon that usually occurs

at high temperatures (55 – 60°C), causes Mn^{2+} to dissolve in the electrolyte[19]. The limitation of LNMO is thus mainly due to the incompatibility of the cathode with the electrolyte. The electrolyte contains carbonate compounds that decompose at the working voltage of LNMO (~4.7V), producing gasses and decomposition products. These products are electrically insulating species, and they reform into a film onto the cathode surface, forming a solid-electrolyte interface (SEI) that impedes lithium-ion transfer from the lattice. Furthermore, the presence of trace amounts of water can produce hydrogen fluoride (HF) with the use of the advanced $LiPF_6$ electrolyte, etching the SEI in tandem with the transition metal ions (Mn and Ni) within the lattice [6]. The constant breakdown and rebuilding of the SEI layer increases the polarization, negatively affecting the electrochemical performance of the cell. Furthermore, the metal ions that dissolve in the electrolyte from the cathode surface migrate to the anode causing cell failure. Also, the gas produced during operation can damage the electrodes due to volumetric changes within the cell, exposing fresh electrode surface and leading to more SEI growth. An amalgamation of these procedures can increase polarization and cause capacity fading at cycling or complete degradation of the cell[20,21].

Hence, approaches to improving the cycling stability of LNMO requires modifications of the electrode or electrolyte materials. Both developments of new cathode materials and material level optimizations are viable options for the battery manufacturing industry in order to improve LIB performance. While material level optimizations such as surface coatings only require minor changes to existing battery manufacturing capacities[21]. Doping of LNMO with metal ions and surface coatings have been reported to suppress the cathode materials limitations and improve electrochemical performance at room temperature[22]. However, doping LNMO does not essentially limit the progression of side reactions between the electrolyte and the

cathode[13,23]. Hence, surface modification techniques like surface coatings can be utilized to reduce the side reactions between the electrolyte and the cathode and stabilize the SEI. When it comes to the improvement of existing cathode materials, cathode surface coatings are regarded as the most viable method. Therefore, research into the influence of coatings on structural integrity and electrochemical performance of the cathode material is required[9]. Various surface coatings for cathodes are described in the literature, from metal-based coatings to polymer-based coatings. As a result of a wide range of coating materials and methods, coating thickness, morphology and performance may vary widely. Occasionally, different cathode materials have been used as surface coatings over desired cathodes to obtain desired performance advantages. Finding the optimum cathode surface coating methods has been difficult due to the abundance of research papers accessible in this large study field. Figure 1c illustrates the trend in literature distribution for LNMO coatings in the past decade. The issue of the optimum surface coating and the best coating technique has been addressed in a number of previous studies, but the answer is far from clear.

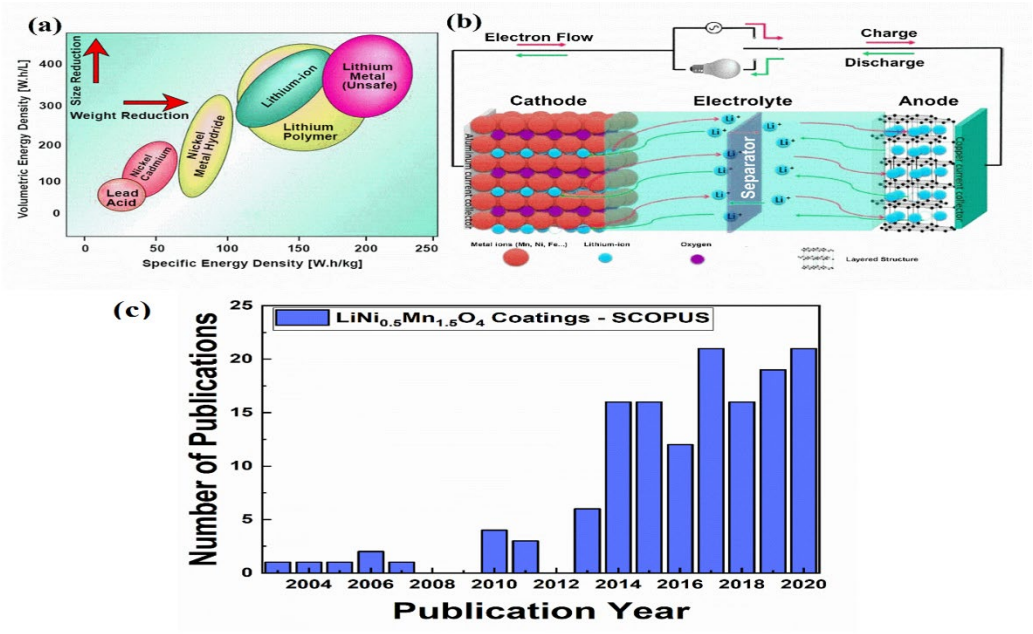

Figure 1: (a) A comparison of different battery technologies in terms of energy density[2] (b) charge/discharge mechanism of LIBs[4] (c) Distribution of literature from 2003 to 2020 for coated $LiNi_{0.5}Mn_{1.5}O_4$ cathode material for lithium-ion batteries, retrieved from SCOPUS by ELSEVIER.

Evaluation of Surface Coatings

Surface coatings on cathode materials act as physical barriers that primarily limit the direct contact of the active cathode material with the electrolyte, inhibiting unfavorable side reactions that may impair battery performance. Surface coatings have been shown to be efficient in suppressing these undesirable surface interactions, especially at elevated temperatures and high-voltage operations. Surface coatings may thus be used to enhance the performance of LIBs with regard to capacity retention, and high-temperature operation, among other things. As a result, surface coating techniques have gained widespread acceptance in both the industry and the academic communities as a potential means of improving the performance of LIBs in general. However, the precise function and process of surface coatings continue to be a subject of interest for the battery research community, as new mechanisms are still being investigated and explored. Ideally, surface coatings over cathode materials must possess certain criteria,

which include the following:

i. Surface coatings must be thin and homogeneous in order to be effective. This aids in the improvement of charge transfer between the electrode/electrolyte interface, which is beneficial. It is possible that if the coating is too thick, it may impair Lithium-ion mobility across the interface and therefore raise interfacial charge transfer resistance, resulting in suboptimal battery performance.

ii. Ionically and electrically conductive surface coatings should be utilized to enable efficient Lithium-ion diffusion or electron migration during battery cycling. It is possible to enhance the charge transfer between the electrode/electrolyte interface by utilizing ionically conductive coatings. Electronically conductive coatings, on the other hand, may aid in the acceleration of electron transport between the cathode and the current collector, resulting in enhanced battery performance, particularly at high current rates.

iii. It is important that the coatings be mechanically stiff and stable throughout cycling. Lithium-ion intercalation and de-intercalation within the cathode cause volume change within the cell, leading to the production of mechanical stresses. Because of the repeated cyclic mechanical forces that occur during cycling, material fatigue may occur, resulting in the development of fractures and the peeling of coating material from the cathode surface. This has the potential to expose the bare cathode surface to the electrolyte, resulting in capacity degradation as a consequence of the exposure. This phenomenon is exacerbated during the delithiated state, causing the release of oxygen and simultaneous unfavorable phase change of the cathode surface resulting in poor structural and electrochemical properties. Consequently, a suitable coating

material should reduce these stresses to the greatest extent possible, allowing for efficient mitigation of the produced stresses associated with volumetric changes during cycling. Moreover, an appropriate coating material can enhance structural stability by quelling phase transitions and decreasing the cation disorder within the crystal. This leads to a reduction in the production of heat evolved due to the side reactions that occur between the electrolyte and the electrode. Furthermore, suitable coatings can also suppress the dissolution of metal ions from the cathode surface and can enhance the scavenging of HF from the non-aqueous electrolytic solution[24].

iv. The coating procedure should be straightforward and scalable. Wet coating techniques are widely used in the manufacture of commercial electrodes. However, these wet methods may alter the cathode's surface chemistry owing to lithium leaching and result in additional costs associated with drying the electrode and treatment of associated wastewater. Dry coating techniques, on the other hand, are more appealing in terms of simple material processing and low post-processing costs. Nevertheless, the dry coating method has a number of drawbacks that limit its economic viability. Dry coating techniques, in general, result in uneven coatings because of the difficulty of controlling the homogeneity and thickness of the coating during the coating process. As a result, additional improvement of coating processes is required before commercial applications can be successfully deployed. Finally, the coating material and methods used should be affordable, with easily accessible raw materials, and must be ecologically benign.

Coating Technologies/Processes

The selection of the coating material and obtaining a thin uniform layer of coatings are the most difficult challenges that dictate the subsequent performance of the cathode.

The amount of coating on the surface of the cathode material can inhibit or enhance electronic and ionic conductivity. Also, the type of coating material and nature of technology utilized for coating can have a major influence on the performance of the LNMO cathode. The subsequent discussion is focused on some of the commonly used coating techniques utilized to develop coated LNMO cathode materials.

Chemical Vapor Deposition (CVD) process

The technique of chemically reacting a volatile component of a material to be deposited with other gases to generate a nonvolatile solid that deposits atomistically on a suitable substrate is known as chemical vapour deposition (CVD).

The essential sequential phases in every CVD process are as follows:

- Convective and diffusive transfer of reactants from gas inlets to the reaction zone
- Gas-phase chemical processes that generate new active species.
- Transport of the starting reactants and their products atomistically to the target substrate.
- Adsorption and diffusion of these substances on the substrate surface (chemical and physical).
- Surface-catalyzed heterogeneous processes that result in film formation.
- Desorption surface reaction of volatile derivatives.
- Convective and diffusive transfer of byproducts of the reaction away from the reaction zone

As Figure 2a shows; the cathode is coated by exposing it to the coating precursor material that flows in a liquid or vapor stream within a chamber. The coating uniformity depends upon a variety of factors like precursor type, reaction temperature, flow rates, and seeding, to name a few. Hou et al.[25] used CVD to coat carbon sourced from sucrose

over NMC cathode, and the resulting sample provided approximately 94% capacity retention at 0.1 C for 100 cycles and an incredibly high discharge capacity of 104.5 mAh g^{-1} at a high current rate of 10C. Hybrid methods that combine physical and chemical vapor deposition characteristics have also evolved. Although the CVD process can be cost-effective to employ in large scale applications, this process does not guarantee homogenous and uniform coverage of the cathode particles consistently[26].

Dry coating technology

Dry coating technology is the most commonly utilized coating technique in industrial applications for coating electrodes, as it is economical. The dry coating method involves the coating of the core material by mechanical impact forces instead of utilizing any solvents or binders. To achieve uniform coating on the cathode material, the coating material particle size should be small so the coating content could best disperse on the cathode surface under high calcination temperatures to ensure a consistent and full coating layer. Moreover, the calcination temperature for the coating material depends on its physio-chemical properties and thus is an important factor for adhesion. Figure 2b illustrates an example of dry coating technology: ball milling[27]. Using a dry coating technique, Nisar and colleagues recently coated silica over LNMO to create a uniform and homogeneous coating layer that provides fast charge (10 min) and slow discharge at C/3 for over 500 cycles with high-capacity retention, illustrating the high-performance, cost-effective, and scalable nature of dry coating technology[28].

Atomic Layer Deposition (ALD)

Atomic layer deposition (ALD) is a cyclic vapor phase deposition method during which precursors and reactants are successively fed into the reactor chamber (see Figure 2f), and the reactions are governed by surface chemistry rather than thermal degradation. The surface chemistry in the half-reactions of the ALD cycles must be self-limiting as

a requirement for ALD. This enables fine growth control with Angstrom-level precision, as well as good uniformity and conformality on difficult substrate topologies. ALD technology is a class of CVD and provides careful control of the amount of coating over the core material, usually less than 1 nm per cycle[29]. ALD technique is sequential, and the coating thickness can be increased by increasing the number of cycles. Kim et al.[30] compared a bare LNMO sample and LNMO coated with alumina coating; the alumina coated LNMO outperformed the bare sample in terms of electrochemical performance significantly. The coated sample, on the other hand, showed much weaker surface reactions and low charge-transfer resistance[30]. However, multiple thin atomic level layers can decrease the electrical conductivity and lithium-ion diffusion by disrupting pathways; also, like CVD, this technology is best utilized in large-scale surface modifications. Pulsed Laser Deposition (PLD) and Molecular Laser Deposition (MLD) are similar in nature to ALD and can be used to obtain thin, uniform coating layers of coating material[31].

Co-precipitation

Coprecipitation has attracted attention among the most often described techniques in the literature for producing precursors for lithium-ion battery active materials due to its simplicity, adaptability, homogenous mixing at the atomic scale, and processability over particle morphology. The co-precipitation approach is usually chosen for the synthesis of nanoparticles because it provides for morphological control and the availability of low-cost raw ingredients. The co-precipitation technique is a common coating technology utilized on a lab scale but holds the advantage of being scalable. The process utilizes precipitation reactions of inorganic compounds to create a coated film or a multilayer film on the surface of cathode particles (Figure 2e). This method is advantageous as it is easy, economical, and has been commonly used to formulate metal

oxides, fluorides, and phosphate coatings[29,32,33]. For instance, Pan et al. prepared LNMO coated with V_2O_5 via the co-precipitation route; the coated sample exhibited improved rate capability compared to the bare LNMO sample; this may be attributed to an increased lithium-ion diffusion coefficient as well as a decreased charge-transfer reaction resistance[34]. There are, however, different process parameters that influence the properties of the prepared coatings, like pH, temperature, the solvent used, and flow rate, etc. Monodisperse spherical particles are frequently sought in the synthesis of battery materials, where tap density of particle powders is a primary goal, which typically includes a high spinning rate, the employment of a chelating agent, and thorough evaluation of pH solution concentrations of reagents.

Radio Frequency (RF) Magnetron Sputtering

The growing need for micro-power applications necessitates the development of thin-film cathode materials for Li-ion micro-batteries. In this coating technique, the substrate is coated by utilizing sputtering of the coating material by accelerated argon ions. Sputtered atoms fly off in a ballistic fashion to impact the target in typical magnetron-sputtering pressures of a few millitorrs. Gas-phase interactions and dispersion at high pressures are avoided because they randomize the directional nature of the sputtered-atom flow and reduce the deposition rate. The shift of the Paschen curve to lower levels relative to simple discharges is a major cause of these positive effects. As a result, at lower pressures, a steady discharge may be established with the same electrode spacing and minimal desired voltage. Radio Frequency **(**RF) magnetron sputtering has a faster coating growth rate compared to ALD; however, the technique is expensive to be utilized at an industrial scale. In the manufacturing of modular and flexible thin-film batteries, RF sputtering has received a lot of interest. According to Lv. et al.[35] LNMO was coated with a 15nm thick lithium phosphorus oxynitride (LiPON) solid electrolyte

coating using RF magnetron sputtering.

Sol-gel Method

The sol-gel technique is based on the creation of a colloidal suspension, a sol, and its transformation into a gel, from which polycrystalline material can be produced by inorganic polymerization processes in solution. A solid phase is generated in the sol-gel method by gelation of a colloidal solution. The gel can then be dried to form a "dry gel" (xerogel), and heat treatment can be employed to remove unreacted organic residues, stabilise the gel, densify it, and induce crystallinity. Figure 2c exhibits a schematic diagram for the sol-gel process. In the sol-gel method, the coating precursors along with the solvent are mixed to form a gel by the subsequent addition of a chelating agent. The gel is then heat-treated to obtain the coated sample. The process is simple to execute, although morphological control is difficult to achieve, making reproducibility of results challenging. An additional caveat is the adhesion of the gel to the reactor surface on drying, complicating the retrieval of the coated material. This makes the sol-gel method fairly problematic for large scale coating purposes. However, this method is commonly utilized to obtain metal oxide coatings on cathode surfaces due to its facile nature[36].

Organic Pyrolysis Technology

To achieve the required phase, an oxidizer (metal nitrate) and an organic fuel (carboxylic acid, carbo hydrazide (CH), oxalyl dihydrazide (ODH), tetra formal tri-azine (TFTA), acid dihydrazide, urea, etc.) undergo an exothermic chemical reaction. The metal nitrate to fuel stoichiometry is calculated assuming full burning to generate metal oxide phase and CO_2, N_2, and H_2O as byproducts. A few of the precursors utilized were discovered to be specialized for a certain class of oxides, for example, urea for alumina and related oxides, carbo hydrazide for zirconia, ODH for Fe_2O_3 and ferrites, TFTA for TiO_2, and glycine for chromium and related oxides. There are two ways to

synthesize combustion: self-propagating high-temperature synthesis (SHS) and volume combustion synthesis (VCS). To begin an exothermic reaction, the samples are heated by an external source, either locally (SHS) or uniformly (VCS). The usual products produced by combustion reactions are submicron in size with a high surface area, which is a consequence of the gaseous gases created during combustion. The carbon precursor is thermally decomposed and deposited over a cathode substrate, followed by high-temperature treatment. Chudzik et al.[37] used pyrolysis of a water-soluble polymer, modified poly(N-vinyl formamide), to coat a two to three-nanometer carbon coating over $LiMn_2O_{3.99}S_{0.01}$ (LMOS). The carbon modified LMOS exhibited improved cyclability at higher current rates of 50 C, retaining up to 67.5 percent of the original 1C discharge capacity. Electrochemical impedance spectroscopy analysis illustrated that the carbon coated LMOS sample showed a reduction in internal resistance due to charge transfer reactions.

Solvothermal Method

A solvothermal process is described as "a chemical reaction occurring in a closed system that consists of a solvent (aqueous and non-aqueous solution) at a temperature greater than the boiling point of such a solvent." The technique uses a solvent at moderate to high pressure (usually between 1 atm and 10,000 atm) and temperature (generally between 100 °C and 1000 °C) to promote the interaction of precursors during synthesis. The process is known as "hydrothermal synthesis" when water is employed as the solvent. Under hydrothermal circumstances, synthesis is typically carried out below the supercritical temperature of water (374°C). This coating method may be used to obtain a variety of coating morphologies such as thin films, bulk powders, single crystals, and nanocrystals. The process is simple in terms of execution; the precursors for the coating material are dissolved in solution, using an organic or non-aqueous

solvent; the cathode material that needs to be coated is added as well. The mixture is then heated at a high temperature within an autoclave (Figure 2d), providing a product that could be filtered and washed to obtain the coated sample. A similar hydrothermal technique is a coating synthesis process through which coatings could be achieved by utilizing hydrolysis reaction with the use of aqueous solvent; the dried sample is then sintered at elevated temperature to obtain the coated cathode material[38]. Carbothermal treatments are the most widely employed synthetic methods in industry, with the benefits of a simple technological process, cheap cost, and mass production. These techniques, however, are ineffective in controlling the morphology and orientation of particles, resulting in greater grain size and poor electrical conductivities. Although, the solvo/hydrothermal procedures omit the need for extra synthesis steps like grinding and calcination. But the amount of coating and coverage is difficult to control using the solvo/hydrothermal technique. Moreover, the morphology of the coated material is dependent on the type of precursor and reaction conditions like pH, temperature, and pressure, making the procedure tedious[39].

Electroless Plating

This technique is used commonly to coat the cathode surface with metal ions by the action of a reducing agent within the solution. LNMO has been coated with copper (Cu), silver (Ag), and gold (Au) using this technique. The electroless method produces porosity by using a galvanic shift between noble metal, such as Ag, and the base material. The studies indicate that all coated LNMO cathodes exhibited increased performance due to higher lithium-ion diffusion because of reduced interfacial impedance[40–42]. However, the procedure is expensive to perform, and control of coating amount is difficult; thus, scalability is unfeasible.

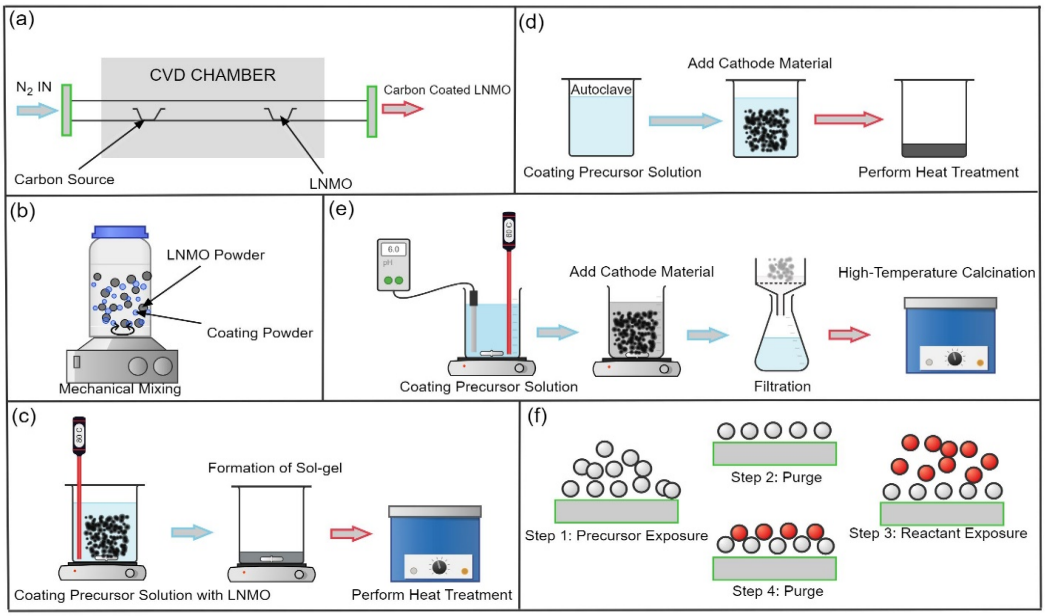

Figure 2: Coating synthesis methods schematic diagrams for (a) CVD, (b) Ball Mill, (c) Solgel, (d) Solvothermal, (e) Co-precipitation and (f) ALD methods.

Chapter 2: Coating Materials

Only the particular requirements of the application, as well as the cathode material itself, determines the kind of coating material to be used. The electrochemical performance of oxide-based cathode materials such as layered oxides (NCM, NCA) and spinel oxides (LMO, LNMO) is often improved by covering them with an oxide-based coating. As opposed to these materials, phosphate-based cathodes (such as LFP) are usually coated with carbon materials, which aids in enhancing their overall electrochemical performance by increasing electronic conductivity. The coating material of choice has to serve as a physical separation shield between LNMO and the electrolyte. The material of choice has to have the required characteristics to retain chemical stability in order to suppress the unexpected side reactions between the active cathode material and the electrolyte. Moreover, the coating should also allow for rapid diffusion of lithium ions and enhance electronic conductivity. The material itself has to be stable against oxidative decomposition at the working voltage of LNMO and also provide homogenous coverage of the cathode material, limiting the formation of a high impedance SEI layer. Hence, the selection of the coating material may have a significant impact on the performance of LNMO, and the appropriate choice is based on the above-mentioned criteria. The following discussion summarizes the major coating material families and their impact on the electrochemical performance of the LNMO cathode. Furthermore, a comprehensive examination of the electrochemical performance of coated LNMO has been collected and tabulated in the succeeding sections.

Metal Oxides

The oxide coating materials generally can be divided into active and inert oxides. Active oxide coatings can be doped on the surface of the cathode, enhancing

the ionic conductivity, and suppressing cationic disorder within the crystal structure by providing active sites for ionic diffusion. In comparison, inert oxides contain metals that are relatively stable and unable to change their oxidation states, thus not participating in any electrochemical reactions and only providing a protective layer that inhibits the reactions between the cathode and the electrolyte [43]. The inert metal oxide coatings also shield the active cathode material from HF attack by scavenging HF from the non-aqueous electrolyte. Metal oxides as coating materials are commonly utilized to improve the electrochemical performance of numerous Lithium-ion battery cathode materials, including LNMO. These coatings are inexpensive and simple to synthesize using common coating technologies such as dry coating techniques, CVD, ALD, sol-gel, solvothermal and co-precipitation. One major caveat regarding metal oxide coatings is that they provide poor ionic conductivity due to being inert towards lithium ions. Hence, careful control of coating thickness is required, or else the thicker coating might result in low-rate capability and/or failure. Nonetheless, metal oxide coatings have widely been utilized to improve the thermal stability and cycling performance of cathode materials within LIBs. Figure 3 illustrates typical images obtained from scanning electron microscopy (SEM) and transmission electron microscopy (TEM) of a coated LNMO cathode.

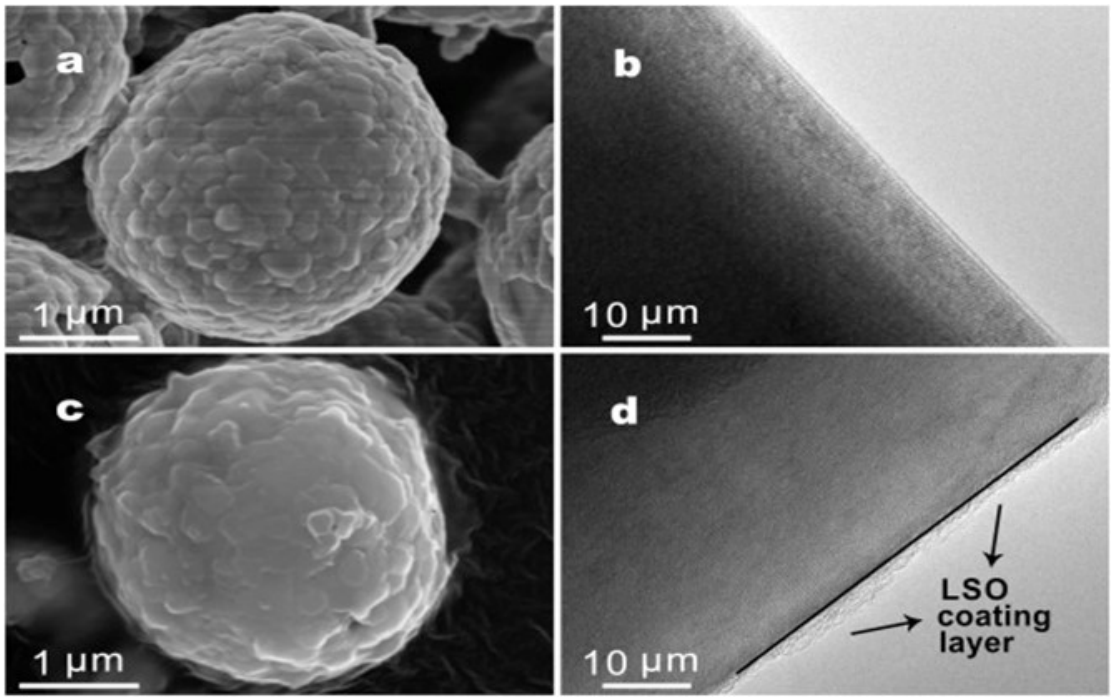

Figure 3: SEM and TEM images: (a) SEM and (b) TEM of LNMO, (c) SEM and (d) TEM of F-doped, Li_4SiO_4 coated $LiNi_{0.5}Mn_{1.5}O_4$.[44]

TiO_2 coated LNMO

LNMO has been reported to be coated with titanium(IV) oxide TiO_2 using the sol-gel method, delivering a discharge capacity of 113 mAh/g vs Li/Li^+ at room temperature for 100 cycles and at 55°C for 55 cycles, when cycled at 3.5 to 5 V at 1 C current rate[45]. Similarly, TiO_2 coated LNMO using ALD conveyed a specific capacity of 103 mAh/g at a C/7.5 rate[46]. Furthermore, the solvothermal coating technique was used to obtain 88.5% (108 mAh/g) capacity retention after 500 cycles at 2 C[47], and 87.9% capacity retention after 200 cycles[48]. Also, a dry coating method was utilized to coat TiO_2, providing 112 mAh/g capacity with a capacity retention of 91.6% at 1 C after 100 cycles [49]. Nearly all TiO_2 coated LNMO studies demonstrated improved electrochemical performance and higher capacity retention at elevated temperature due to reduced charge transfer resistance and electrode polarization that lead to the significantly low amount of electrolytic decomposition and metal ion dissolution. However, TiO_2

coatings are poor electronic conductors and lower the initial charge capacity of the cells. Figure 4(i) shows the cycling capability of various metal oxide coated LNMO cathodes at 25°C [49].

MgO coated LNMO

Magnesium oxide (MgO) coated LNMO reportedly provided enhanced discharge capacity, high coulombic efficiency, and promising rate capability at 50°C, producing 85-90% capacity retentions at 1C[50]. However, the MgO coatings did not provide any significant improvement in electrochemical performance at room temperature. The improvements were realized at elevated temperature cycling. Moreover, LNMO half cells (vs Li/Li^+) were produced with MgO co-coated with tantalum pentoxide (Ta_2O_5). The co-coated LNMO exhibited 88.2% capacity retention at 55°C and 100 cycles. The MgO behaved like an HF scavenger, and the Ta_2O_5 coating helped protect the cathode from HF, thus increasing electrochemical performance[51].

ZnO coated LNMO

Another coating that protects the LNMO cathode structure by scavenging HF is zinc oxide (ZnO)[52]. 1.5 wt% of ZnO was stated to be coated using the solvothermal technique, and the coated LNMO provided 137 mAh/g discharge capacity at 55°C[52–54]. Sun et al.[55] prepared an Al-doped ZnO coating layer that outperformed both the pristine LNMO and ZnO coated LNMO by retaining 95% capacity at 50°C for 50 cycles at a high charge/discharge rate of 5C. The increased electrochemical performance purportedly is a result of lattice stabilization due to Zn^{2+} ions within the crystal structure, protecting the cathode from electrolytic decomposition[56].

Ta_2O_5 coated LNMO

Recently, LNMO coated with Ta_2O_5 has been reported to offer high resistance against HF attacks. A Ta_2O_5 modified LNMO half-cell delivered 93% capacity

retention at 55°C after 100 cycles. This was mainly due to the surface modification of the LNMO by Ta^{5+} that diminished the metal-ion dissolution from the cathode [57].

SnO_2 coated LNMO

Tin(IV) oxide (SnO_2) surface modification also improves the rate capability of LNMO by conserving the structural and morphological aspects of the cathode material. The SnO_2 coated LNMO synthesized using CVD exhibited high performance at room temperature; 95.2% capacity retention after 100 cycles at 1 C [58,59]. The tin oxide coating enabled high energy storage at an elevated temperature of 60°C[58].

CeO_2 coated LNMO

LNMO surface coated with cerium(IV) oxide (CeO_2) provided increased electrochemical performance at high charge/discharge rates. A 3 wt% coating layer can achieve 118.1 mAh/g discharge capacity at 1 C; the coating helps to enhance the electronic conductivity and provides fast lithium diffusion whilst reducing electrochemical polarization[60,61].

La_2O_3 coated LNMO

An active lanthana (La_2O_3) coating was reported to improve the rate capability of LNMO cathode. LNMO was coated with 1.5 wt% lanthana that provided 126.5 mAh/g capacity at 1 C on cycling between 3.5 to 5 V in the LNMO half-cell[62]. A detailed study of LNMO coated with lanthana was conducted by Gao et al.[63], employing varying amounts of coating material (0 to 3 wt%). An optimum amount of 2 wt% lanthana coating provided 93% capacity retention at 55°C for 50 cycles. La_2O_3 coating protects the LNMO cathode from the undesired reactions between the cathode surface and electrolyte, while providing a slight increase in the conductivity. Other active transition metal oxides that have been used to coat LNMO have been reported in the literature that all have positive performance effects, coatings like Mn_3O_4[64], V_2O_5[34,65],

Fe_2O_3[66], CuO[67], Co_3O_4[68–70] and CdO[71].

Al_2O_3 coated LNMO

The most commonly utilized inert metal oxide coating is alumina (Al_2O_3). Alumina coated LNMO have been synthesized utilizing various coating technologies like ALD[72–74], PLD[75], CVD[76], solvothermal[77], and co-precipitation[8]. The alumina has reportedly been coated in ultra-thin layers of nanometric scales (nm) using ALD, and a 5 to 20 nm thickness of coating has demonstrated enhanced performance at elevated temperatures, as alumina can scavenge HF[57]. Song et al.[72] reported a 6 nm coating of alumina over the LNMO surface helped retain 98% discharge capacity after 200 cycles at room temperature by reducing the side reactions that occur due to the oxidation of the organic species within the electrolyte. Fang et al.[73], used a similar ALD process to ascertain the performance at an elevated temperature of 55°C, obtaining 116 mAh/g capacity after 100 cycles. The relation of cathode surface morphology on electrochemical performance was investigated by Kim et al.[78], observing that the alumina coated LNMO outperformed the bare LNMO cathode because of the coating acting as a barrier and protecting the cathode surface from electrolytic oxidation reactions. Furthermore, nanoscale coatings of alumina have also been reported to suppress the JTE by subduing Mn^{2+} formation[79]. Recently, Chang et al.[77], studied the performance of 0.5 alumina coating prepared by a facile solvothermal technique, a 0.5 wt% amount of alumina provided a 90.9% capacity retention at 1 C during high temperature cycling at 55°C[77]. Figure 4(ii) illustrates the cycling capability of alumina coated LNMO along with other ceramic oxide coated LNMO samples at an elevated temperature of 55°C, the lower performance is due to poor electronic conductance of Alumina. Song et al.[80] coated 10 nm inert alumina on the surface of LNMO to insulate the cathode from coming in contact with the electrolyte, a one wt% coating amount

provided a significant 96% capacity preservation after 300 cycles at 1 C, reducing the Mn^{3+} concentration by changing the ordering of the LNMO structure [81].

ZrO_2 coated LNMO

Inert oxide coatings have been reported to provide benefits based on the toughness of the coating layer. In this class, zirconia (ZrO_2) has also been employed as a coating material for LNMO due to its high toughness [82]. Wu et al. [83] reported improved electrochemical performance of 1wt% zirconia coated LNMO using a solvothermal technique at an elevated temperature of 55°C; 4% capacity loss after 150 cycles. The zirconia coatings reduced the heat generation and lowered the charge transfer resistance leading to a low amount of side reactions between the electrolyte and the cathode. Nisar et al.[84] studied the fast-charging characteristics of zirconia modified LNMO half-cell batteries. 1wt% ZrO_2 coated LNMO delivered 86% capacity retention at a high charge rate of 40 C, and a 2wt% provided 76% capacity retention at 55°C for a thousand cycles at the same C-rate. The reported findings signify that zirconia coated LNMO cathode can be utilized in portable electronics as they offer the advantage of fast charging over a large number of cycles.

SiO_2 coated LNMO

Silica (SiO_2) modified LNMO cathode was reportedly synthesized using the sol-gel method. The LNMO half-cell was cycled at 55°C between 3.5 and 5 V for 100 cycles, providing 86% capacity at 1wt% coating[85]. Pang et al.[86] employed a solvothermal technique to obtain silica coated LNMO. The coated LNMO reduced capacity fading on cycling to about 65% at an elevated temperature of 55°C. The performance improvement can be attributed to the silica coating layer protecting the LNMO cathode from HF while enhancing lithium-ion diffusion. A dry method using ball milling to coat nanoparticles of silica on the LNMO surface was employed by Nisar

et al.[28] to study the high-rate performance of the cathode at an elevated temperature of 55°C. 1wt% amount of coating exhibited 87.9% capacity retention at 40 C for 400 cycles, providing a cheap coating material that could be utilized in commercial LNMO battery applications. Other inert metal oxides studied as surface coatings to improve the performance of LNMO are Y_2O_3 and RuO_2[87–89].

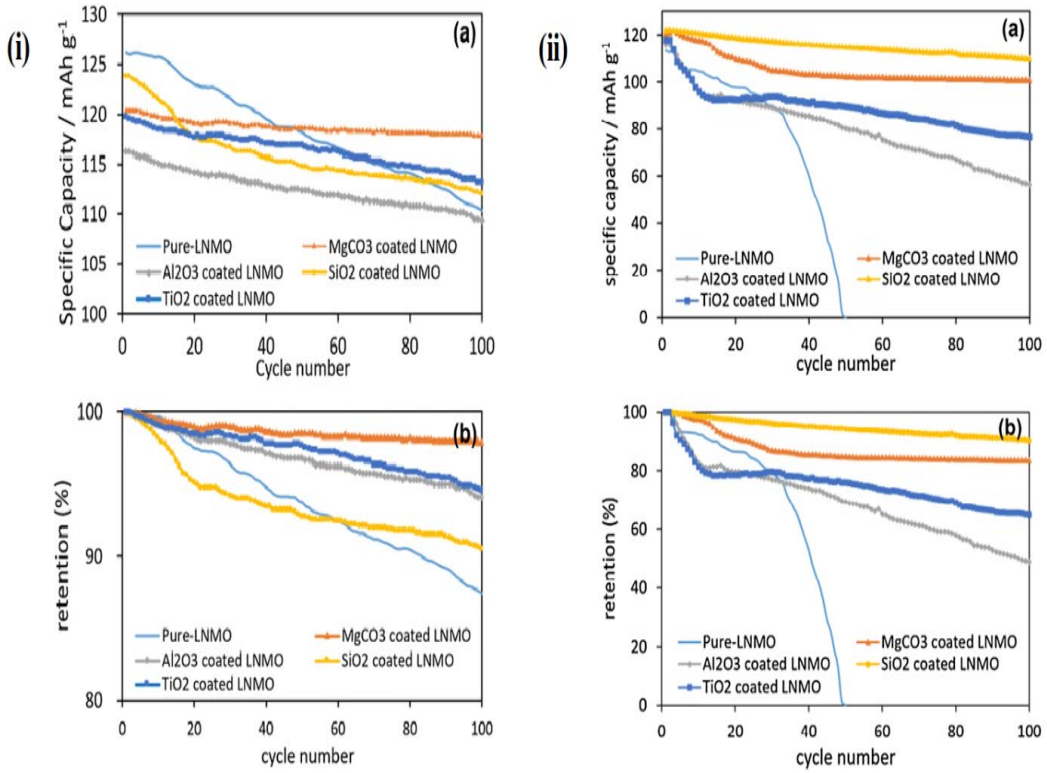

Figure 4: Cycling performance of various metal oxide coated LNMO cathodes at 1C charge-discharge for 100 cycles between 3.5-4.9 V vs. Li+/Li at (i) 25°C and (ii) 55°C, where (a) Cycling capability, (b) Capacity retention[49].

Metal oxides coating materials are extensively studied in various industries. They are cheap and can be easily reformed into compositions according to the application needs. Table 1 lists the metal oxide coated LNMO performance provided in the literature.

Table 1. $LiNi_{0.5}Mn_{1.5}O_4$ Coated with Metal Oxide and the Corresponding Electrochemical Performance.

COATING MATERIAL	COATING TECHNOLOGY	DISCHARGE CAPACITY [mAh/g]	CAPACITY RETENTION [%]	REF.
TiO_2	Sol-gel	113@1C, 25°C	-@100 Cycles	[45]
		113@1C, 55°C	-@55 Cycles	
	ALD	103@C/7.5, 25°C	-@30 Cycles	[46]
	Solvothermal	108@2C, 25°C	88.5@500 Cycles	[47]
		97.6@7C , 25°C	-	
		88.3@10C, 25°C	-	
		74.5@15C, 25°C	-	
	Dry Coating	102.3@5C, 25°C	87.9@200 Cycles	[48]
		72.1@7C, 25°C		
		112@1C, 25°C	91.6@100 Cycles	[49]
		95@1C, 55°C	70@100 Cycles	
MgO	Solvothermal	118@C/10, 25°C	85-90 @ 16 Cycles	[50]
		113@C/10, 50°C	85-90@ 16 Cycles	
ZnO	Solvothermal	96.9@C/4, 25°C	-@50 Cycles	[52]
		88.6@C/4, 55°C	-@50 Cycles	
		137@C/3, 55°C	99@50 Cycles	[53]
		120@C/10, 25°C	92@20 Cycles	[56]
	Sol-gel	141.6@C/10, 25°C	97@50 Cycles	[90]
Ta_2O_5	Dry Coating	129.5@C/5, 25°C	97@100 Cycles	[57]
		122@C/10, 55°C	93@100 Cycles	
SnO_2	CVD	132@1C, 25°C	95@100 Cycles	[58]
	Solvothermal	139.9@2C, 25°C	75@500 Cycles	[59]
CeO_2	Solvothermal	129.7@C/5, 25°C	-	[60]
		121.2@C/2, 25°C	-	
		118.1@1C, 25°C	98.3@100 Cycles	
		109.8@2C, 25°C	-	

COATING MATERIAL	COATING TECHNOLOGY	DISCHARGE CAPACITY [mAh/g]	CAPACITY RETENTION [%]	REF.
La_2O_3	Sol-gel	131.9@C/5, 25°C	-	[62]
		127.1@C/2 , 25°C	-	
		126.5@1C, 25°C	95.8@35 Cycles	
		120.7@2C, 25°C	-	
		101.5@5C, 25°C		
		112.2@1C, 25°C	75.5@500 Cycles	[63]
		127.1@1C , 55°C	93@50 Cycles	
Mn_3O_4	Solvothermal	108@10C, 55°C	78@100 Cycles	[64]
V_2O_5	Solvothermal	123.9@C/5, 25°C	-	[65]
		119.2@C/2 , 25 °C	-	
		131.5@1C, 25°C	92.2@100 Cycles	
		117.5@2C, 25°C	-	
		111.9@5C, 25°C	-	
		105.3@10C, 25°C	-	
		126.3@5C, 55°C	92@100 Cycles	
	Co-precipitation	131.4@C/5, 25°C		[34]
		122@C/2 , 25°C	-	
		108.9@1C, 25°C	-	
		93.8@2C, 25°C	96.6@100 Cycles	
		52.1@5C, 25°C	85.3@100 Cycles	
			-	
Fe_2O_3	Co-precipitation	124.2@1C, 25°C	98.6@100 Cycles	[66]
CuO	Co-precipitation	131.5@C/2, 25°C	95.6@100 Cycles	[67]
		125.6@2C , 25°C	-	
		115.7@5C, 25°C	-	
		108.4@7C, 25°C	-	
		98.7@10C, 25°C	-	
CdO	Solvothermal	133.3@1C, 25°C	95.2@300 Cycles	[71]
		120@10C, 25°C	92.3@300 Cycles	
Co_3O_4	Solvothermal	120@10C, 25°C	95.8@300 Cycles	[68]
		120@1C, 55°C	93@200 Cycles	[70]
		93@5C, 25°C	81@2000 Cycles	
	Co-precipitation		96.8@300 Cycles	[69]

COATING MATERIAL	COATING TECHNOLOGY	DISCHARGE CAPACITY [mAh/g]	CAPACITY RETENTION [%]	REF.
		122@1C, 25°C		
Al_2O_3	ALD	99@1C, 25°C	76.6@300 Cycles	[46]
		115@C/2, 25°C	92@200 Cycles	[72]
		120@C/2, 25°C	91@200 Cycles	[73]
		116@C/2, 55°C	63@100 Cycles	
	PLD	120@1C, 55°C	84.1@100 Cycles	[75]
	Dry Coating	117.9@1C, 25°C	91.5@100 Cycles	[49]
		60@1C, 55°C	50@100 Cycles	
	CVD	106.8@C/5, 25°C		
		112.9@C/5, 25°C	81@400 Cycles	[76]
		118.1@1C, 25°C	90@50 Cycles	
	Solvothermal	115.7@1C, 55°C	92.6@200 Cycles	[77]
			90.9@200 Cycles	
		118.2@1C, 25°C	93@500 Cycles	[81]
		124@1C, 25°C	96@300 Cycles	[80]
ZrO_2	Co-precipitation	114@1C, 55°C	96@150 Cycles	[83]
	Dry Coating	110@40C, 25°C	86@1200 Cycles	[84]
		100@40C, 55°C	76@1000 Cycles	
SiO_2	Dry Coating	109.4@1C, 25°C	86.7@100 Cycles	[49]
		113.8@1C, 55°C	90.2@100 Cycles	
		125@10C, 55°C	96.7@400 Cycles	[28]
		115@40C, 25°C	87.9@400 Cycles	
		89@80C, 25°C	82.4@400 Cycles	
	Solvothermal	112@C/2, 55°C	86@100 Cycles	[85]
		130@C/10, 25°C	97.5@200 Cycles	[86]
		115@C/10, 55°C	85@200 Cycles	
Y_2O_3	Co-precipitation	123.2@1C, 25°C	97.7@300 Cycles	[87]

COATING MATERIAL	COATING TECHNOLOGY	DISCHARGE CAPACITY [mAh/g]	CAPACITY RETENTION [%]	REF.
		115.5@1C, 55°C	91.6@100 Cycles	
RuO_2	Solvothermal	100@C/2, 25°C	96.1@300 Cycles	[88]
	Co-precipitation	131.7@C/2, 25°C	97.7@100 Cycles	[89]
		129.7@C/2, 60°C	97.2@100 Cycles	
		104.5@5C, 25°C		
		66.1@10C, 25°C		
$CoAl_2O_4$	Solvothermal	125.7@1C, 25°C	95@100 Cycles	[91]
		119@5C, 55°C	90@200 Cycles	
$MgAl_2O_4$	Co-precipitation	112@C/5, 25°C	91.5@100 Cycles	[92]
		110.8@5C, 55°C	88.2@100 Cycles	
$ZnAl_2O_4$	Sol-gel	121.6@1C, 25°C	97.3@100 Cycles	[93]
		108.8@1C, 60°C	87@100 Cycles	

Metal Phosphates

Similar to metal-oxide coatings, metal-phosphate coatings can also be active or inactive depending on the valence state of the metals (see Table 2). As a result, they may enhance the ionic transport characteristics of the coated cathode material. In most cases, to obtain metal-phosphate coatings, dry coating techniques, hydrothermal and sol-gel processes are used, creating a crystalline coating layer on the surface of the active cathode material. LNMO cathode on operation at high voltages causes decomposition of the electrolyte, as the carbonates within conventional electrolyte are decomposed at such potentials: ~4.5 V[94]. This causes rapid and severe capacity fading on cycling at high temperatures. Metal phosphate coatings can increase the ionic diffusion by forming a double layer with the LNMO cathode and can help decrease the Jahn-Teller Effect (JTE). The subsequent increase in electrochemical performance utilizing phosphate coatings is thus mainly due to a reduction in the dissolution of

manganese[95]. Yubuchi et al.[96] utilized pulsed laser deposition (PLD) to coat LNMO with Li_3PO_4 while utilizing Li_2S-P_2S_5 solid electrolyte that would not decompose at high operating potentials of the cathode material. This combination provided a discharge capacity of 62 mAh/g at ten cycles. Ren et al.[97] also synthesized 5wt% Li_3PO_4 coated LNMO through a facile co-precipitation method; the coating provided lower charge transfer resistance, increasing ionic and electronic conductivity. $FePO_4$ has also been investigated as a coating material due to it being inexpensive, stable, and electrochemically active[98]. The $FePO_4$ material, itself being a cathode material for LIBS, can behave like a reservoir for lithium ions, increases electronic conductivity, and has a buffering effect upon cycling. These properties can improve ionic and electronic diffusion and lead to high performance compared to common coating materials like alumina[99]. Other metal phosphate compounds like $Co_3(PO_4)_2$, $Ni_3(PO_4)_2$, and $Mn_3(PO_4)_2$ have also been utilized as surface modifiers for LNMO cathode[100,101]. Figure 5 illustrates the cycling capability of YPO_4 coated LNMO; a 3wt% coating provided a higher discharge capacity of 107 mAh g^{-1} with a capacity retention of 77.5% compared to the pristine LNMO material. This is mainly due to the formation of the Lewis acid YF_3, which forms due to the interaction of the phosphate coating with HF, a byproduct gas produced at elevated temperature due to the fluorine content within the PVDF binder and within the commercial electrolyte $LiPF_6$. YF_3 formation assists in increasing ion exchange on the surface of the cathode, creating a solid solution of Li-Ni-Mn-Y-O that can be attributed to the improvement in electrochemical performance of the cell[102].

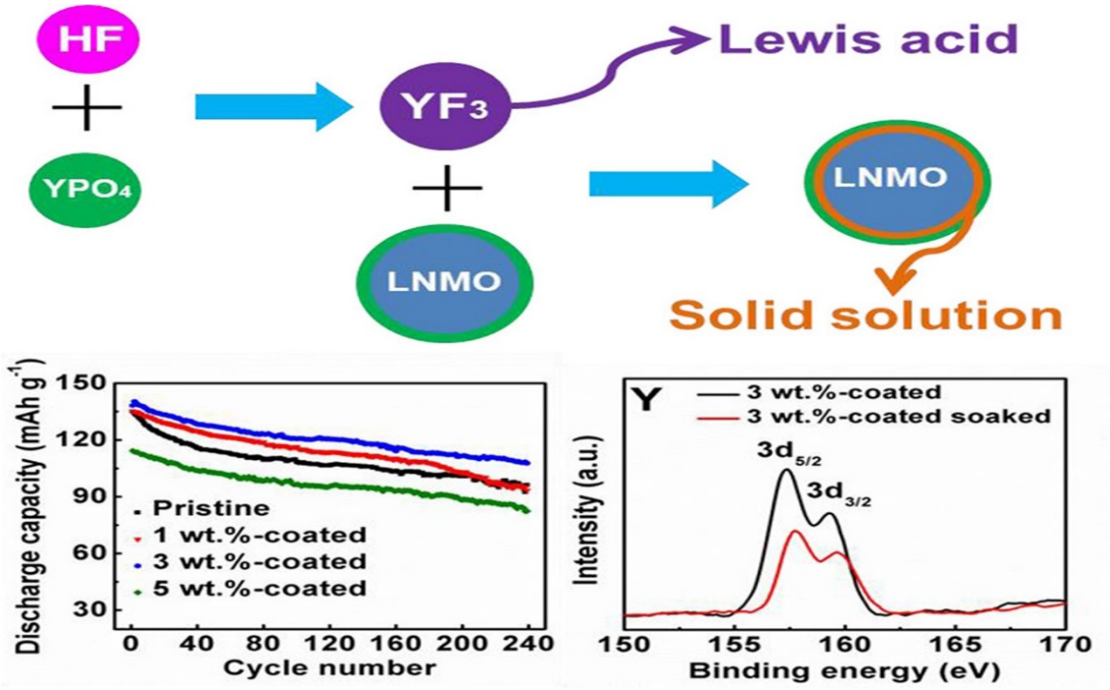

Figure 5: Performance of YPO_4 coated LNMO at C/10 and 25°C. Reprinted (adapted) with permission from[102]. Copyright (2021) American Chemical Society.

Table 2. Electrochemical Performance of Phosphate Coated LNMO.

COATING MATERIAL	COATING TECHNOLOGY	DISCHARGE CAPACITY [mAh/g]	CAPACITY RETENTION [%]	REF.
Li_3PO_4	PLD	62@-,25°C	-@10 Cycles	96
	Co-precipitation	-@-, 25°C	90.7@20 Cycles	95
		-	-	97
$FePO_4$	Sol-gel	117@2C, 25°C	102@80 Cycles	98
	Co-precipitation	120.1@C/5, 25°C	99.3@50 Cycles	103
	ALD	105.8@C/2, 25°C	94@100 Cycles	99
		80@5C, 25°C	71@50 Cycles	

COATING MATERIAL	COATING TECHNOLOGY	DISCHARGE CAPACITY [mAh/g]	CAPACITY RETENTION [%]	REF.
$AlPO_4$	ALD	94@C/2, 25°C 73.5@C/2, 25°C	94@100 Cycles 74.9@350 Cycles	[104]
$Co_3(PO_4)_2$	Solvothermal	128@C/10, 25°C 121@C/2, 55°C	98.4@100 Cycles 96.8@100 Cycles	[105]
$BiPO_4$	Solvothermal	116.6@C/2, 25°C 100@10C, 25°C	93.6@50 Cycles 96.2@100 Cycles	[106]
YPO_4	Co-precipitation	107@C/10, 25°C	77.5@240 Cycles	[102]
ZrP_2O_7	Sol-gel	90@1C, 55°C	75@150 Cycles	[83]

Metal Fluorides

To address the poor capacity retention and rate performance of LNMO cathodes due to decomposition of electrolyte at high operating voltages, metal oxide and phosphate coatings have been utilized, Table 3, that provide structural integrity to the LNMO. However, these coatings undergo an in-situ transformation into metal fluorides by reacting with HF, causing disintegration or dissolution of the coating material[107]. Hence, the use of metal fluorides as coating materials constitutes a novel approach in terms of improving cyclic performance at elevated temperatures by the reduction in corrosion due to HF and electrolyte decomposition. Metal fluorides are resistant to attack by HF and are used in electronics as they offer outstanding thermal stability and high hardness. Li et al.[108] found AlF_3 coating to be effective in stabilizing the SEI layer

leading to increased cyclic performance due to reduction in interface impedance. Wu et al.[109] also reported increased cyclic performance utilizing, AlF_3 and MgF_2 coatings. The coatings effectively reduced the dissolution of transition metal ions within by protecting the cathode against exposure from the electrolyte, which in turn inhibited the formation of a thick SEI layer during cycling[109,110].

Table 3. Electrochemical Perfromance of Fluoride Coated LNMO.

COATING MATERIAL	COATING TECHNOLOGY	DISCHARGE CAPACITY [mAh/g]	CAPACITY RETENTION [%]	REF.
AlF_3	Solvothermal	107.2@C/5, 25°C	81@50 Cycles	[111]
		100.5@10C, 25°C	92.1@100 Cycles	
		119.1@C/5, 25°C	98.1@100 Cycles	[112]
		118.1@C/5, 55°C	81.7@100 Cycles	
	Co-precipitation	115.5@2C, 25°C	92.4@45 Cycles	[108]
		97@C/10, 25°C	93.6@50 Cycles	[109]
LaF_3	Co-precipitation	108.6@C/10, 25°C	92@150 Cycles	[113]
YF_3	Co-precipitation	108@C/10, 25°C	84@100 Cycles	[107]
		95@1C, 25°C	73.8@100 Cycles	
		78@2C, 25°C	60.6@100 Cycles	
		32@5C, 25°C	24.9@100 Cycles	
ZrF_4	Co-precipitation	117.1@C/10, 25°C	95.5@120 Cycles	[114]
		106@2C, 25°C		
MgF_2	Co-precipitation	103.7@C/10, 25°C	89.9@100 Cycles	[115]

Carbon Compounds

The surface coating prevents undesired reactions between a cathode and an electrolyte, eliminating ion dissolution. The coatings also suppress the formation of a passivating SEI layer that reduces lithium diffusion rates. However, it is commonly known that most metal oxides have considerable resistance to electrical conductivity,

which results in broad polarization of the cathode because of their isolating or semi-conductive nature[116]. Hence, coating with carbon materials is a common method of enhancing electrochemical performance to make up for the low electronic conductance of the cathodes. The carbon-coating layer is typically formed under an inert environment by the thermal decomposition of organic material known as pyrolysis. This approach is not generally acceptable for LNMO, as heating in an inert atmosphere contributes to oxygen depletion, which could affect structural stability and electrochemical efficiency of the cathode[117,118]. Thus, effective coating technologies like the dry method and solvothermal techniques can offer innovation in preparing surface modified LNMO. Different carbon compounds and their rate performance, along with coating technology utilized to coat them, are provided in Table 4. As an example, the discharge behavior of graphene coated LNMO cathodes at different temperatures is presented in Figure 6a. From Table 4, it can be observed that graphene coated LNMO provided the best cycling performance compared to other carbon coatings.

Table 4. Surface Modification of $LiNi_{0.5}Mn_{1.5}O_4$ with Various Carbonaceous Compounds.

COATING MATERIAL	COATING TECHNOLOGY	DISCHARGE CAPACITY [mAh/g]	CAPACITY RETENTION [%]	REF.
Conductive Carbon	Solvothermal	130@1C, 25°C 114@5C, 25°C	92@100 Cycles	[119]
Graphene Oxide	Solvothermal	67.1@1C, 25°C	61@1000 Cycles	[120]
		123.2@1C, 25°C	94@280 Cycles	[121]
Carbon	Organic Pyrolysis	64@10C, 25°C	71@500 Cycles	[122]
OCNTs	Dry Coating	130.8@1C, 25°C	95.5@80 Cycles	[123]
Graphene	Dry Coating	91@20C, 25°C	82.5@1000 Cycles	[124]

COATING MATERIAL	COATING TECHNOLOGY	DISCHARGE CAPACITY [mAh/g]	CAPACITY RETENTION [%]	REF.
Reduced Graphene Oxide	Solvothermal	83.8@2C, 55°C 100@1C, 25°C	94.5@100 Cycles 91@100 Cycles	[117]
p-phenyline diamine reduced graphene oxide (pPD-rGO)	Electrophoresis	100@-, 25°C	81.7@1000 Cycles	[125]
Sandwiched Graphene Sheet	Solvothermal	130.8@1C, 25°C	95.5@80 Cycles	[118]

Conductive Polymers

Conductive polymers have been employed as surface modification chemicals for LNMO due to the low ionic conductivity offered by inorganic coatings. Uniformity of the coating is another parameter that is difficult to control, especially for carbon coating materials owing to the complex nature of the coating technologies utilized. Table 5 lists the different conductive coatings utilized by researchers in order to modify the surface properties of LNMO. Moreover, inorganic coatings like metal oxides, phosphates, and fluorides do not uniformly deposit at the surface of the cathode, and deposition methods, like ALD, that achieve uniformity face scalability limitations. Hence, the family of polymeric coatings are utilized as they provide high ionic conductivity and can deposit in uniform thin films upon the cathode surface. Furthermore, these kinds of polymer-based coatings are capable of accommodating any

significant volume changes in the cathode material that may occur during cycling. Because of the soft and flexible coating layer, it is anticipated that the likelihood of fracture formation and delamination of the coating layer as a result of volume fluctuations would be reduced. Conductive polymers like polyimide (PI) wrapped LNMO cathodes have been proven to offer protection against side reactions at the interface between LNMO and the electrolyte and increase ionic conduction at high temperatures. This was because the PI was deposited uniformly on the surface in (~10 nm)[124]. However, the PI coating did not perform well at high current rates of 5C and 10 C, possibly due to higher electronic resistance at these rates. Conductive Polypyrrole (PPy) coating, on the other hand, was investigated as a coating material and provided better stability at high current rates of 5 C and 10 C. PPy coating provided 91% capacity retention at the higher temperature (55°C) at 1 C for 100 cycles[126]. Cyclized polyacrylonitrile (cPAN) exhibited a 95.2% capacity retention at a high charge rate of 5C after 100 cycles at an elevated temperature of 55°C (Figure 6b). One advantage of conductive polymer coatings is the facile synthesis method that does not require high-temperature heat treatments. Most conductive polymer coatings can be prepared in solutions using oxidative polymerization reactions that require heating of the solution below 100°C, compared to other synthesis methods that require heat treatments in the range of 400°C to 600°C.

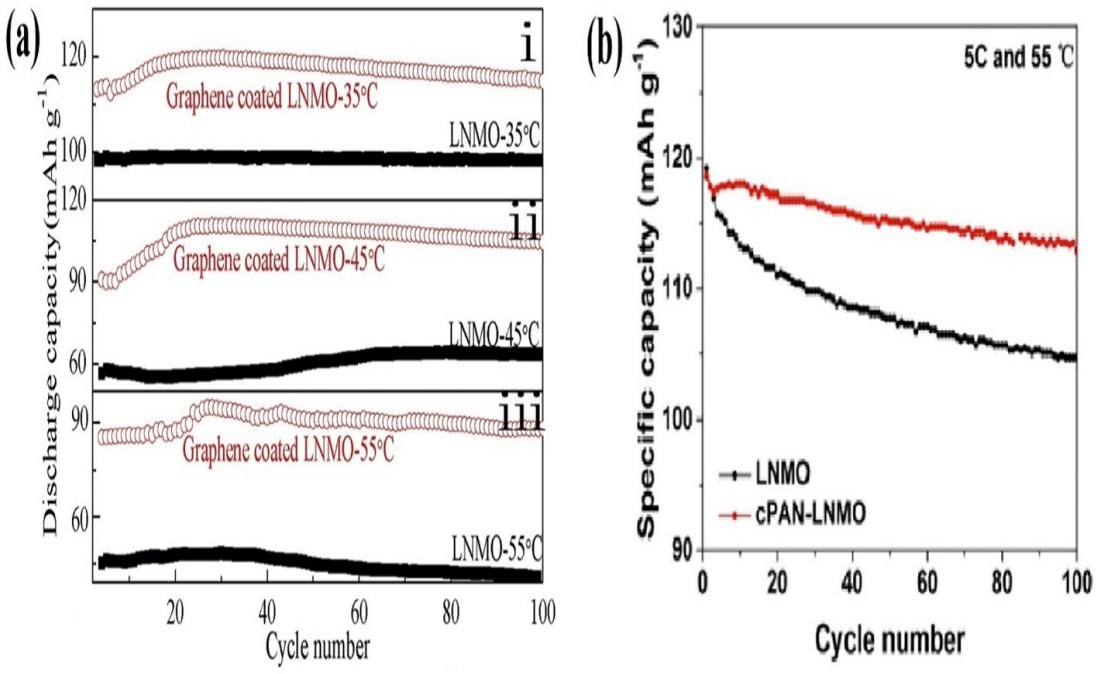

Figure 6: (a) Discharge capacity for graphene-coated LNMO and bare LNMO at 2C for 100 cycles at (i) 35°C (ii) 45°C (iii) 55°C[127]. (b) Comparison of cycling performance of bare LNMO and cPAN-coated LNMO at 5C and 55°C[128].

Table 5. $LiNi_{0.5}Mn_{1.5}O_4$ Coated with Conductive Polymers and the Corresponding Electrochemical Performance.

COATING MATERIAL	COATING TECHNOLOGY	DISCHARGE CAPACITY [mAh/g]	CAPACITY RETENTION [%]	REF.
Polyimide (PI)	Oxidative polymerization	120@1C, 55°C	95@50 Cycles	[127]
Conductive Polypyrrole (PPy)	Oxidative polymerization	112.9@1C, 25°C	91@300 Cycles	[128]
		105.2@1C, 55°C	91@100 Cycles	
Cyclized Poly-acrylonitrile (cPAN)	Oxidative polymerization	112.9@5C, 55°C	95.2@100 Cycles	[126]
Polythiophene (PTP)	Oxidative polymerization	105@1C, 55°C	78.8@100 Cycles	[129]
		123.4@C/2, 25°C	99.7@200 Cycles	[130]

COATING MATERIAL	COATING TECHNOLOGY	DISCHARGE CAPACITY [mAh/g]	CAPACITY RETENTION [%]	REF.
Polyaniline (PANi)	Oxidative polymerization	106.6@C/2, 25°C	94.5@100 Cycles	
Poly-(ethylα -cyano-acrylate) (PECA)	Oxidative polymerization	110@1C, 25°C	92@100 Cycles	131
3, 4-ethylene-dioxy-thiophene (PEDOT)	Oxidative polymerization	114.5@C/5, 25°C	91.6@200 Cycles	132
		110@5C, 25°C	-	
		63@10C, 25°C	-	
		-@1C, 25°C	92.8@200 Cycles	133
Polyvinylidene fluoride (PVDF)	Solvothermal	-@-, 25°C	97.8@300 Cycles	134
		-@-, 55°C	86.1@300 Cycles	
Lithium Polyacrylate (PAALi)	Solvothermal	111.6@1C, 25°C	90@200 Cycles	135

Conductive Coatings

Careful control of coating amount is necessary for the optimal performance of LIBs utilizing LNMO cathode. Too much amount of oxide, phosphate, fluoride, or carbon coatings, although effective, can impede the diffusion of lithium-ions, reducing rate capability and cycling performance[44]. Therefore, incorporating Li^+ conductors as coating materials might help to protect the cathode from electrolytic decomposition and HF attacks while ensuring increased lithium-ion diffusion. According to Deng et al.[136], Li_2SiO_3, a lithium-ion conductor, can increase the rate capability of LNMO by providing three-dimensional lithium diffusion pathways in its layered structure, thus

improving capacity retention at 500 cycles[137]. $Li_4P_2O_7$, a type of ionic conductive glass, is also utilized to coat LNMO, providing high-capacity retention of 74.3% at around 800 cycles at 0.5C and also shows a high stability at 40 C-rates[138]. Elsewhere, a superconductive coating of $YBa_2Cu_3O_7$ (YBCO) has also been reported to offer increased electrochemical performance. While $Li_{0.33}La_{0.56}TiO_3$ (LLTO), an ionic conductor, can help to increase the rate capability due to low charge transfer resistance at the interface, leading to faster lithium-ion diffusion. Other conductive coatings used for enhancement of LNMO cycling at elevated temperatures are Li_4SiO_4 and $YBa_2Cu_3O_7$ (YBCO) and $La_{0.7}Sr_{0.3}MnO_3$ (LSM)[44,116,139]. Li_2ZrO_3 has been utilized as a coating material due to its high thermal stability and lithium-ion conductivity owing to having three-dimensional pathways for lithium diffusion. Figure 7 illustrates the cycling performance of Li_2ZrO_3[140] and Table 6 tabulates the performance of various conductive coating materials on LNMO.

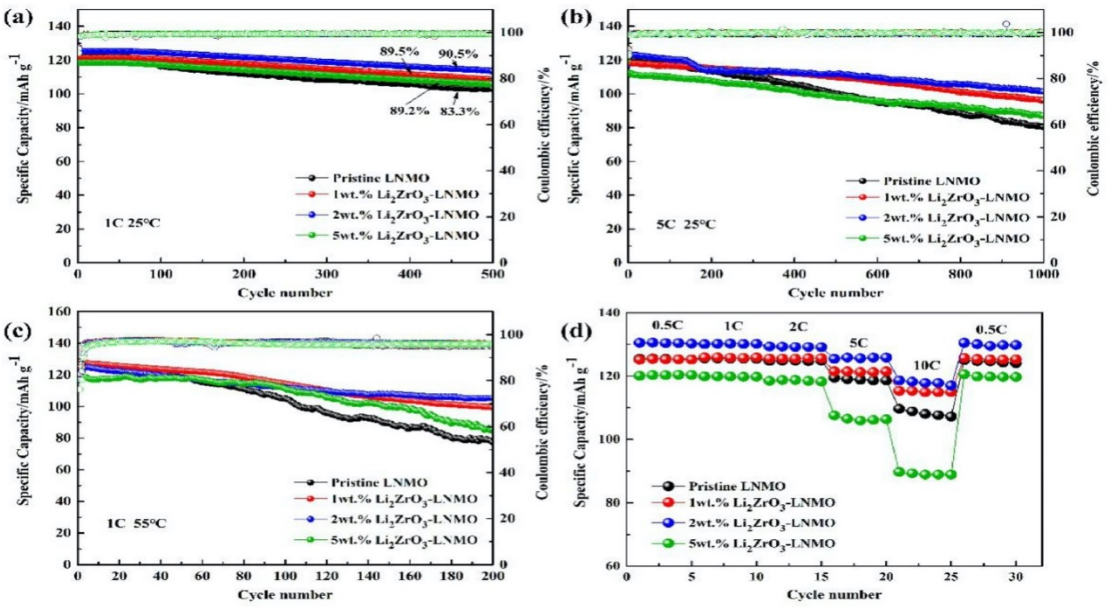

Figure 7: Cycling performance of Li_2ZrO_3 coated LNMO at (a) 1C and 25°C (b) 5C and 25°C (c) 1C and 55°C and (d) rate capability at current rates of 0.5/1/2/5/10[140].

Table 6. Surface Modification of $LiNi_{0.5}Mn_{1.5}O_4$ with Various Conductive Coatings.

COATING MATERIAL	COATING TECHNOLOGY	DISCHARGE CAPACITY [mAh/g]	CAPACITY RETENTION [%]	REF.
Li_2SiO_3	Solvothermal	-@C/10, 25°C	95.2@100 Cycles	[136]
		111@C/10, 25°C	99.4@500 Cycles	
	Aerosol Spray Pyrolysis	95.89@1C, 25°C	93.3@500 Cycles	[141]
		91.8@1C, 50°C	81.2@400 Cycles	
$Li_4P_2O_7$	Dry Coating	92@C/2, 25°C	74.3@893 Cycles	[138]
Li_2ZrO_3	Solvothermal	-@5C, 25°C	82.4@1000 Cycles	[140]
		-@1C, 55°C	83.5@200 Cycles	
Li_3BO_3	Solvothermal	127@1C, 25°C	92@500 Cycles	[142]
$LiAlO_2$	ALD	92@C/3, 25°C	78@50 Cycles	[143]
F-doped Li_4SiO_4	Sol-gel	117.36@5C, 25°C	97.8@150 Cycles	[44]
		113.04@5C, 55°C	94.2@150 Cycles	
$Li_{6.4}La_3Al_{0.2}Zr_2O_{12}$ (LLAZO)	Sol-gel	92.1@1C, 25°C	72.6@600 Cycles	[144]
$YBa_2Cu_3O_7$ (YBCO)	Sol-gel	112@2C, 60°C	87@100 Cycles	[116]
$Li_{0.33}La_{0.56}TiO_3$ (LLTO)	Sol-gel	130.8@1C, 25°C	95.5@80 Cycles	[145]
$La_{0.7}Sr_{0.3}MnO_3$ (LSM)	Sol-gel	122.3@1C, 25°C	97.71@100 Cycles	[139]
		116.6@1C, 55°C	93.17@100 Cycles	
Li_2O-Al_2O_3-TiO_2-P_2O_5 (LATP)	Sol-gel	110@2C, 55°C	83@100 Cycles	[146]
		82.2@C/10, -20°C	61@100 Cycles	[147]
Li_2O-$2B_2O_3$ (LBO)	Solvothermal	136@1C, 30°C	97@50 Cycles	[148]

COATING MATERIAL	COATING TECHNOLOGY	DISCHARGE CAPACITY [mAh/g]	CAPACITY RETENTION [%]	REF.
		106.9@1C, 60°C	87@50 Cycles	[149]
		-@1C, 25°C	91.4@100 Cycles	

Electrode and Solid Electrolyte Materials

A wide range of materials has been researched to be employed as either electrodes or electrolytes within LIBs. Commercial cathode, anode, and electrolyte materials have also been reported to be utilized as surface coating materials for LNMO cathodes, Table 7. Every material comes with its own set of pros and cons; as such, LNMO cathode material has its own aforementioned limitations that could be offset by the use of surface coatings of other common electrode materials utilized in LIBs. Normally, the more stable performing material should be coated over the less stable material to enhance total material performance. Commonly used electrode materials as surface coatings are $LiCoO_2$ (LCO), $Li_4Ti_5O_{12}$ (LTO), $LiFePO_4$ (LFP), to name a few. The advantage of these coatings is that they provide a physical barrier between the cathode and the electrolyte, thus reducing unwanted side reactions. These coatings enhance the charge transfer kinetics of the cathode material, resulting in improved electrochemical performance. However, applying a homogeneous and thin covering of this type is difficult. Additionally, high heat treatment temperatures are needed to produce a suitable coating, which may result in the breakdown of the cathode to be coated. As a result, the selection of the optimal coating material and optimal coating conditions for various kinds of coatings remains a problem. Additionally, owing to the complexity required and the high cost of the precursor materials utilized, these kinds of coatings significantly raise the total cost of cathode material. LNMO coated with LCO

has been reported by Deng et al.[150] to increase lithium-ion diffusion and protect the electrode from degradation, providing enhanced performance compared to the bare LNMO material. LFP, a common cathode material for LIBs, offers excellent thermal and structural stability, conductivity, and enhanced electrochemical performance at high temperatures; when coated on LNMO using a sol-gel method, it provided increased cyclability at 55°C[151]. LTO is a common anode material utilized for commercial LIBs; it is a spinel material instead of the traditional layered graphite. LTO has a high lithium insertion voltage resulting in the development of a thinner SEI layer resulting in faster Li^+ diffusion, compared to graphite[152]. Moreover, LTO offers no significant structural change resulting from lithium intercalation and de-intercalation as it is termed as a zero-strain material, so LTO has been utilized as a coating material to increase the cycling stability of LNMO, especially at elevated temperatures[153–155]. Other anode materials like Li_2SnO_3 and Li_2TiO_3 are also utilized as coating materials due to their high Li^+-ion conductivity, along with their protective qualities[156,157].

Apart from active electrode materials, solid electrolytes with high lithium-ion conductivities have also been utilized as coating layers for LNMO. They have been considered due to their low charge transfer resistance at the cathode electrolyte interface and high lithium-ion diffusion near the cathode surface, providing stability at high discharge rates and at elevated temperatures[158–160]. However, solid electrolytes possess poor electronic conductivities, and like other coating materials, thick coatings can negatively affect electrochemical performance. Ceramic based solid electrolyte coatings like $Li_{0.33}La_{0.56}TiO_3$(LLTO) and $Li_{1.4}Al_{0.4}Ti_{1.6}(PO_4)_3$ (LATP) are reported to provide enhancement in rate capability and cyclability due to their protective function; shielding the active cathode material from electrolytic oxidation. $Li_{1.4}Al_{0.4}Ti_{1.6}(PO_4)_3$ (LATP) is a commonly utilized solid electrolyte that offers high Li^+ ion conductivity.

Wu et al.[161] determined the cycling performance of LNMO coated with 0.5 wt% LATP. The LATP coated samples were tested at a current rate of 1 C (147 mAh/g), providing 98% capacity retention at 25°C and 96% capacity retention at 55°C after 100 cycles[161].

Table 7. Electrode and Electrolyte Materials Utilized as Coating Materials for Surface Modification of LNMO.

COATING MATERIAL	COATING TECHNOLOGY	DISCHARGE CAPACITY [mAh/g]	CAPACITY RETENTION [%]	REF.
$LiCoO_2$ (LCO)	Sol-gel	122@10C, 25°C	-	[150]
		-@-, 55°C	96.2@100 Cycles	
$LiCoPO_4$ (LCP)	-	130@20C, 25°C	-@100 Cycles	[162]
$Li_{1.2}Ni_{0.2}Mn_{0.6}O_2$ (LIR)	Co-precipitation	124.8@C/2, 25°C	97.2@300 Cycles	[163]
		116.3@1C, 25°C	92.3@300 Cycles	
$LiFePO_4$ (LFP)	Sol-gel	-@-, 25°C	97@50 Cycles	[151]
		-@-, 55°C	89@50 Cycles	
	Dry Coating	82@1C, 25°C	75@140 Cycles	[164]
$Li_4Ti_5O_{12}$ (LTO)	Solvothermal	132.3@1C, 25°C	93.7@500 Cycles	[155]
		136.3@1C, 55°C	97@140 Cycles	
		112.8@C/2, 25°C	93.6@100 Cycles	[154]
		107.5@C/2, 55°C	88.1@100 Cycles	
	Sol-gel	99@1C, 25°C	99@10 Cycles	[153]
Li_2SnO_3	-	-@C/10, 25°C	88.2@150 Cycles	[156]
		-@1C, 55°C	86.8@150 Cycles	
Li_2TiO_3	Solvothermal	-@1C, 25°C	90@50 Cycles	[157]
		-@1C, 55°C	94.1@50 Cycles	
$BiFeO_3$	Solvothermal	105.6@C/10, 25°C	89.1@100 Cycles	[165]
		110@C/10, 55°C	92.9@100 Cycles	
$LaFeO_3$	Solvothermal	122.3@1C, 25°C	97.71@100 Cycles	[166]

COATING MATERIAL	COATING TECHNOLOGY	DISCHARGE CAPACITY [mAh/g]	CAPACITY RETENTION [%]	REF.
		116.6@1C, 55°C	93.17@100 Cycles	
$LiNbO_3$	Sol-gel	122.3@-, 60°C	90@100 Cycles	[167]
		100@10C, 25°C	-	
$Li_{1.4}Al_{0.4}Ti_{1.6}(PO_4)_3$ (LATP)	Sol-gel	84.8@-, 25°C	68.9@500 Cycles	[168]
		-@-, 55°C	85.7@100 Cycles	
		-@1C, 25°C	98.1@100 Cycles	[161]
		-@1C, 55°C	96.1@100 Cycles	
$Li_{0.1}B_{0.967}PO_4$ (LBPO)	Dry Coating	125.1@1C, 25°C	91.3@400 Cycles	[160]
		119.3@20C, 25°C	87@50 Cycles	
		81.1@50C, 25°C	59.2@50 Cycles	

Composites

Composite coatings, as listed in Table 8, can be used to improve both the ionic and electronic conductivity on the surface of LNMO while offering protection from interfacial side-reactions that occur between the electrode and the electrolyte. Composite coatings consist of one type of coating material that could be employed for its electronic conductance property, while the other material would offer a high ionic conductance. $Li_2O–2B_2O_3$ (LBO)/Carbon composite coating is an ideal example, as it improves the cyclability and capacity retention by providing more ionic and electronic conductance, in addition to suppression of interfacial side reactions. The LBO/Carbon composite coating provides around 90% capacity retention at both room temperature (20°C) and elevated temperature (55°C) after 100 cycles at 1C (147 mAh/g) current rate[169]. Another composite coating such as La_2O_3/Al_2O_3 also contributes a similar performance alleviating the formation of SEI and alumina shielding the cathode from corrosive effects of HF[170]. Metal oxide coatings, while offering protection to the

cathode, increases the interfacial impedance that might increase cycling stability but at the expense of lower capacity[171]. Hence, composite coatings are commonly a combination of Li^+ conductor and a metal oxide; examples include Li_3PO_4/TiO_2, $LiCoO_2/Co_3O_4$, $Al_2O_3/LiAlO_2$[171–173].

Table 8. Composite Materials Utilized as Surface Coatings for LNMO Perfromance Enhancement.

COATING MATERIAL	COATING TECHNOLOGY	DISCHARGE CAPACITY [mAh/g]	CAPACITY RETENTION [%]	REF.
LBO/Carbon	Solvothermal	-@1C, 25°C	>90@100 Cycles	[169]
		-@1C, 60°C	>90@100 Cycles	
Li_3PO_4/TiO_2	ALD	96.5@C/2, 25°C	81.2@300 Cycles	[171]
$LiCoO_2/Co_3O_4$	Sol-gel	107.6@5C, 25°C	97.8@200 Cycles	[172]
La_2O_3/Al_2O_3	Solvothermal	-@1C, 25°C	94@200 Cycles	[170]
		-@1C, 55°C	95@100 Cycles	
		-@5C, 25°C	93.3@500 Cycles	
$Al_2O_3/LiAlO_2$	Co-precipitation	-@C/2, 55°C	88@50 Cycles	[173]
		-@C/2, 25°C	90.9@200 Cycles	

Other Materials

Some other types of coating materials apart from oxide, fluorides, phosphates, carbon materials, polymers, and composite coatings are also employed to coat LNMO. $LiMg_{0.5}Mn_{1.5}O_4$ (LMgMO) is a spinel-type compound that possesses a similar crystal structure to LNMO. It can be grown epitaxially on the surface of LNMO, providing alignment of 3-dimensional lithium-ion diffusion channels. This enhances ionic

conductivity while offering protective characteristics similar to other coating materials. The LMgMO coating is prepared using the common sol-gel method and can provide 91.4% capacity retention at room temperature at 1 C to provide a discharge capacity of 125.1 mAh/g after 500 cycles. It can also provide better cyclability at an elevated temperature of 55°C, 119.3 mAh/g at 2 C after 100 cycles[174]. Fluoroalkyl Silane (FAS17), $F_3C(CF_2)_7(CH_2)_3Si(OCH_3)_3$, is a self-assembling coating layer that forms strong siloxane bonds with the LNMO surface, resulting in a thin yet dense coating that provides complete coverage of the LNMO, while being highly stable.

As illustrated in Figure 8, a 2-nm coating is achieved by the vapor deposition method that provides 97% capacity retention at 1 C and 25°C after 100 cycles, greatly improving the cycling capacity of LNMO[175]. Moreover, (pentafluorophenylpropyl)trimethoxysilane (PFPPS) is also a chemically and mechanically stable perfluorinated benzene precursor that can act as a self-assembling coating layer. PFPSS coating over LNMO provides 91.7% capacity retention at C/2 rate over 100 cycles at both room temperature and elevated temperatures; a thin coating layer is achieved by molecular vapor deposition (MLD)[176]. Furthermore, Wei et al.[177] tested the cycling capacity of surface-sulfidized LNMO. The 3-aminopropyltriethoxysilane (APTES) precursor utilized was done so as it forms a 3D matrix that aligns with the LNMO matrix. The aligned lattices facilitate the efficient transfer of ions through the cathode interface upon cycling, providing 74.9% capacity retention at 93.4 mAh/g after 2500 cycles at 2C[177].

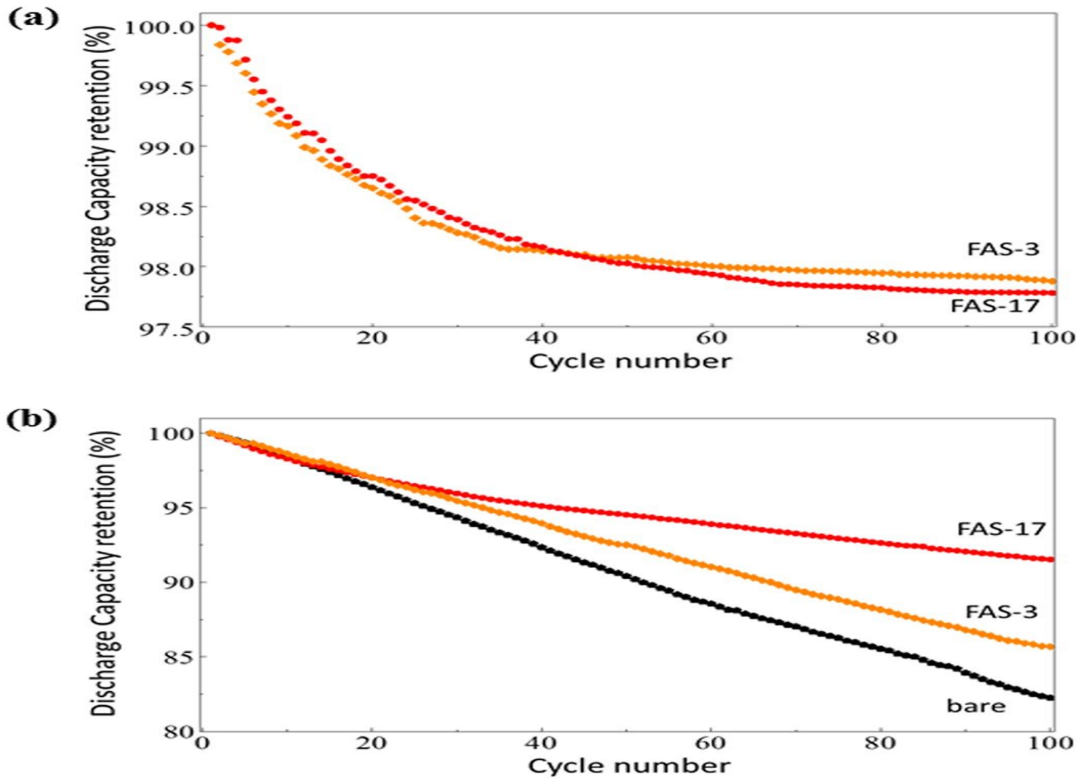

Figure 8: Cycling performance of FAS17 coated LNMO at 1C and (a) 25°C (b) 55°C[175].

Numerous types of surface coatings have been employed over LNMO and tested in a half-cell configuration. An extensive literature review has been carried out to collect information regarding the discharge capacity and capacity retention for such materials.

Scope and Objectives

The thesis will focus on the synthesis, characterization, and performance evaluation of LNMO cathode materials coated with metal oxides wrapped with graphene. The metal oxides chosen as coating materials are aluminum oxide (Al_2O_3) and cerium oxide (CeO_2). A comparison of structural, thermal, and electrochemical performance (cyclic voltammetry, galvanostatic charge/discharge behavior, cyclability, rate capability, and GITT) of pristine material with the coated LNMO will be accomplished. The coatings are anticipated to provide enhanced cycling stability, rate

capability, and electrochemical performance compared to bare pristine LNMO.

Numerous research groups have utilized a variety of coating materials, including metal oxides[84], conductive coatings [142], polymers[131], and carbon coatings[122] that can enhance the performance of LNMO. Widely available and cheap metal oxide coating materials such as alumina (Al_2O_3) have been utilized in a variety of industries as a common coating material. LNMO with an alumina coating has been made using a variety of coating methods, including as ALD [72–74], PLD [75], CVD [76], solvothermal [77], and co-precipitation[8]. By reducing the side reactions generated by the oxidation of organic molecules inside the electrolyte, Song et al.[72] found that a 6 nm layer of alumina on the LNMO surface helped sustain 98% discharge capacity after 200 cycles at ambient temperature. Kim et al.[30] looked into how cathode surface morphology affected electrochemical performance, they discovered that an alumina coated LNMO cathode outperformed an uncoated LNMO cathode by acting as a barrier to prevent electrolytic oxidation processes from damaging the cathode surface. The Jahn-Teller effect can be mitigated by using nanoscale alumina coatings, which have been shown to prevent Mn^{2+} formation[79].

Moreover, rare-earth metal oxides have superior electrochemical properties and are more electrically stable than the host ionic species, facilitating the migration of electrical and ionic species. It is stated that CeO_2 is an electrochemically active and feasible coating material for LNMO, providing rapid transformation between Ce^{3+} to Ce^{4+}[60,178,179]. Previous reports state the improvement in cyclic performance due to the use of ceria coating over $LiCo_{1/3}Ni_{1/3}Mn_{1/3}O_2$, $LiCoO_2$, $LiFePO_4$, $Li_4Ti_5O_{12}$ and other Lithium rich cathodes[178,180–184]. However, the coating methods employed for accomplishing the ceria coating provide difficulty in controlling the homogeneity of the coating layer[143,185].

Metal oxide coatings lend extra resistance to the mobility of ions and electrons and lower the rate capability of LNMO[186]. Hence, due to graphene's exceptional electrical characteristics, stable chemical properties, and large surface area, it has been keenly investigated for energy storage applications[187]. Graphene and Graphene oxide have been stated to enhance the cyclability and rate performance of spinel LNMO, $LiCo_{0.1}Ni_{0.8}Mn_{0.1}O_2$, $LiFePO_4$ and $LiMn_2O_4$ by enhancing the conductivity and decreasing the charge transfer resistance[118,124,188–192]. Graphene is usually dispersed or wrapped around the cathode particles instead of being coated on the surface, due to its hydrophobic nature. Hence, Graphene oxide is often utilized as a coating precursor as it attaches easily to the cathode surface owing to the oxygen-containing groups that it possesses[193]. However, the electronic conductivity of graphene oxide is lower compared to graphene, so a calcination process is often utilized that reduces the graphene oxide into graphene sheets and enables efficient coverage of the cathode material[121186].

Careful control of reaction parameters is required to obtain LNMO spinel with increased metal-ion disorder and resultantly enhanced electrochemical performance. LNMO particles of various structure and sizes have been prepared by common processes like sol-gel, hydrothermal, solid-state, Atomic Layer deposition, microwave-assisted process etc. [60,194–196]. For manufacturing LIB active materials, coprecipitation has been documented extensively in the literature for its simplicity, flexibility, uniform mixing, and control over particle shape. Co-precipitation is commonly used to synthesize nanoparticles due to its straightforward morphological control and low-cost raw materials[197]. However, nanoparticles decrease the tap density of the cathode because they provide a large surface area. Therefore, it is required to develop an approach that can be utilized to synthesize LNMO secondary microspheres that contain

primary nanoparticles, without the formation of secondary phases. Such an approach would enable the realization of enhanced electrochemical performance along with a high volumetric specific energy. Furthermore, microwave heating is an efficient method for preparing $LiNi_{0.5}Mn_{1.5}O_4$ that can save time and energy. Other cathode materials ($LiMn_2O_4$, Li_2FeSiO_4, and $LiFePO_4$) have been developed utilizing microwave-assisted methods[198–201]. Microwave irradiation is critical for grain development in microwave-assisted processes. During the heat treatment process, microwave sintering has been reported to enhance the crystal structure and thus boosts the capacity of the spinel LNMO[202,203].

Using existing metal oxide coatings, graphene coatings, and microwave sintering techniques, this work proposes a unique way for synthesizing Alumina (Al_2O_3)/Ceria (CeO_2) coated LNMO microspheres that are wrapped with graphene. The required cathode material, $LiNi_{0.5}Mn_{1.5}O_4$, is generated using a combination of microwave irradiation and chemical precipitation. The ceramic coatings over the secondary microspheres of LNMO are also realized by utilizing co-precipitation technique, succeeded by a simple hydrothermal method for achieving the graphene wrapping. While several spinel structures have been synthesized using microwave assisted processes, to the authors' knowledge, Al_2O_3-coated or CeO_2-coated $LiNi_{0.5}Mn_{1.5}O_4$ microspheres covered in graphene have not been previously disclosed. The significant increase in cyclic stability suggests that the proposed synthesis approach and subsequent design are an effective method of improving the electrochemical performance of LNMO as a cathode material. The material architecture is meant to minimize parasitic interactions between the cathode and the electrolyte, hence increasing cyclability (see Figure 9). The approach of material development described herein may be successfully applied to different families of cathode materials

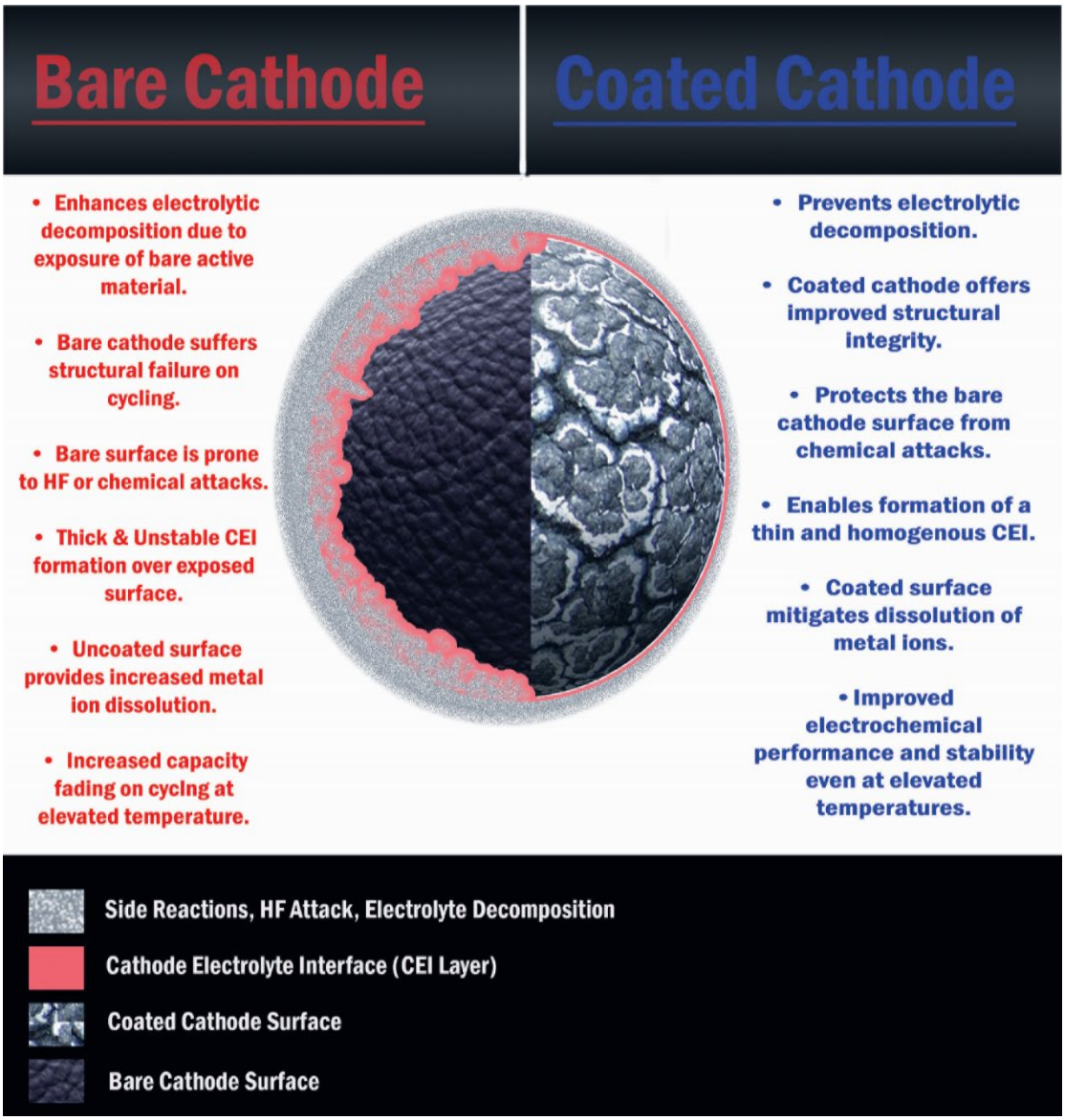

Figure 9: Schematic illustrating advantages of surface coatings.

Chapter 3: Methodology

The methodology to study the influence of metal oxide coatings on LNMO performance includes three significant tasks: material synthesis, structural characterization, electrochemical characterization.

Material Synthesis

The synthesized LNMO cathode material will be initially coated with ceramic coating and subsequently encapsulated with graphene; a simplified version of the process is illustrated in Figure 10.

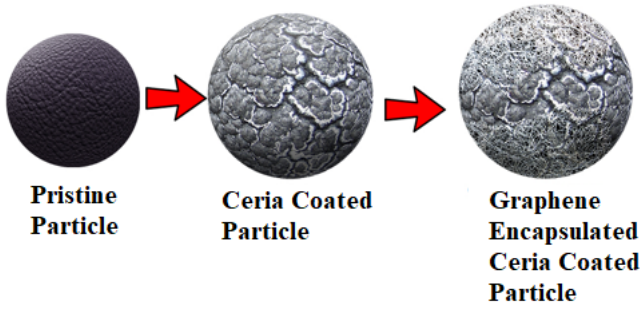

Figure 10: Proposed synthesis procedure.

Synthesis of spherical $LiNi_{0.5}Mn_{1.5}O_4$

For the pristine LNMO synthesis a co-precipitation technique is utilized as exhibited in Figure 11(a). Stoichiometric amounts of precursors $NiSO_4.(H_2O)_6$ (Nickel Sulfate Hexahydrate; purity >98%, Carl Roth GmbH + Co. KG, Germany) and $MnSO_4.H_2O$ (Manganese (II) sulfate monohydrate; AnalaR NORMAPUR ACS/Reagent, VWR Chemicals, USA) are prepared in an aqueous solution (500 mL of deionized water) in a continuous stirred tank reactor. Na_2CO_3 (Sodium carbonate; purity >99.5%, ACS reagent, Sigma-Aldrich, USA) solution is added dropwise as a reagent to initiate the precipitation reaction; a pH of 8 is maintained to ensure an alkaline environment. The Na_2CO_3 solution to the metal ion ratio will be kept as 2:1; the temperature of the reaction is kept constant at 80°C for 2 hours while holding the pH steady by utilizing

ammonia solution (35% (W/W) pure assay, Honeywell Riedel-de Haen, Germany); which also behaves like a chelating agent. Afterwards, the solution is vacuum filtered, and the resulting precipitate (Spherical ($Ni_{0.25}Mn_{0.75})CO_{3)}$ is stored in a vacuum oven at 120°C. The resulting$(Ni_{0.25}Mn_{0.75})CO_3$ is ground using a mortar and pestle; calcinated in a microwave furnace (VBCC HYTHERM, VBCC/MF/14/15) at 550°C for 15 minutes at the rate of 10°C/min, to convert the carbonate into oxide. Subsequently, a 5% excess stoichiometric amount of lithium carbonate (Li_2CO_3; purity >99%, Honeywell Fluka, USA) is added, for lithiation, to the sample by grinding them together using a mortar and pestle. The resulting sample is then be sintered at 850°C at $10°C.min^{-1}$ for 30 minutes in a microwave furnace, followed by annealing to 700°C at the rate of at $10°C.min^{-1}$ for 15 minutes to obtain phase pure $LiNi_{0.5}Mn_{1.5}O_4$, this sample is labelled as LNMO.

Formulation of Ceria (CeO_2) coated $LiNi_{0.5}Mn_{1.5}O_4$

Microwave assisted co-precipitation technique was also utilized for preparing LNMO coated with a 1 wt% cerium oxide layer (CeO_2). 0.05g of cerium (III) nitrate hexahydrate ($Ce(NO_3)_3.6H_2O$; purity >99% trace metals basis, Sigma-Aldrich, USA) was added to 100mL of de-ionized water and made into a solution. Next, 2g of solid pristine LNMO was added into the solution and heated at 60°C in a continuous stirred tank reactor; with the pH maintained at 6. Subsequently, 0.0369g of Na_2CO_3 solution is prepared in 50mL de-ionized water and added dropwise as a reagent to initiate the precipitation reaction. The resulting precipitate is vacuum filtered and sintered at 500°C for 15 min in a microwave furnace to obtain cerium-oxide coated LNMO labelled as LNMO-Ce, as illustrated in Figure 11(b).

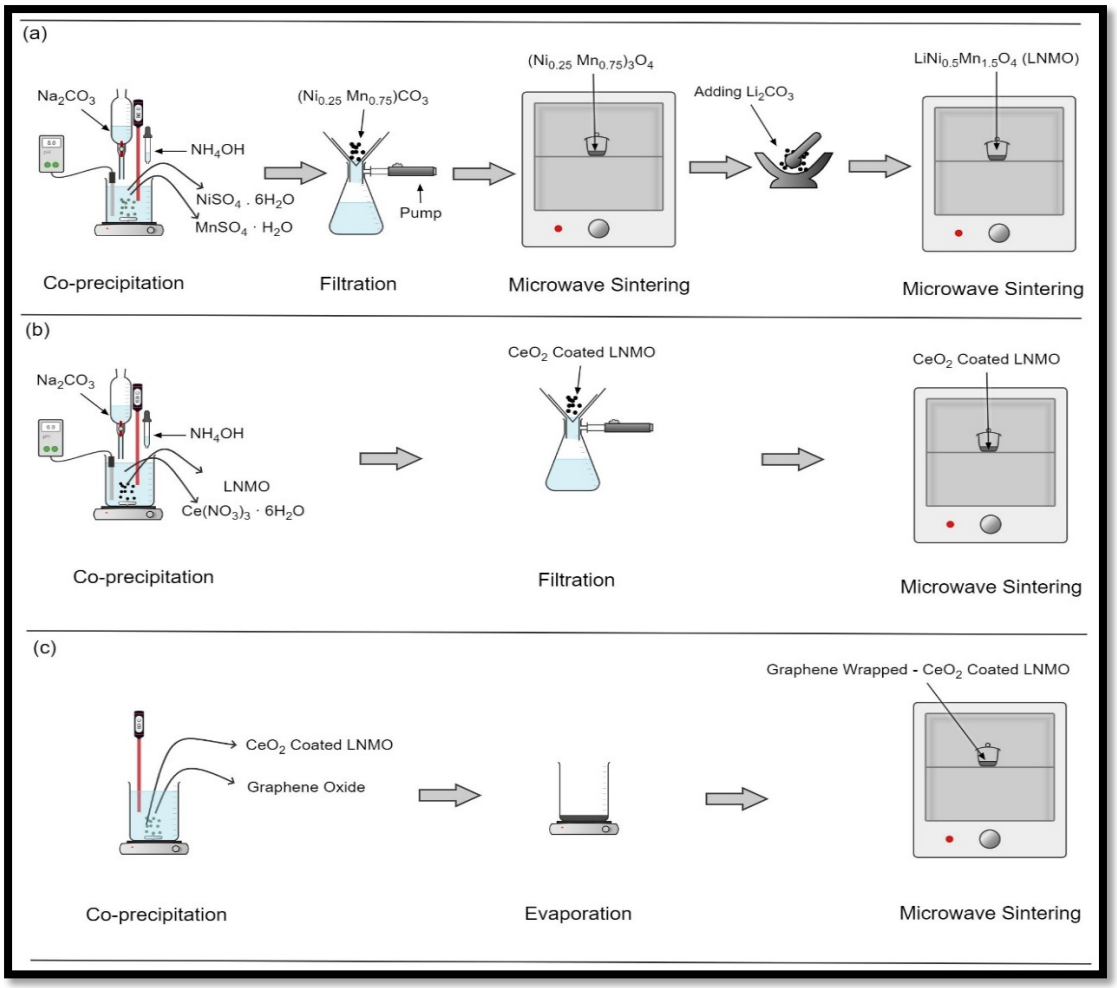

Figure 11: Schematics for the synthesis of; (a) pure $LiNi_{0.5}Mn_{1.5}O_4$ (LNMO), (b) CeO_2 coated $LiNi_{0.5}Mn_{1.5}O_4$ (LNMO-Ce), and (c) Graphene wrapped CeO_2 coated $LiNi_{0.5}Mn_{1.5}O_4$ (LNMO-Ce-GO).

Synthesis of graphene wrapped CeO_2 coated $LiNi_{0.5}Mn_{1.5}O_4$

2g of LNMO-Ce powder was added to 300mL de-ionized water with 0.02g (1wt%) graphene oxide (graphene oxide water dispersion 0.4wt%, Graphenea, USA) the solution was stirred gently to form graphene wrapped CeO_2 coated LNMO, indicated in the text as LNMO-Ce-GO. After 30 minutes of sonication, the mixture was homogenized. Finally, the suspension was filtered, and dried at 60°C. The filtrate was then sintered in a microwave at 600°C for 15 minutes, to cure the coatings. Due to the size difference between the LNMO-Ce microspheres and the graphene sheets, graphene

may not completely coat the LNMO particles but will possibly wrap around them. This procedure, Figure 11c, resulted in graphene-wrapped CeO_2-coated $LiNi_{0.5}Mn_{1.5}O_4$ spinel particles that retained their original spherical shape.

Formulation of Alumina (Al_2O_3) coated $LiNi_{0.5}Mn_{1.5}O_4$

LNMO coated with alumina was also synthesized by microwave assisted co-precipitation method. In 100 mL of de-ionized water, 0.0737 g (1wt%) of $Al(NO_3)_3.9H_2O$ (aluminum nitrate nonahydrate; Sigma-Aldrich, >98%) was dissolved. 2g of LNMO, as synthesized earlier, was then mixed with the Al^{3+} containing solution, and heated to 70°C while maintaining the pH within 7.5-8.5. Next, to initiate the precipitation reaction, 0.0416g of Na_2CO_3 solution is dissolved in 50mL deionized water and added dropwise as a reagent. The obtained precipitate, LNMO coated aluminum oxide (LNMO-Al) is vacuum filtered and sintered in a microwave furnace at 500°C for 15 min, as shown in Figure 12.

Synthesis of graphene wrapped Al_2O_3 coated $LiNi_{0.5}Mn_{1.5}O_4$

In 300mL de-ionized water, 2g of LNMO-Al was dissolved with 5 mL (1wt%) graphene oxide (water dispersion 0.4wt%, Graphenea) and stirred uniformly to obtain graphene wrapped Al_2O_3 coated LNMO, abbreviated in the literature as LNMO-Al-GO. The mixture was then sonicated for homogenization for 30 minutes. Lastly, the suspension was filtered and dried at 60°C. To cure the coatings, the filtrate was treated in an argon tube furnace at 600°C for 6 hours. Graphene may not completely coat the LNMO particles but instead wrap around them because of the size disparity between the LNMO-Al microspheres and the graphene sheets. This process, Figure 12, formed graphene wrapped Al_2O_3 coated LNMO spinel particles that preserved their spherical form.

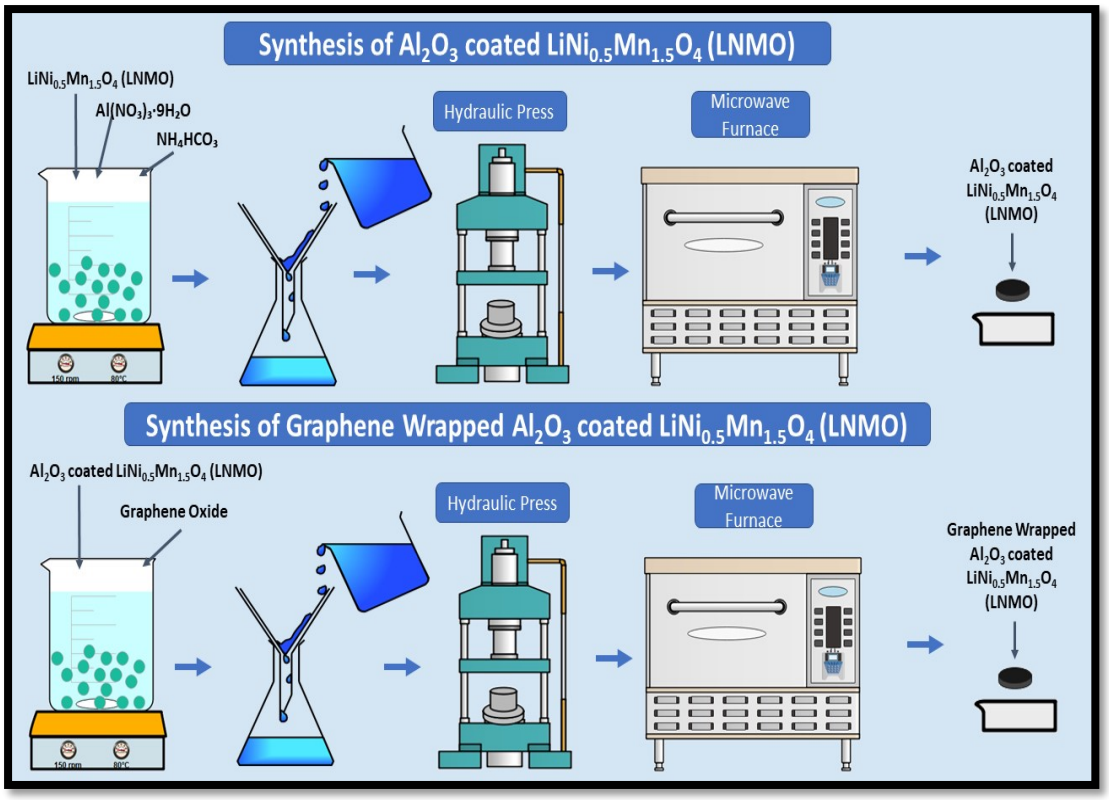

Figure 12: Experimental representation for the synthesis of Al_2O_3 coated $LiNi_{0.5}Mn_{1.5}O_4$ (LNMO-Al), and Al_2O_3 coated $LiNi_{0.5}Mn_{1.5}O_4$ wrapped with graphene (LNMO-Al-GO).

Physical Characterization

The crystal structure arrangement and phase purity of synthesized materials was studied using an X-ray diffractometer (XRD, PANalytical diffractometer, Almelo, Netherlands) at a scan rate of 2 degrees per minute and a step size of 0.02°, using Cu-$K\alpha$ radiation between 20° and 70°. The data was analyzed using PANalytical X'Pert Highscore software.

The morphologies, microstructures and elemental composition of the materials were investigated using a field emission scanning electron microscope (FE-SEM) coupled with energy-dispersive X-ray spectroscopy (EDX) (Nova NanoSEM 450 with Bruker EDX Detector, FEI). The FE-SEM utilized a Schottky FEG hot tip with acceleration voltage from 50V to 30kV and a magnification scale from 35x to 1 000 000x. Moreover,

to study the topographical, crystallinity and morphological aspects of the synthesized samples a 200kV high-resolution transmission electron microscope (HR-TEM, TECNAI G2 TEM TF20, FEI) was utilized.

Vibrational spectroscopic analysis for the samples were carried out using Thermo fisher scientific DXR Raman Microscope with a wavelength of 532nm, 40 times scan, and the laser power was 10 using 10X microscope objectives. Also, Fourier Transform Infrared Spectroscopy (FTIR; PerkinElmer, USA) instrument was used to analyze the presence of functional groups within the synthesized samples. All the spectra were recorded from 4000 to 500 cm^{-1} at a spectra resolution of 4.0 cm^{-1}.

Thermal gravimetric analysis was used to determine the thermal stability of the created materials using a TGA analyzer (Pyris 4000, PerkinElmer-USA); TGA profiles were obtained at temperatures ranging from 25 to 700°C at a rate of 10°C/min in the presence of nitrogen. The thermal stability of the lithiated and the de-lithiated samples were conducted to analyze the interfacial interaction between the samples and the electrolyte; investigated using differential scanning calorimetry (DSC 8500, PerkinElmer-USA). Initially, to prepare the de-lithiated samples the coin cells were first charged at the rate of 0.1C and equilibrated at 4.9V. Subsequently, the cells were moved into an argon-filled glovebox and the cells were disassembled to obtain the electrode. Approximately 5mg of the cathode material was scraped from the aluminum current collector and collected within a 30 μL stainless steel pan that was sealed shut by use of a gold-plated copper seal. The DSC was conducted from room temperature up to 300°C at a rate of $10°.min^{-1}$ in a nitrogen environment.

Electrochemical Characterization

A battery cycler equipment (Won A Tech; WBCS3000L, Seoul, South Korea) will be used for performing galvanostatic charge/discharge tests in a voltage range of 3.5 to 4.9 V (vs. Li/Li+). The electrochemical tests will be carried out to determine the charge

and discharge profiles of the cell, analyze the behavior of the redox couples, and determine the cathode material's storage capacity. Cyclability tests (Constant Current Constant Voltage (CCCV)) will be carried out to determine the battery's capacity change over a range of cycles and at various charge rates. Moreover, Galvanostatic Intermittent Titration Technique (GITT) will be used to provide insight; respective to electronic and structural changes during intercalation/deintercalation cycles, the kinetics of intercalation and electrochemical stability. GITT was measured at a rate of C/10 with a 10 min galvanostatic stage and a 1 h relaxation interval. Cyclic Voltammetry (CV) was conducted at 0.1 mV/s.

Electrode Fabrication

To test the electrochemical performance of the graphene wrapped-alumina coated LNMO, alumina coated LNMO, and pure LNMO cathodes, the samples will initially be made into coin cells (CR-2032) in an argon glovebox. To initiate coin cell fabrication, the cathode samples will be converted into a slurry coated on a battery grade aluminum foil, using the doctor blade procedure. The ratio of cathode material, acetylene black, and polyvinyl difluoride in the slurry will be 80:10:10. The chemicals are mixed and stirred for 6 hours using N-Methyl-2-pyrrolidone solvent (NMP). The aluminum foil is then coated with the slurry and placed in a vacuum oven for 2 hours at 120°C to effectively evaporate the solvent. Utilizing a punching machine, the coated foil is cut into 14 mm diameter electrodes and returned to the vacuum oven for 24 hours prior to getting transferred to an argon-filled glovebox. The coin cells will be made inside the glove box using lithium metal anode (half-cell) and an electrolyte solution of 1 M lithium hexafluorophosphate ($LiPF_6$) in ethyl carbonate (EC)/dimethyl carbonate (DMC) (1:1 v/v). A glass fiber separator (Whatman GF/D) will be utilized as the separator. The entire process is illustrated in Figure 13.

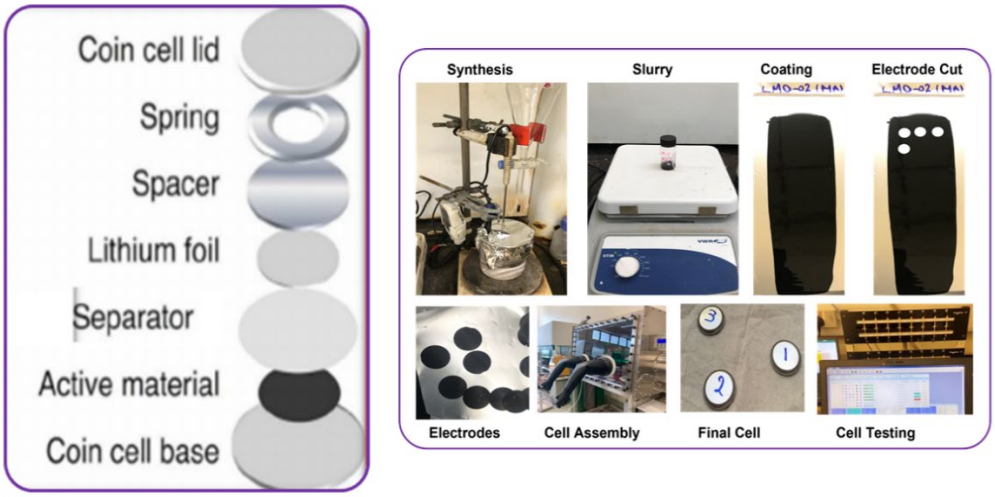

Figure 13: Fabrication procedure for a coin-cell battery, from start to finish.

Chapter 4: Results & Discussion

Influence of Ceria (CeO_2) Coated Graphene Wrapped LNMO

The X-ray diffractograms of $LiNi_{0.5}Mn_{1.5}O_4$ (LNMO), Ceria coated $LiNi_{0.5}Mn_{1.5}O_4$ (LNMO-Ce) and Graphene wrapped ceria coated $LiNi_{0.5}Mn_{1.5}O_4$ (LNMO-Ce-GO) are exhibited in Figure *14*. All spectra exhibit the LNMO structure's signature peak. The sharp and strong peaks demonstrate that the materials are extremely pure and crystalline, with (111) peak position being the most intense. All of the Bragg peaks may be assigned to the disordered spinel F$\overline{d3}$m space group, where Lithium ions occupy tetrahedral (8a) sites while Manganese and Nickel ions statistically remain in the octahedral (16d) sites; with a = b = c = 8.15 (ICSD #98-018-7804). Due to the high temperature synthesis process, minor amounts of rock-salt secondary phases such as $Li_xNi_{1-x}O$ or NiO are observed in the pristine LNMO sample. These minor impurities correspond to the weak peaks at 37.5° and 63.2°, these peaks are characteristic to the disordered space group and are denoted by asterisks in Figure *14*. However, these other phases are not present in the cerium oxide coated or the graphene wrapped ceria coated sample; illustrating the feasibility of using microwave sintering to synthesize pure disordered coated LNMO. The lack of the CeO_2 and graphene peaks in the LNMO-Ce and LNMO-Ce-GO spectra is due to their extremely low concentrations, approximately 1 wt%. The lack of the (220) peaks indicates that the tetrahedral (8a) locations within the crystal structure are not occupied by larger transition metal ions [60]. The prepared materials' lattice parameters are listed in Table 9. The diffusion of Ce^{4+} into the surface lattice causes contraction of the LNMO particles resulting in cell volume reduction due to the higher bonding energy of the Ce-O bond compared to the Mn-O and Ni-O bonds, lowering the lattice constant of the LNMO-Ce sample compared to bare LNMO [204,205]. Moreover, the coating layer can generate slight ordering of the lattice structure towards

ordered $P4_332$ phase, reducing the lattice constant. However, this phenomenon might happen at a very small scale as the XRD spectra is typical of the disordered spinel $F\overline{d}3m$ spinel space group. This reduction of lattice constant is in agreements with other studies published in the literature pertaining to coated LMO or LNMO spinel oxides [110,203,205,206]. Additionally, the graphene wrapping and ceria coating of LNMO did not enter the spinel system but remained attached to the particle surface, as seen by a modest increase in cell volume. Additionally, it implies that the specified microwave sintering did not alter the parent LNMO spinel structure. According to XRD patterns, there are no noticeable differences in the crystalline structure of the samples. The ratio of the I_{311}/I_{400} peaks, on the other hand, is significantly different between LNMO and LNMO-Ce samples, which may indicate the structural stability of the $[Mn_2]O_4$ spinel framework. According to previous research, spinel $LiMn_2O_4$ with I_{311}/I_{400} ratios between 0.96 and 1.1 typically exhibits superior electrochemical properties than those with ratios outside this range [89,207]. According to Table 9, the I_{311}/I_{400} ratio value of both LNMO-Ce and LNMO-Ce-GO can be comparable with that of spinel $LiMn_2O_4$ with the I_{311}/I_{400} ratios within the optimal range. As a result, it is plausible to conclude that LNMO-Ce and LNMO-Ce-GO samples exhibit superior electrochemical performance.

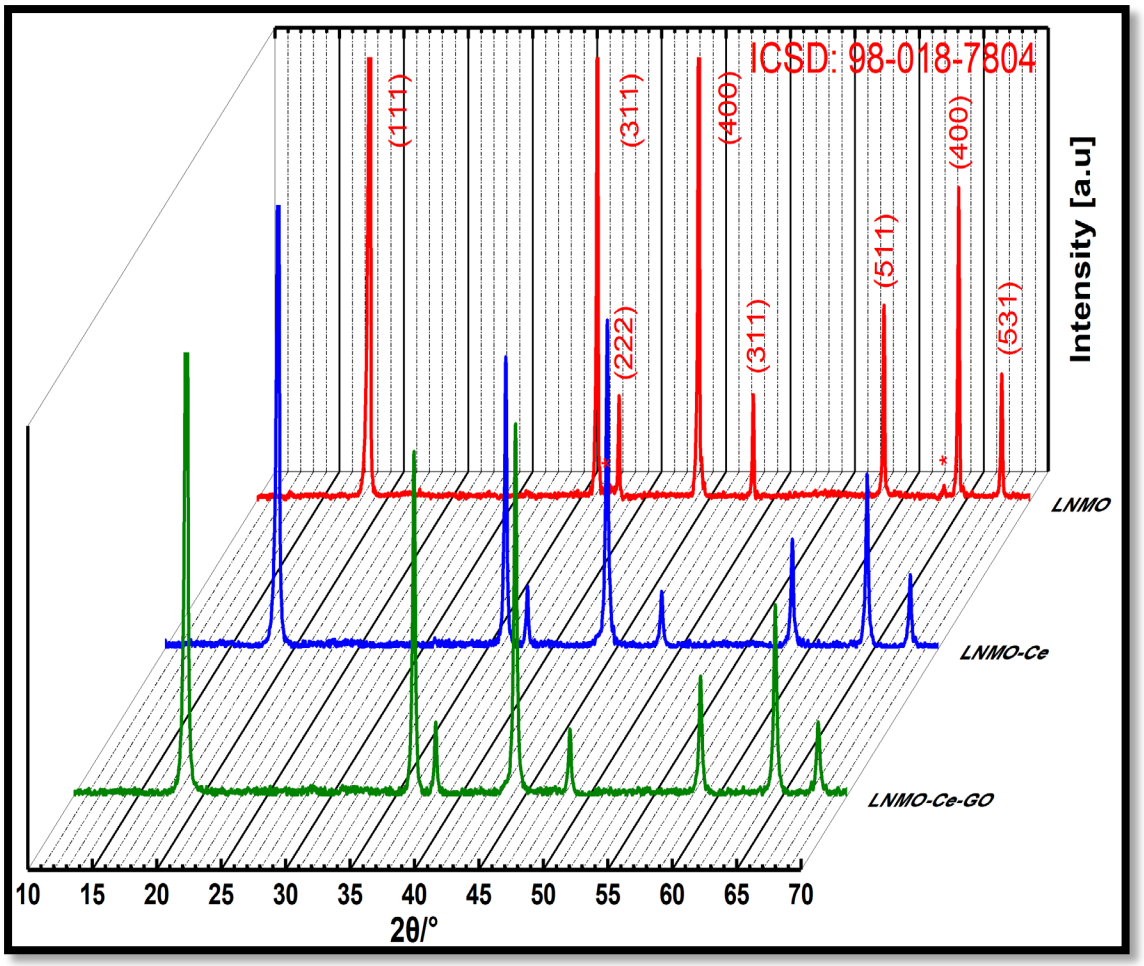

Figure 14: XRD patterns of synthesized samples.

Table 9. Lattice Parameters for the Synthesized Samples.

Sample	Lattice Constant (Å)	Volume (Å^3)	I_{311}/I_{400}
LNMO-Ce-GO	**8.174**	**546.1**	**0.9863**
LNMO-Ce	**8.128**	**536.9**	**0.9670**
LNMO	**8.151**	**541.6**	**0.9952**

Since manganese and nickel have comparable X-ray light scattering patterns, Raman and FTIR spectroscopy were used to highlight the distinctive vibrational bands of the ordered ($P4_332$) and disordered ($Fd\bar{3}m$) structures of the synthesized LNMO samples [208]. Figure 15(a) illustrates two main peaks at 490 and 630 cm^{-1}, exhibiting the Ni-O and Mn-O stretching modes on the Raman spectrum, respectively. The absence of intense peaks at 220 and 240 cm^{-1} along with the distinctive split peaks for the Mn-O bands at around 630 cm^{-1} are characteristics of the disordered spinel [124,192]. Additionally, Figure 15(b) illustrates the characteristic Mn-O and Ni-O bonds on the FTIR spectrum at 750 and 500 cm^{-1}, respectively. These bonds were utilized to assess the order of cations in the spinel lattice's 16d sites. The synthesized sample was verified to be the disordered spinel at the 16d octahedral sites due to the extremely low intensity of the distinctive bands at 650 and 556 cm^{-1}.The vibrational band at 628 cm^{-1}, accredited to the Mn–O stretching mode, was more intense than the band at 590 cm^{-1}, symptomatic of the disordered structure. Moreover, the Ni–O stretching mode in the structure was attributed to the two vibrations at 584 and 507 cm^{-1}, and the results were in good accord with prior studies[203].

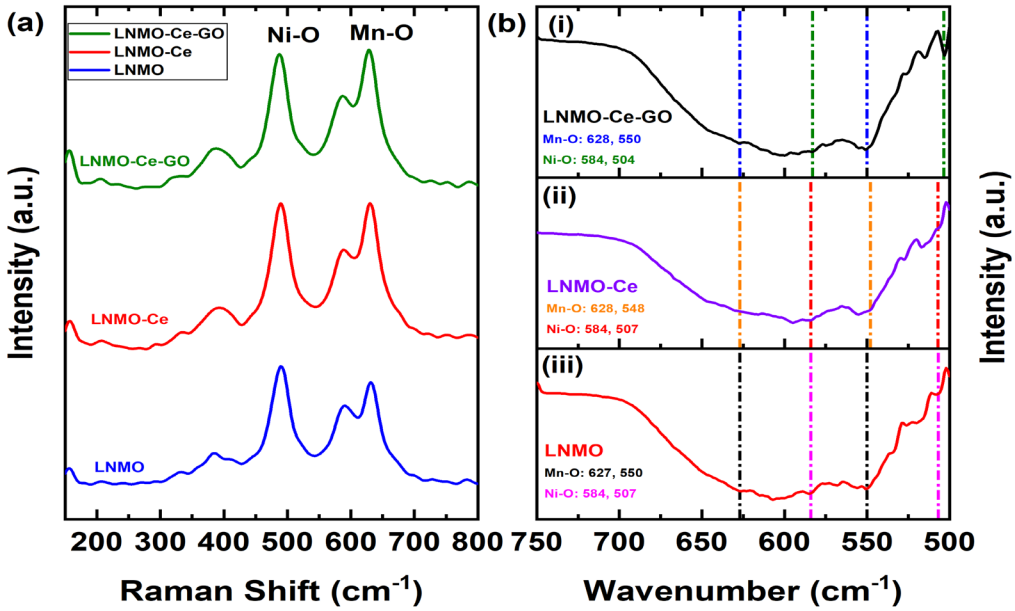

Figure 15: (a) Raman spectra and (b) FTIR spectra of (i) Graphene wrapped cerium coated $LiNi_{0.5}Mn_{1.5}O_4$ (LNMO-Ce-GO) (ii) Cerium coated $LiNi_{0.5}Mn_{1.5}O_4$ (LNMO-Ce) and (iii) $LiNi_{0.5}Mn_{1.5}O_4$ (LNMO), samples.

Thermal gravimetric analysis was utilized to assess the thermal stability of the produced materials and estimate the graphene wrapping of the LNMO particles. The temperature-induced shift in sample weight was monitored, resulting in a variation in graphene concentration. From Figure 16, no substantial measurable weight loss occurs over the full heating range. Because of the inclusion of a cerium oxide coating that may enhance thermal stability, the LNMO-Ce sample has the smallest extent of weight reduction. However, as the samples are heated from ambient temperature to 700°C, the LNMO-Ce-GO sample loses more weight than LNMO. The weight-loss region in the TGA plot for the LNMO-Ce-GO sample extends beyond 700°C, indicating carbon degradation. The overall computed carbon loss value for the LNMO-Ce-GO sample is roughly around 1.2 percent. Furthermore, it can be noted that all three created materials have good thermal stability up to 700 °C, since no substantial weight loss is seen.

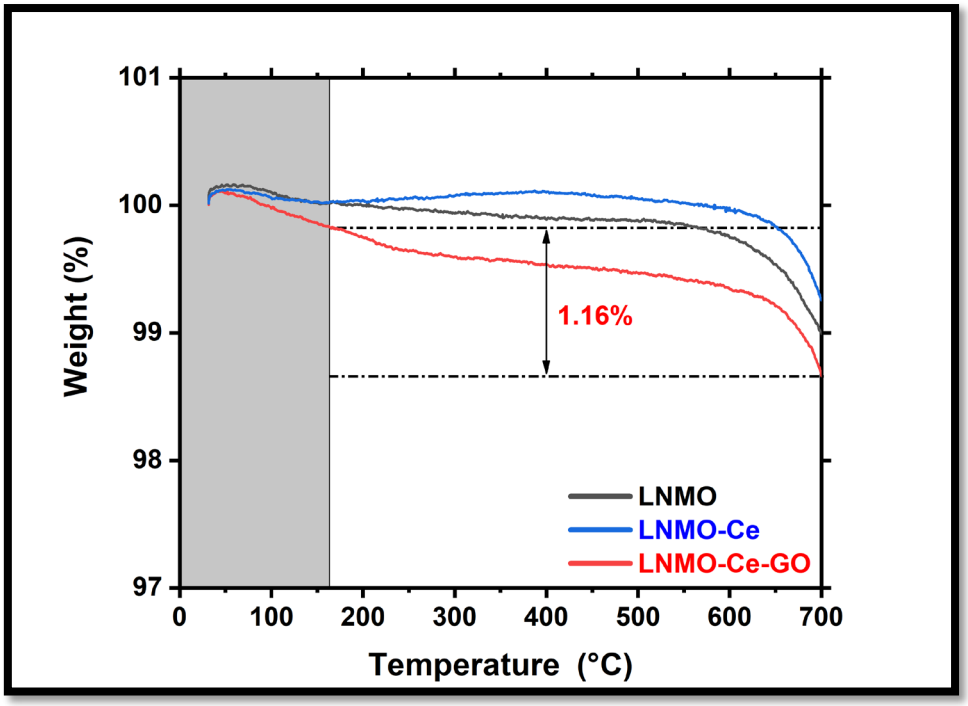

Figure 16: Thermal gravimetric analysis of $LiNi_{0.5}Mn_{1.5}O_4$ (LNMO), ceria coated $LiNi_{0.5}Mn_{1.5}O_4$ (LNMO-Ce) and graphene wrapped ceria coated $LiNi_{0.5}Mn_{1.5}O_4$ (LNMO-Ce-GO), in nitrogen environment.

Figure 17 exhibits FE-SEM micrographs of LNMO, LNMO-Ce, and LNMO-Ce-GO, samples. Even following high-temperature microwave sintering, the LNMO retains its characteristic spherical form. The LNMO sample is composed up of spheres with diameters ranging from 1-3 µm. However, many tiny holes on the surface of the LNMO particles may be detected, which may have been caused by carbon dioxide escape during sintering. In comparison, because of the thin nano size coating, the FE-SEM images of LNMO (Figure 17a-b) and LNMO-Ce (Figure 17c-d) do not differ significantly. The surface of the ceria coated sample is partially wrapped by graphene in the LNMO-Ce-GO sample (Figure 17e-h); its crinkled cover has the shape of sheets

(Figure 17h). Figure 17(i-j) depicts an EDX examination of the LNMO-Ce and LNMO-Ce-GO samples, which validates the presence of the elements that the produced material is composed of. The EDX studies shows that the LNMO particles were effectively coated with CeO_2 and enveloped by the graphene nanosheets. The homogenous CeO_2 nano-coating is intended to minimize unwanted contact between the electrolyte and the electrode surface, thereby improving cycling performance. The nanoscale layer would not restrict the internal channels that might prevent lithium-ion diffusion. The LNMO-Ce-GO microspheres include internal radial channels that enable regulated electrolyte-protected wettability, enhanced electronic conductivity, and ionic leaching protection.

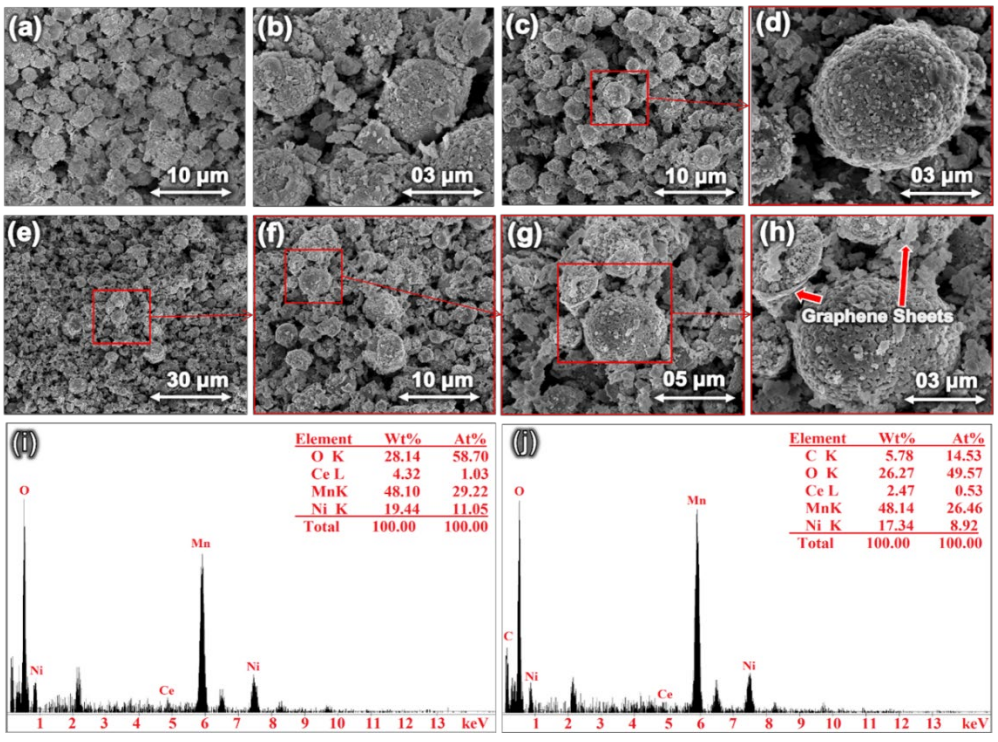

Figure 17: FE-SEM micrographs of; (a-b) $LiMn_{1.5}Ni_{0.5}O_4$ particles (c-d) Ceria coated $LiMn_{1.5}Ni_{0.5}O_4$ particles (e-h) Ceria coated $LiMn_{1.5}Ni_{0.5}O_4$ particles wrapped with 1wt% graphene; EDX analysis of (i)Ceria coated $LiMn_{1.5}Ni_{0.5}O_4$ particles and (j) Ceria coated $LiMn_{1.5}Ni_{0.5}O_4$ particles wrapped with 1wt% graphene.

To further corroborate the presence of ceria coating and graphene wrapping over $LiMn_{1.5}Ni_{0.5}O_4$, High-resolution transmission electron microscopy (HR-TEM) was utilized. The HR-TEM figures for LNMO, LNMO-Ce and LNMO-Ce-GO are presented in Figure 18. The sample particles were ground by a mortar before mounted on a carbon-coated copper TEM grid. The smooth particles observed in Figure 18(a-b) are attributed to pristine LNMO. Figure 18(c-f), on the other hand, exhibit grainy appearance, mainly due to the existence of ceria film and graphene sheets [203]. The nanometric coating of CeO_2 can be clearly observed in Figure 18(d), the film has an approximate thickness of 1-3 nm. The electrochemically active ceramic ceria coating ensures protection of the LNMO cathode from direct exposure to the electrolyte, minimizing undesirable reactions between the active material and the electrolyte. Furthermore, due to the ceramic nature of the coating, the LNMO cathode is also protected from HF attack and the integrity of the cathode is preserved due to suppression of Mn dissolution. In general, when the thickness of the cerium oxide coating increases, the contact resistance and load transfer resistance rise significantly, particularly as coating thickness exceeds 10 nm [209]. However, in this work, the ceria coating thickness is 1-3 nm (Figure 18d-f), guaranteeing that polarization and power depletion are successfully circumvented. Furthermore, the presence of graphene enhances the cathode's electrical conductivity, hence improving its electrochemical performance. Figure 18(h) exhibits the selected area diffraction (SAED) pattern of an independent graphene wrapped ceria coated LNMO particle, the pattern demonstrates that the increased crystallinity results in a lower energy barrier for lithium-ion insertion, resulting in rapid ionic diffusion. Additionally, as shown in Figure 18g, the distance between lattice fringes is 0.472 nm, corresponding to the interplanar division of the

$LiMn_{1.5}Ni_{0.5}O_4$ (111) plane in accordance with the XRD data. On the basis of the energy dispersive X-ray analysis and selected area diffraction, it can be determined that microwave-assisted chemical co-precipitation is a feasible method to manufacture phase pure spinel cathodes.

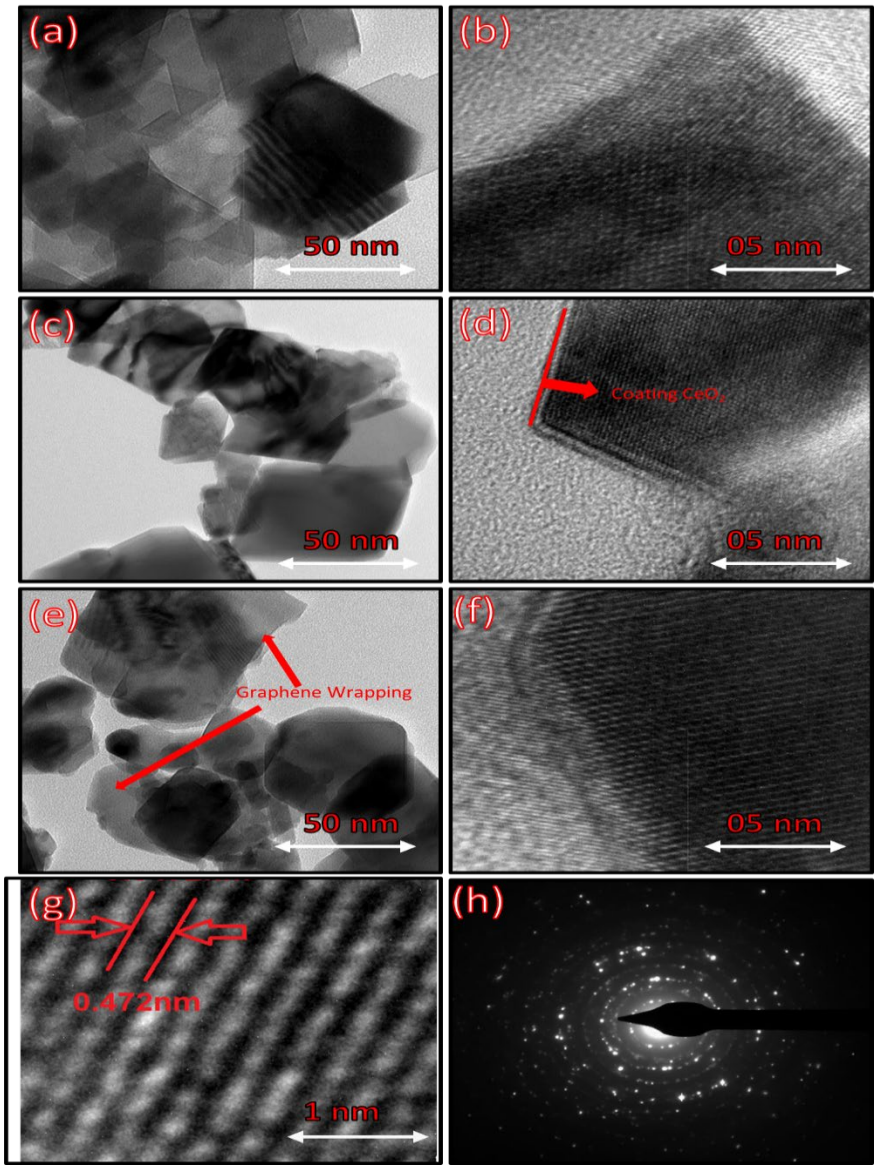

Figure 18: HR-TEM micrographs: (a, b) pristine LNMO particles (c, d) CeO_2 (5~8nm) coated LNMO particles (e, f) 1wt% graphene wrapped CeO_2 coated LNMO particles (g) Lattice fringes of LNMO-Ce-GO and (h) SAED pattern of LNMO-Ce-GO.

After coin-cell fabrication the charge and discharge behaviour for the three samples were conducted in the voltage window of 3.5 V to 4.9 V, characteristic of the redox couples for Mn and Ni within LNMO. The cells were tested at a constant current rate of 0.1C. Figure 20 illustrates the cyclability and the charge/discharge profiles for $LiNi_{0.5}Mn_{1.5}O_4$ (LNMO), Ceria coated $LiNi_{0.5}Mn_{1.5}O_4$ (LNMO-Ce) and Graphene wrapped ceria coated $LiNi_{0.5}Mn_{1.5}O_4$ (LNMO-Ce-GO) cells. The lithium intercalation may be traced back to the two-stage extraction process as the cycles advance; the charging plateau climbs upwards to greater potential owing to cathode polarization, while the discharging plateau lowers down to lower potential. The voltage plateaus at around 4 V and at 4.7V are distinctive to the Mn^{3+}/Mn^{4+} and Ni^{2+}/Ni^{4+} redox couples, respectively. From Figure 20(b), the coin-cell with the pristine LNMO sample provides a high initial discharge capacity of approximately 133 $mAhg^{-1}$ but dropping down to 112.6 $mAhg^{-1}$ after 100 cycles. According to reports, the first charge/discharge cycle is commonly disregarded since there is persistent capacity degradation due to the formation of a solid electrolyte interface (SEI) layer [210]. From Figure 20(c-d), the LNMO-Ce and LNMO-Ce-GO cells provide an initial discharge capacity of 137.3 $mAhg^{-1}$ and 139 $mAhg^{-1}$ respectively. And a reversible capacity of 125.8 $mAhg^{-1}$ and 132.4 $mAhg^{-1}$ respectively after cycling 100 times. This translates into a capacity retention of 95.3% for LNMO-Ce-GO sample, compared to 91.6% and 84.7% for LNMO-Ce and LNMO, respectively. Moreover, on comparison of Figure 20(b-d), it can be observed that the capacity fading observed on cycling diminishes for the LNMO-Ce-GO sample. A similar observation can be made about the columbic efficiency, the cell with the graphene wrapping (LNMO-Ce-GO) exhibits high performance compared to both LNMO-Ce and LNMO. Previous reports illustrate the efficacy of

electrochemically active ceria coated LNMO. According to Yi et al., 3 wt% CeO_2 coated LNMO provided a high-capacity retention of 98.3% at 1C rate, over a 100 cycles [60]. However, the spinel LNMO synthesized by Yi's group was ordered spinel LNMO, with a lower initial discharge capacity, that already is much more stable while cycling compared to the disordered spinel synthesized in the current study. Similarly, Tang et al. studied the effect of 4.7 wt% graphene wrapping over ordered LNMO nanorods, declaring that the LNMO-graphene wrapped rods provided a 94% capacity retention and a reversible capacity of 115 $mAhg^{-1}$ after 200 cycles at 0.1C rate [193]. As elucidated earlier, the disordered spinel has a high discharge capacity with low cyclability, while the ordered spinel exhibits good cyclability at the compromise of discharge capacity. The aim of this work was to improve the cyclability of disordered LNMO spinel by using a combination of ceria coating and graphene wrapping, resulting in a high-voltage cathode material that is energy dense and exhibits good cyclability. Hence, it can be concluded that the novel method of utilising ceramic coating and graphene wrapping combination can improve the electrochemical performance of the disordered spinel LNMO.

Statistical analysis was performed to evaluate the capacity fading for the modified LNMO cathodes. 20 coin-cells were cycled up to 100 cycles and the initial and final capacities were recorded. These are illustrated for the synthesized samples in Table 10 below. From Table 10 it can be noticed that the mean discharge capacity after the initial cycle increases from 133 $mAhg^{-1}$ for pristine LNMO to 137.3 $mAhg^{-1}$ for the ceria coated LNMO cells (LNMO-Ce) to 139 $mAhg^{-1}$ for the graphene wrapped ceria coated LNMO cathode (LNMO-Ce-GO). A similar trend can be observed for the cells after constant current charge and discharge for 100 cycles, resulting in an average capacity

retention of 95.8% for the LNMO-Ce-GO cells which is significantly better compared to the 84.5% capacity retention exhibited by the uncoated LNMO.

Moreover, the ceria-coated-graphene-wrapped LNMO (LNMO-Ce-GO) cells were hypothesized to provide a capacity retention of more than 94%. A one sample mean one-tailed t-test was performed (Figure 19) to determine if the coin cells containing LNMO-Ce-GO on average provide more than 94% capacity retention. From the t-test it can be concluded with 95% confidence that the cells containing LNMO-Ce-GO cathode consistently provide more than 94% capacity retention after 100 cycles.

Test to determine with 95% Confidence wether the cycled cells provide more than 94% capacity retention		
Hypothesis:	Mean	95.8
Null hypothesis, $H_0: \mu \leq 94$	Variance	6.33
Alternative hypothesis, $H_1: \mu > 94$	Observations	20
Rejection Region:	Hypothesized Mean Difference	94
$Reject\ H_0\ if\ t > 1.73$	df	19
$Reject\ H_0\ if\ p \leq 0.05$	t	3.22
Conclusion:	P(T<=t) one-tail	0.0022
Since, $t > 1.73\ and\ p < 0.05$	t Critical one-tail	1.73
$We\ Reject\ H_0, the\ capacity\ retention\ for\ LNMO - Ce - GO\ is\ more\ than\ 94\%$		

Figure 19: A t-test to determine performance evaluation of LNMO-Ce-GO sample.

Table 10. Statistical Analysis for Ceria Modified LNMO Cathode Samples.

	LNMO			**LNMO-Ce**			**LNMO-Ce-GO**		
Cell	**Cycle 1**	**Cycle 100**	**Capacity Retention (%)**	**Cycle 1**	**Cycle 100**	**Capacity Retention (%)**	**Cycle 1**	**Cycle 100**	**Capacity Retention (%)**
1	140.0	113.7	81.2	137.5	119.8	87.1	144.5	137.2	95.0
2	125.5	112.7	89.7	141.6	128.2	90.6	135.9	132.6	97.6
3	129.7	110.5	85.2	139.9	122.0	87.2	133.5	127.2	95.3
4	146.7	117.9	80.4	131.5	125.8	95.6	138.2	132.4	95.8
5	135.3	115.1	85.0	139.0	123.5	88.8	144.5	132.1	91.4
6	126.3	107.3	84.9	140.1	128.0	91.3	140.4	135.8	96.7
7	124.5	103.6	83.2	144.8	126.2	87.1	138.7	134.7	97.1
8	135.7	121.7	89.7	141.7	131.4	92.8	141.9	134.0	94.4

	LNMO			LNMO-Ce			LNMO-Ce-GO		
Cell	**Cycle 1**	**Cycle 100**	**Capacity Retention (%)**	**Cycle 1**	**Cycle 100**	**Capacity Retention (%)**	**Cycle 1**	**Cycle 100**	**Capacity Retention (%)**
9	130.7	111.5	85.3	126.6	122.1	96.5	136.0	130.7	96.1
10	133.2	100.8	75.7	133.5	121.2	90.8	142.3	136.9	96.2
11	144.2	118.1	81.8	128.2	125.0	97.5	141.1	131.3	93.1
12	138.3	123.3	89.2	143.7	122.3	85.1	135.5	128.5	94.8
13	127.8	115.2	90.1	129.3	126.9	98.2	130.1	129.7	99.7
14	127.7	120.3	94.2	135.6	120.2	88.7	139.9	130.6	93.4
15	134.2	116.4	86.7	138.4	122.2	88.3	136.4	132.6	97.3
16	137.7	107.8	78.3	141.1	134.6	95.4	137.9	132.3	96.0
17	131.8	109.6	83.1	141.3	121.4	86.0	132.8	134.5	101.2
18	135.6	113.7	83.8	135.6	122.4	90.3	136.7	134.0	98.0
19	133.3	104.3	78.2	143.2	125.1	87.4	143.8	130.4	90.7
20	135.0	112.4	83.3	128.9	125.7	97.5	137.1	132.2	96.4
Mean	133	112.6	84.5	137.3	125.8	91.1	139	132.4	95.8
Std. Dev.	6.5	5.5	4.5	4.7	4.2	4.2	3.6	2.3	2.5

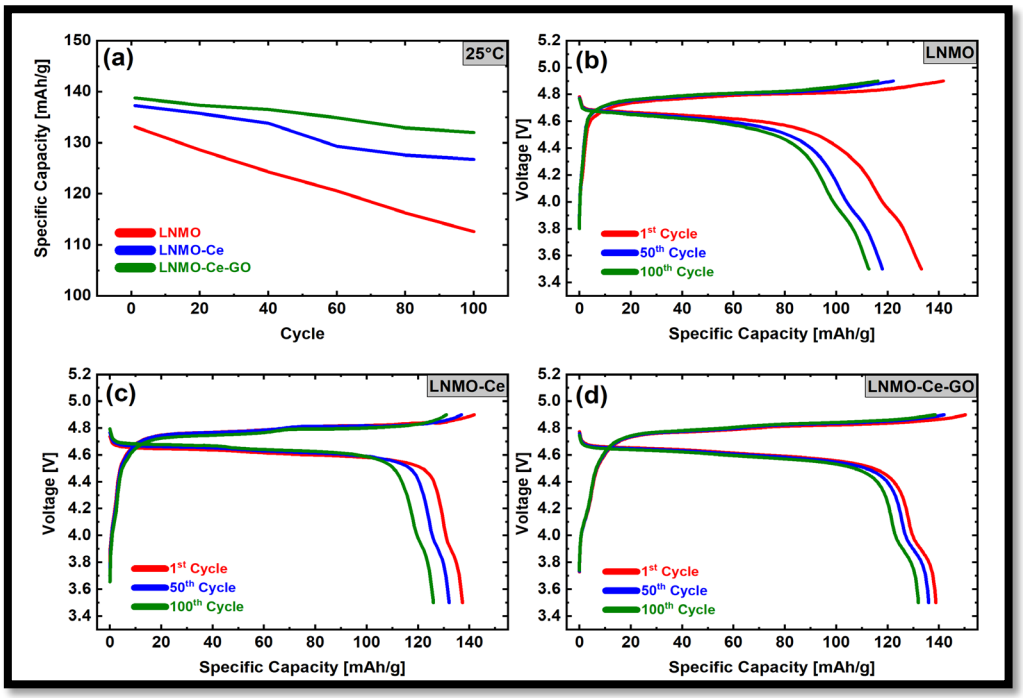

Figure 20: (a) Cycling performance of the synthesized samples at 25℃, galvanostatic charge/discharge profiles of, (b) Pristine $LiMn_{1.5}Ni_{0.5}O_4$ (LNMO), (c) 1wt% ceria

coated $LiMn_{1.5}Ni_{0.5}O_4$ (LNMO-Ce), and (d) 1wt% ceria coated $LiMn_{1.5}Ni_{0.5}O_4$ particles wrapped with 1wt% graphene (LNMO-Ce-GO).

The cyclic voltammograms shown in Figure 21 for the cells are used to determine the lithium intercalation kinetics for LNMO, LNMO-Ce, and LNMO-Ce-GO, by analysing the energy levels of the redox couples present within LNMO. The prominent peaks at 4.7 V are caused by the oxidation of Ni^{2+} to Ni^{4+}, whereas additional peaks at 4.0 V are caused by the lower current required to oxidize Mn^{3+} to Mn^{4+}. The maximal intensity of the manganese redox pair in the pure LNMO cell is larger than that of ceria coated LNMO (LNMO-Ce) cell and the graphene wrapped ceria coated LNMO (LNMO-Ce-GO) at 4.0 V. This signifies that the ceramic ceria coating somehow suppresses manganese oxidation, providing credulity to the cycling data as can be observed from the weak voltage plateau at 4.0 V in Figure 20(c). In contrast, the nickel redox couple is more prevalent in LNMO-Ce and LNMO-Ce-GO, compared to that of the pure LNMO cell. Peak-to-peak differentiation is greater in the LNMO-Ce and LNMO-Ce-GO cells, suggesting superior lithium intercalation reversibility and faster kinetics.

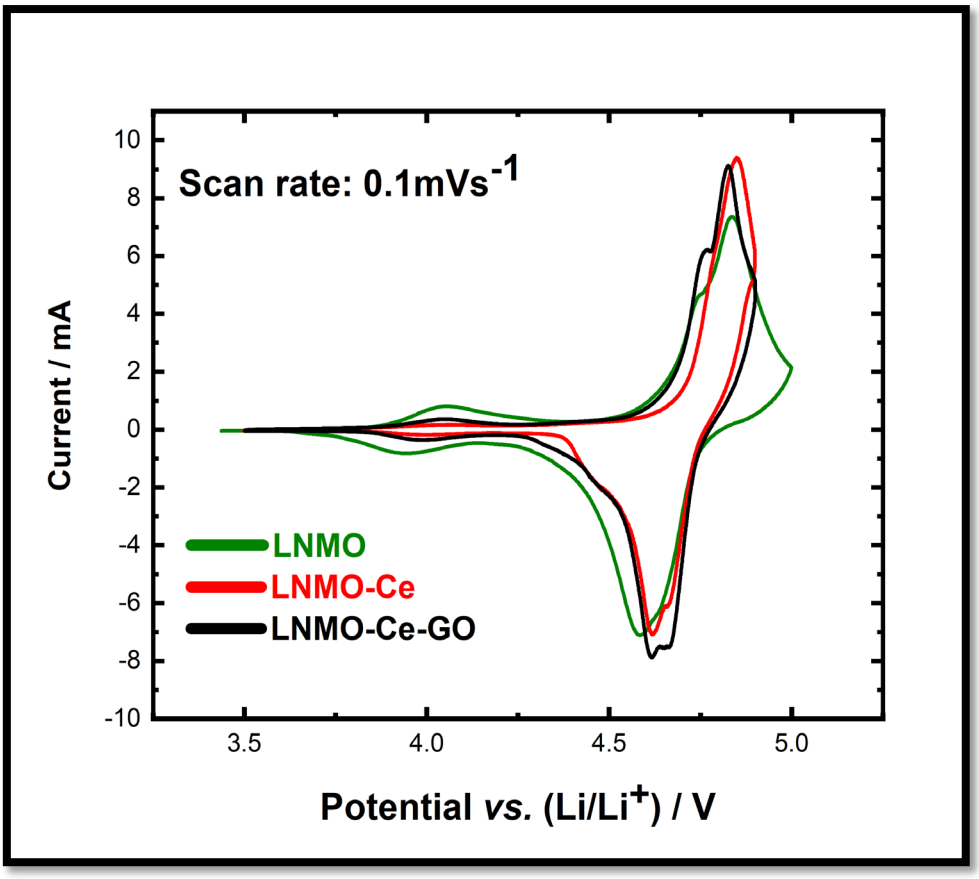

Figure 21: Cyclic voltammograms of the synthesized samples, at a scan rate of 0.1mV/s.

Between 3.5 V and 4.9 V, the fabricated cells were charged and discharged at 0.1C, 0.5C, and 1C to test their effectiveness at higher current rates. Diverse capacities are attained, which can be related to the different current rates used and the regulating electrochemical processes that contribute to the cells' degradation in efficiency. From Figure 22(a), the LNMO cell's discharge capacity is significantly reduced from 136 $mAhg^{-1}$ at 0.1C to 124 $mAhg^{-1}$ at 1C rate. At 0.1C, the discharge capacities of the LNMO-Ce and LNMO-Ce-GO cells are 132 $mAhg^{-1}$ and 138 $mAhg^{-1}$, respectively. More crucially, at 1C, LNMO-Ce and LNMO-Ce-GO cells demonstrate a considerable increase in discharge behaviour, with discharge capacities of 127 $mAhg^{-1}$ and 135 $mAhg^{-1}$, respectively. The outcomes from the rate capability analysis indicate that

increasing the rate of charge transfer at the cathode-electrolyte boundary or lithium-ion transport can limit the electrochemical performance of the fabricated cells. The results suggest that the resultant higher discharge capacity of LNMO-Ce and LNMO-Ce-GO might be a result of the ceramic coating in tandem with the graphene packaging. But mainly due to graphene's influence on enhancing electrical conductivity and shortening lithium diffusion paths [120]. In comparison to the uncoated LNMO cell, the LNMO-Ce and LNMO-Ce-GO cells exhibit outstanding discharge behaviour and no discernible fading on rapid discharging.

To get insight into the electrochemical performance of developed cathode materials, galvanostatic intermittent titration (GITT) tests were conducted. To allow adequate time for possible equilibrium, the cells were cycled in phases separated by rest intervals [203]. At C/10, measurements were taken to determine the quasi-equilibrium profile for the reaction kinetics, which are depicted in Figure 22 (b-d). Comparing the GITT curves of the three cells in the nickel redox window, reveals a smooth lithium insertion and extraction profile due to minor polarization. Lithium ions reside at 8a sites and travel along over to the vacant octahedral 16c sites within the LNMO spinel lattice. Increased applied voltage results in a decrease in lithium diffusion due to the high polarization of the LNMO sample, which may be attributed to $Ni^{2+/3+}$ and $Ni^{3+/4+}$ redox couples. However, this phenomenon is not observed for the LNMO-Ce and LNMO-Ce-GO cells, as they display smoother profiles. In comparison to the LNMO sample, the short relaxation spikes seen for LNMO-Ce and LNMO-Ce-GO indicate faster kinetics with low polarization. The LNMO-Ce-GO sample displays the smoothest profile, exhibiting superior electrochemical performance and complete lithium extraction. The relaxation spikes are smaller during charging, indicating that the oxidation phase is outperforming the reduction phase. The oxidation peak regions are significantly larger than the

reduction peak areas, which is consistent with the asymmetry of oxidation and reduction as illustrated by the cyclic voltammograms (Figure 21).

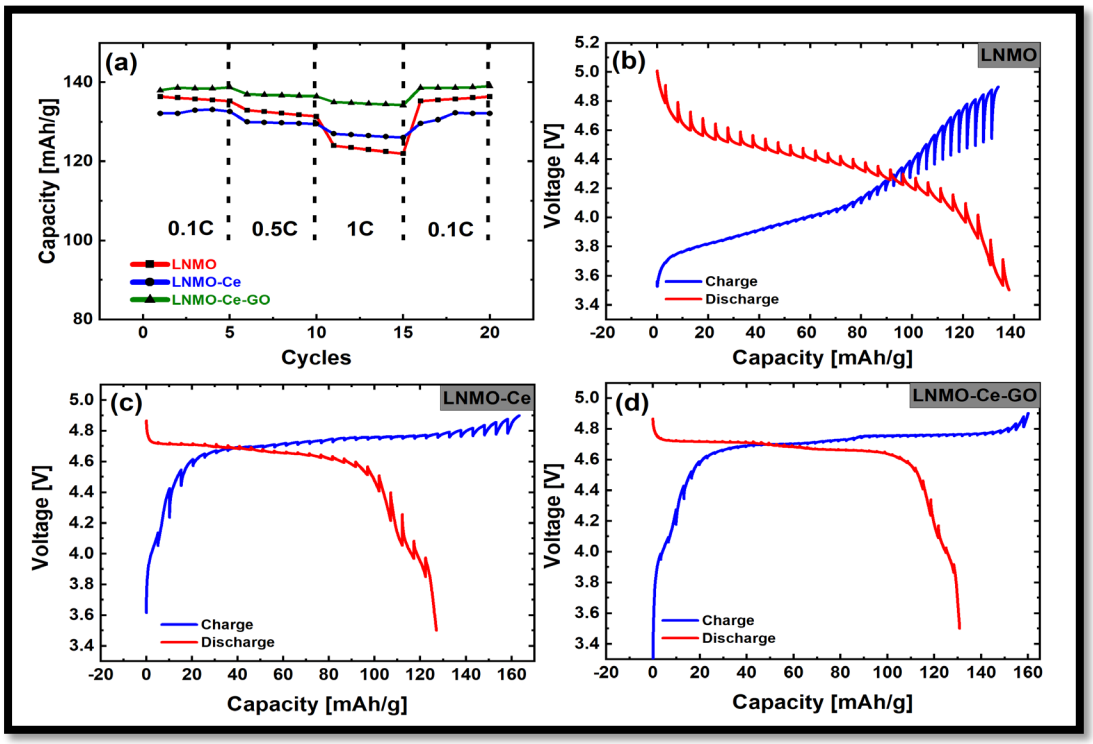

Figure 22: (a) Rate capability of the cells at ambient temperature, and GITT analysis at C/10 rate of (b) LNMO, (c) Ceria coated $LiMn_{1.5}Ni_{0.5}O_4$ (LNMO-Ce), and (d) Graphene wrapped-Ceria coated $LiMn_{1.5}Ni_{0.5}O_4$ (LNMO-Ce-GO) cells.

Lastly, the thermal stability of the lithiated and the delithiated samples were conducted utilizing DSC. Figure 23a illustrates the DSC thermograms for the bare $LiMn_{1.5}Ni_{0.5}O_4$ (LNMO), CeO_2 coated $LiMn_{1.5}Ni_{0.5}O_4$ (LNMO-Ce), and CeO_2 coated $LiMn_{1.5}Ni_{0.5}O_4$ wrapped in graphene (LNMO-Ce-GO) samples after charging the cells to 4.9V at 0.1C. The pristine LNMO sample exhibits an exothermic peak around 256°C, which is consistent with earlier literature reports [211]. The interaction between the electrolyte and the charged spinel cathode is mainly the cause for such a peak. The

oxygen emitted from the delithiated LNMO structure oxidizes the electrolyte solvent at this high operating voltage, resulting in heat being evolved [159]. The protective ceria ceramic coating protects the cathode surface from these exothermic side reactions with the electrolyte, and it can be observed from Figure 23a, that the LNMO-Ce and LNMO-Ce-GO cathode samples do not show any considerable exothermic activity around the same temperature range. Concluding that the microwave-assisted co-precipitation induced surface modification increases the thermal stability of the LNMO-Ce and LNMO-Ce-GO samples compared to the bare LNMO sample. Moreover, for comparison the lithiated or uncharged DSC curves for the samples are also illustrated in Figure 23b. Hence, this work elucidates the physical, structural, and electrochemical basis of performance enhancement of the high-voltage spinel LNMO cathode material surface modified with CeO_2 and wrapped with graphene. This work can also be utilized as a roadmap to improve the other next generation cathode materials for LIBs.

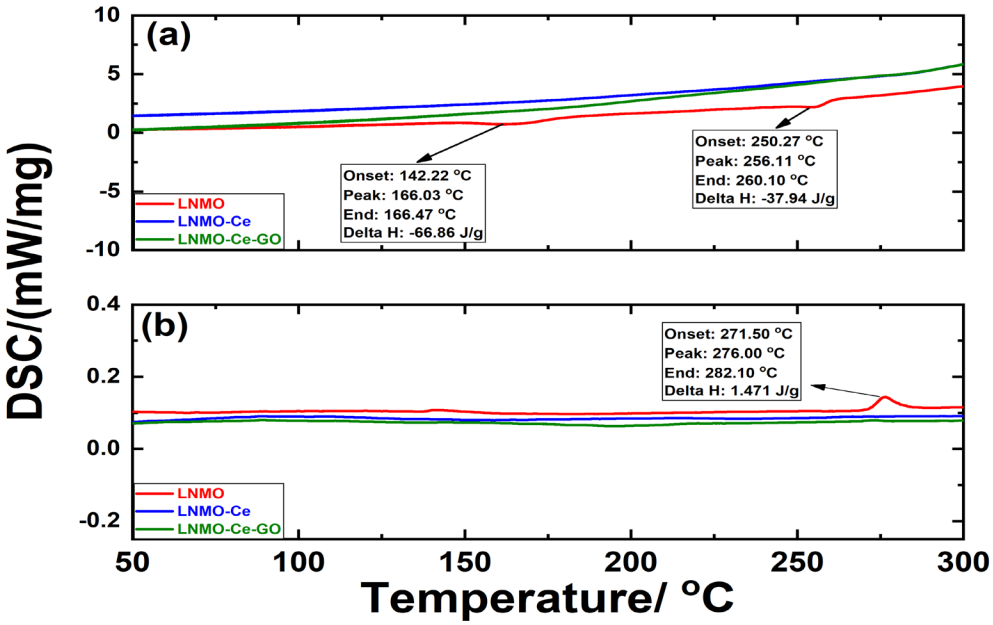

Figure 23: DSC thermograms until 300°C for (a) Charged samples equilibrated at 4.9V at 0.1C and (b) discharged samples: of LNMO, LNMO-Ce and LNMO-Ce-GO.

Influence of Alumina (Al_2O_3) Coated Graphene Wrapped LNMO

Spinel LNMO can be generated in two different cubic versions depending on the synthesis temperature which ultimately dictates the metal-ions (Ni, Mn) ordering at the structure's octahedral sites. As exhibited in Figure 24a, the ordered P-type ($P4_332$) LNMO can be synthesized at annealing temperatures of around 700°C resulting in an ordered structure with Ni ions located at 4b octahedral sites, and Mn ions occupying 12d sites, the Li ions are present at the 8a sites while the O^{2-} ions are located at the 8c and 24e Wyckoff positions. However, when the synthesis temperature is more than 800°C, as in this study, a disordered F-type ($Fd\overline{3}m$) cubic structure is formed with Ni and Mn randomly distributed at 16d octahedral sites[212]. X-ray powder diffractograms of the synthesized materials are exhibited in Figure 24b. From the diffractograms it can be clearly exhibited that the hallmark peak of the disordered LNMO structure may be found in all three spectra. The crisp and defined peaks show that the materials are exceptionally pure and crystalline, with (111) being the most intense peak position. All of the Bragg peaks can be attributed to the disordered spinel ($Fd\overline{3}m$) space group, in which manganese and nickel ions are distributed in the octahedral (16d) sites whereas lithium ions occupy the tetrahedral (8a) sites and O^{2-} are located at the 32e cubic sites (ICSD #98-007-0023). Minuscule amounts of secondary phases with Bragg peaks at $2\theta = 37.5°$ and 63.3° are also characteristic of the $Fd\overline{3}m$ space group and can be assigned to Nickel rich rock-salt impurities ($Li_xNi_{1-x}O$) [212]. Table 11 shows the crystallite sizes and lattice parameter values obtained through Rietveld refinement for the synthesized samples. LNMO's graphene wrapping, and alumina coating did not enter the spinel system, but instead remained attached to the particle surface. Because there are no discernible differences in the crystalline structure of the samples, microwave sintering had no effect on the parent LNMO spinel structure for the alumina

coated or graphene wrapped samples. Additional heat treatment for the coated samples, however, increased the crystallinity of the LNMO-Al and LNMO-Al-GO, as exhibited by crystallite size and the intensity of the peaks illustrated in Figure 24b. The ratio of the I_{311}/I_{400} peaks, on the other hand, is significantly different between LNMO and LNMO-Al samples, which may indicate the structural stability of the $[Mn_2]O_4$ spinel framework. According to previous research, spinel $LiMn_2O_4$ with I_{311}/I_{400} ratios between 0.96 and 1.1 typically exhibits superior electrochemical properties than those with ratios outside this range [213,214]. According to Table 11, the I_{311}/I_{400} ratio value of both LNMO-Al and LNMO-Al-GO can be comparable with that of spinel $LiMn_2O_4$ with the I_{311}/I_{400} ratios within the optimal range.

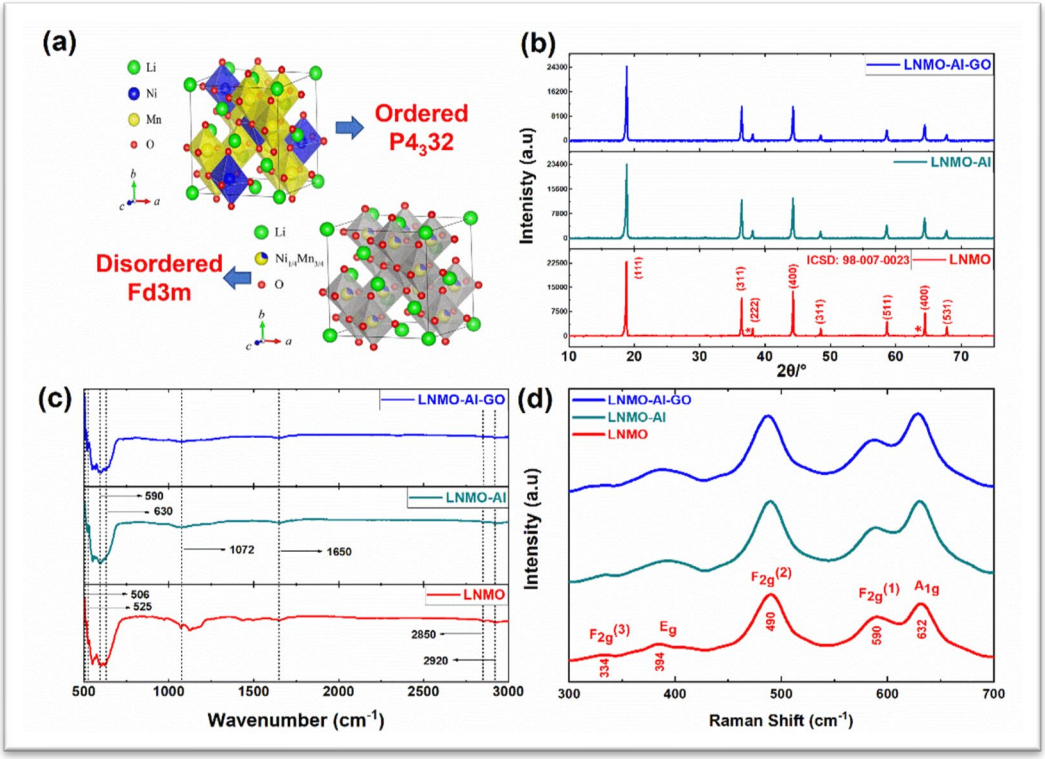

Figure 24: (a) Ordered and disordered cubic phases of LNMO (b) XRD diffractograms, (c) Fourier Transform Infrared Spectroscopy, (d) RAMAN spectroscopy, of the synthesized samples.

Table 11. Crystal Structure Parameters of the Samples Based on Rietveld Refinement.

Sample	Crystallite Size (Å)	Lattice Constant (Å)	d-spacing (nm)	Volume ($Å^3$)	I_{311}/I_{400}
LNMO-Al-GO	**677.8 ± 29.3**	**8.176**	**0.472**	**546.5**	**1.03**
LNMO-Al	**703.5 ± 31.9**	**8.179**	**0.474**	**547.1**	**1.01**
LNMO	**566.2 ± 18.1**	**8.163**	**0.471**	**544.0**	**0.94**

Since, Mn and Ni have similar scattering factors, the XRD technique is not feasible to distinguish both polymorphs of LNMO. The electrochemical performance of LNMO is strongly influenced by the cation ordering, which is determined by the annealing temperature. However, because there is neither absolutely ordered nor completely disordered structure in the synthesized LNMO materials, they cannot be simply classified as ordered or disordered. Depending on the synthesis conditions, the degree of cation ordering ranges from predominantly ordered to predominantly disordered. Evaluating the degree of cation ordering for the LNMO material is critical for understanding the electrochemical performance. For LNMO, the disordered structure undergoes a single-phase change during cycling, but the ordered crystal structure requires a two-step phase transition. The rate of the two-step transition in an ordered crystal structure is determined by the availability of lithium ions and the vacancy between the two phases. The lithium-ions have enough time to de-intercalate from the ordered structure at lower current rates, resulting in good cyclability; however, at higher current rates, this two-step phase transition cannot be completed in time, resulting in

poor rate capability of the ordered structure compared to the disordered structure. The major takeaway regarding the polymorphs of LNMO is that ordered LNMO provides good cyclability at low rates but provides lower capacity, consequently, the disordered LNMO provides high discharge capacity but low cyclability[215]. The objective of this study is to enhance the cyclability of disordered LNMO as this polymorph offers enhanced capacity. Thus, it is important to characterize the synthesized samples to ascertain the degree of ordering. Figure 24c illustrates the FTIR spectra for the synthesized samples, from the spectra distinctive Ni-O bands can be observed at 590 and 506 cm^{-1} [77]. While the characteristic band at 630 is assigned to the Mn-O stretching mode. The ratio of the intensity of the band at 630 and 590 is used to gauge if the synthesized sample is disordered ($Fd\bar{3}m$) or ordered ($P4_332$) , if the band intensity at the higher wavenumber is more compared to the peak at 590 cm^{-1}, the material is deemed to be disordered [216]. However, the FTIR spectra are significantly more difficult to distinguish between the two types of phases, and so Raman spectroscopy can be utilized in tandem with FTIR. Figure 24(d) illustrates the Raman spectra for the synthesized samples. The lack of sharp clearly defined peaks is symptomatic of the existence of disordered LNMO. Moreover, the absence of split peak at 590 and the absence of clear peaks at 221, 241, and 406 cm^{-1}, clearly illustrate that the synthesized samples are indeed LNMO belonging to the $Fd\bar{3}m$ space group[193,217]. The spectra also exhibit existence of main peaks at 490 and 632 cm^{-1}, exhibiting the Ni-O and Mn-O stretching modes on the Raman spectrum, as widely reported [208].

Figure 25 exhibits FE-SEM micrographs and elemental mapping for the $LiMn_{1.5}Ni_{0.5}O_4$ particles, alumina coated $LiMn_{1.5}Ni_{0.5}O_4$ particles, and alumina coated $LiMn_{1.5}Ni_{0.5}O_4$ particles wrapped with graphene. The SEM images for the pristine particles, Figure 25(a) and (b), exhibit that the primary nanoparticles are somewhat octahedral in shape

and are grouped to form secondary microspheres in a core-shell like structure. The subsequent Al_2O_3 coating (Figure 25c) increases the amount of truncation of the LNMO octahedra. For the graphene wrapped alumina coated sample, (Figure 25(d-e)), the highly regular truncated octahedral microstructure with large portions of stable (100) facets are showcased. The exposed faces are proposed to stabilize the spinel structure to effectively suppress the side reactions with the electrolyte at high operating voltage and are also orientated to support Li+ transport kinetics[218]. The truncated octahedra shape on the LNMO particles are a result of the microwave assisted synthesis technique, similar structures have been reported in literature due to microwave sintering[219]. The synthesized microspheres possess diameters ranging from 0.5-2 μm, with primary nanoparticles within 50-75 nm range. Figure 25 (f-t) showcase the EDX elemental mapping for the synthesized samples, confirming the presence of elements utilized in the synthesis route. Moreover, Figure 25(l) and Figure 25(q) confirm the presence of "Al" within the alumina coated LNMO samples, exhibiting uniform coverage of the LNMO particles with Alumina. Moreover, Figure 25(t) illustrates that the alumina coated LNMO particles are successfully wrapped in graphene. The uniform Al_2O_3 nano-coating is expected to avoid unnecessary interaction between the electrolyte and the electrode interface, thus may increase the cycling performance. In addition, the nanoscale coating would not obstruct the internal pathways so that the performance is not hindered. The LNMO-Al-GO microspheres consist of internal radial channels and provide controlled electrolyte wettability, improved electronic conductivity, and protection from ionic leaching. Figure 26 illustrates the EDX analysis of the synthesized samples, from Figure 26b and Figure 26c, it can be noted that the atomic percentage of Al is less than 1 in the alumina coated samples. However, the mapping illustrates uniform coverage of the LNMO particles.

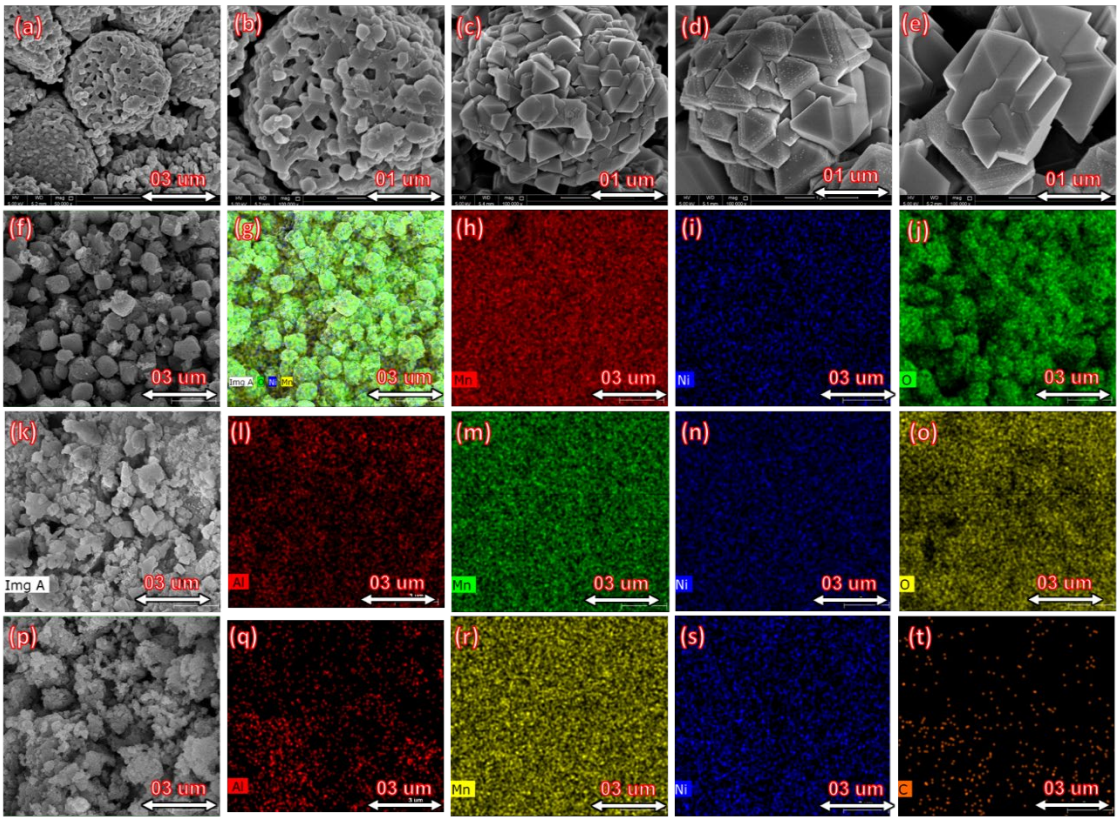

Figure 25: FE-SEM micrographs of; (a-b) $LiMn_{1.5}Ni_{0.5}O_4$ particles (c) Alumina coated $LiMn_{1.5}Ni_{0.5}O_4$ particles (d-e) Alumina coated $LiMn_{1.5}Ni_{0.5}O_4$ particles wrapped with graphene. EDX elemental mapping of (f-j) Pristine LNMO particles, (k-o) Alumina coated $LiMn_{1.5}Ni_{0.5}O_4$ particles and (p-t) Alumina coated $LiMn_{1.5}Ni_{0.5}O_4$ particles wrapped with graphene.

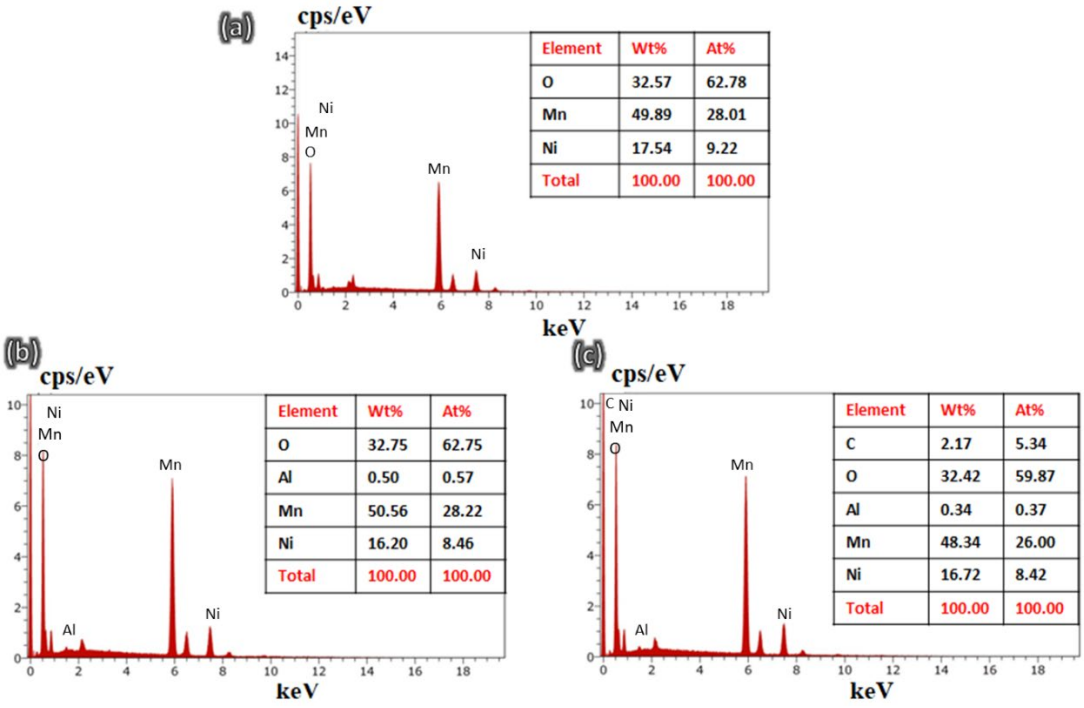

Figure 26: EDX analysis of (a) $LiMn_{1.5}Ni_{0.5}O_4$ particles (b) Al_2O_3 coated $LiMn_{1.5}Ni_{0.5}O_4$ particles (c) Al_2O_3 coated $LiMn_{1.5}Ni_{0.5}O_4$ particles wrapped with graphene.

High-resolution transmission electron microscopy (HR-TEM) was used to confirm the existence of alumina coating and graphene wrapping over $LiMn_{1.5}Ni_{0.5}O_4$. Figure 27 shows the HR-TEM results for LNMO (Figure 27 a-e), LNMO-Al (Figure 27 f-j), and LNMO-Al-GO (Figure 27 k-o). A mortar was used to grind the sample particles before mounting them on a carbon-coated copper TEM grid. The smooth particles seen in Figure 27(a) and (b) are pure LNMO. Figure 27(f)–6(g), on the other hand, have a grainy appearance, owing to the presence of alumina film. The ceramic coating protects the LNMO cathode from direct electrolyte exposure, avoiding undesired electrolyte-active material reactions. Furthermore, due to the scavenging nature of alumina, the LNMO cathode is shielded against HF assault, and the cathode's integrity is conserved due to Mn dissolution suppression. In general, as the thickness of the coating grows, so does the contact resistance and load transfer resistance, especially when the coating

thickness surpasses 10 nm [209]. However, the alumina coating thickness in our study is 2-3 nm (Figure 27h & m), ensuring that polarization and power depletion are effectively avoided. Furthermore, the inclusion of graphene increases the electrical conductivity of the cathode, boosting its electrochemical performance. The selected area diffraction (SAED) pattern of the samples is exhibited in Figure 27(e), Figure 27(j), and Figure 27(o). The SAED patterns shows that higher crystallinity leads to a decreased energy barrier for lithium-ion insertion, resulting in fast ionic diffusion, the SAED patterns confirm the results from XRD that the LNMO-Al-GO sample exhibits high crystallinity. Furthermore, as shown in Figure 27(d), (i) and (n), the distance between lattice fringes is provided and they are in good accordance with the d-spacing calculated from the Rietveld refinement (see Table 11). According to the energy dispersive X-ray analysis and chosen area diffraction, microwave-assisted chemical co-precipitation is a viable approach for producing phase pure disordered spinel cathodes.

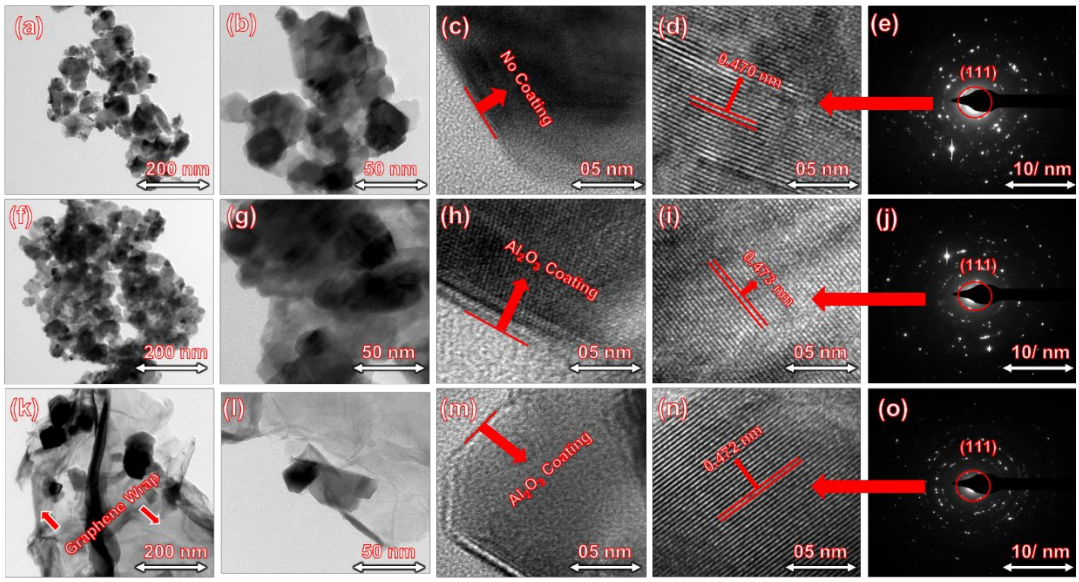

Figure 27: HR-TEM micrographs: (a-c) Pristine LNMO particles (f-h) Al_2O_3 (3~5nm) coated LNMO particles (k-m) Graphene wrapped Al_2O_3 coated LNMO particles. Lattice fringes of (d) LNMO, (i) LNMO-Al and (n) LNMO-Al-GO. Scanning area electron diffraction pictograms for (e) LNMO, (j) LNMO-Al and (o) LNMO-Al-GO.

Following coin-cell production, the charge and discharge behaviour of the three samples was studied in the voltage range of 3.5 V to 4.9 V, which corresponds to the redox couplings for Mn and Ni in LNMO. The cells were tested at 0.1C constant current rate. The cyclability and charge/discharge characteristics of $LiNi_{0.5}Mn_{1.5}O_4$ (LNMO), Al_2O_3 coated $LiNi_{0.5}Mn_{1.5}O_4$ (LNMO-Al), and Graphene wrapped Al_2O_3 coated $LiNi_{0.5}Mn_{1.5}O_4$ (LNMO-Al-GO) cells are shown in Figure 29. As the cycles progress, the lithium intercalation may be traced back to the two-stage extraction process; the charging plateau rises to greater potential due to cathode polarization, while the discharging plateau falls to lower potential. The voltage plateaus at roughly 4 V and 4.7V are unique to the Mn^{3+}/Mn^{4+} and Ni^{2+}/Ni^{4+} redox couples. According to Figure 29(b), the coin-cell with the pristine LNMO sample has a high initial discharge capacity of around 133 $mAhg^{-1}$ but drops to 112.6 $mAhg^{-1}$ after 100 cycles. According to studies, the initial charge/discharge cycle is frequently ignored because of continuous capacity deterioration caused by the creation of a solid electrolyte interface (SEI) layer [210]. According to Figure 29(c) and (d), the initial discharge capacity of the LNMO-Al and LNMO-Al-GO cells is 136.8 $mAhg^{-1}$ and 137.8 $mAhg^{-1}$, respectively. After 100 cycles, the reversible capacity is 120.2 $mAhg^{-1}$ and 134.7 $mAhg^{-1}$, respectively. This equates to 97.7% capacity retention for the LNMO-Al-GO sample, compared to 87.8% and 84.7% for the LNMO-Al and LNMO samples, respectively. Furthermore, a comparison of Figure 29(b-d) shows that the capacity fading seen during cycling lowers for the LNMO-Al-GO sample. A similar conclusion can be found for columbic efficiency; the cell with graphene wrapping (LNMO-Al-GO) outperforms both LNMO-Al and LNMO. The performance of the LNMO-Al-GO cathode material is superior compared to other Al_2O_3 coated LNMO cells are per Table 1. The goal of this research was to increase the cyclability of disordered LNMO spinel by combining ceramic coatings

with graphene wrapping, resulting in a high-voltage cathode material that is both energy dense and cyclable. As a result, the unique strategy of combining ceramic coating with graphene wrapping can improve the electrochemical performance of the disordered spinel LNMO.

Statistical analysis was performed to evaluate the capacity fading for the modified LNMO cathodes. 20 coin-cells were cycled up to 100 cycles and the initial and final capacities were recorded. These are illustrated for the synthesized samples in Table 12 below. From Table 12 it can be noticed that the mean discharge capacity after the initial cycle increases from 133 $mAhg^{-1}$ for pristine LNMO to 136.8 $mAhg^{-1}$ for the alumina coated LNMO cells to 137.8 $mAhg^{-1}$ for the graphene wrapped alumina coated LNMO cathode. A similar trend can be observed for the cells after constant current charge and discharge for 100 cycles, resulting in an average capacity retention of 94% for the LNMO-Al-GO cells which is significantly better compared to the 84% capacity retention exhibited by the uncoated LNMO.

Moreover, the alumina-modified-graphene-wrapped LNMO cells were hypothesized to provide a capacity retention of more than 94%. A one sample mean one-tailed t-test was performed (Figure 28) to determine if the coin cells containing LNMO-Al-GO on average provide more than 94% capacity retention. From the t-test it can be concluded with 95% confidence that the cells containing LNMO-Al-GO cathode fail to provide 94% capacity retention after 100 cycles consistently. Note that the capacity retention of the cerium coated samples were better compared to the alumina coated ones. This might be due to the electrochemically active nature of the ceria material, which might lend some extra capacity to the cell, or it might be due to the fact that the ceria coating better protected the LNMO structure during cycling compared to alumina.

Test to determine with 95% Confidence wether the cycled cells provide more than 94% capacity retention		
Hypothesis:	Mean	94.0
$Null\ hypothesis, \quad H_0: \mu \leq 94$	Variance	15.1
$Alternative\ hypothesis, H_1: \mu > 94$	Observations	20
Rejection Region:	Hypothesized Mean Difference	94
$Reject\ H_0\ if\ t > 1.73$	df	19
$Reject\ H_0\ if\ p \leq 0.05$	t	-0.025
Conclusion:	P(T<=t) one-tail	0.490
$Since, \quad t < 1.73\ and\ p > 0.05$	t Critical one-tail	1.73
$We\ Fail\ to\ Reject\ H_0, the\ capacity\ retention\ for\ LNMO - Al - GO\ is\ less\ than\ 94\%$		

Figure 28: A t-test to determine performance evaluation of LNMO-Al-GO sample.

Table 12. Statistical Analysis for Alumina Modified LNMO Cathode Samples.

	LNMO			LNMO-Al			LNMO-Al-GO		
Cell	**Cycle 1**	**Cycle 100**	**Capacity Retention (%)**	**Cycle 1**	**Cycle 100**	**Capacity Retention (%)**	**Cycle 1**	**Cycle 100**	**Capacity Retention (%)**
1	135.5	110.9	81.8	132.1	119.7	90.6	139.6	130.3	93.3
2	125.3	110.2	87.9	137.8	126.1	91.5	146.8	129.0	87.9
3	143.2	107.6	75.1	135.6	127.2	93.8	146.9	130.6	88.9
4	133.2	118.6	89.0	134.9	123.7	91.7	133.2	132.2	99.3
5	129.5	100.6	77.7	141.3	122.7	86.8	138.6	130.3	94.1
6	137.9	117.0	84.9	130.7	116.4	89.0	150.3	133.5	88.8
7	133.6	110.2	82.5	138.7	119.1	85.9	139.8	134.1	95.9
8	129.7	115.7	89.2	140.1	122.4	87.4	141.4	132.7	93.9
9	136.6	104.8	76.7	129.5	125.1	96.6	135.0	128.7	95.3
10	130.5	111.3	85.3	131.1	122.8	93.7	141.7	138.3	97.6
11	133.6	105.9	79.3	129.9	129.7	99.9	149.8	132.7	88.6
12	124.7	120.4	96.6	137.6	109.2	79.4	143.2	132.6	92.6
13	131.7	108.8	82.6	131.4	121.4	92.4	145.8	129.8	89.0
14	129.3	110.0	85.1	135.5	125.2	92.4	136.6	132.2	96.8
15	132.8	109.8	82.7	134.7	125.6	93.2	149.3	134.3	89.9
16	130.7	118.4	90.6	138.8	113.6	81.9	142.9	136.4	95.5
17	125.3	108.5	86.5	144.8	121.0	83.6	131.1	130.3	99.3
18	130.5	107.0	82.0	145.1	119.5	82.3	134.2	131.6	98.1
19	125.4	113.8	90.7	131.8	123.2	93.5	133.1	128.8	96.7
20	128.3	107.9	84.1	138.0	111.3	80.7	132.3	129.6	98.0
Mean	133	112.6	84.5	136.8	120.2	89.3	137.8	132.4	94.0
Std. Dev.	6.5	5.5	5.3	5.3	4.9	5.6	5.7	3.8	3.9

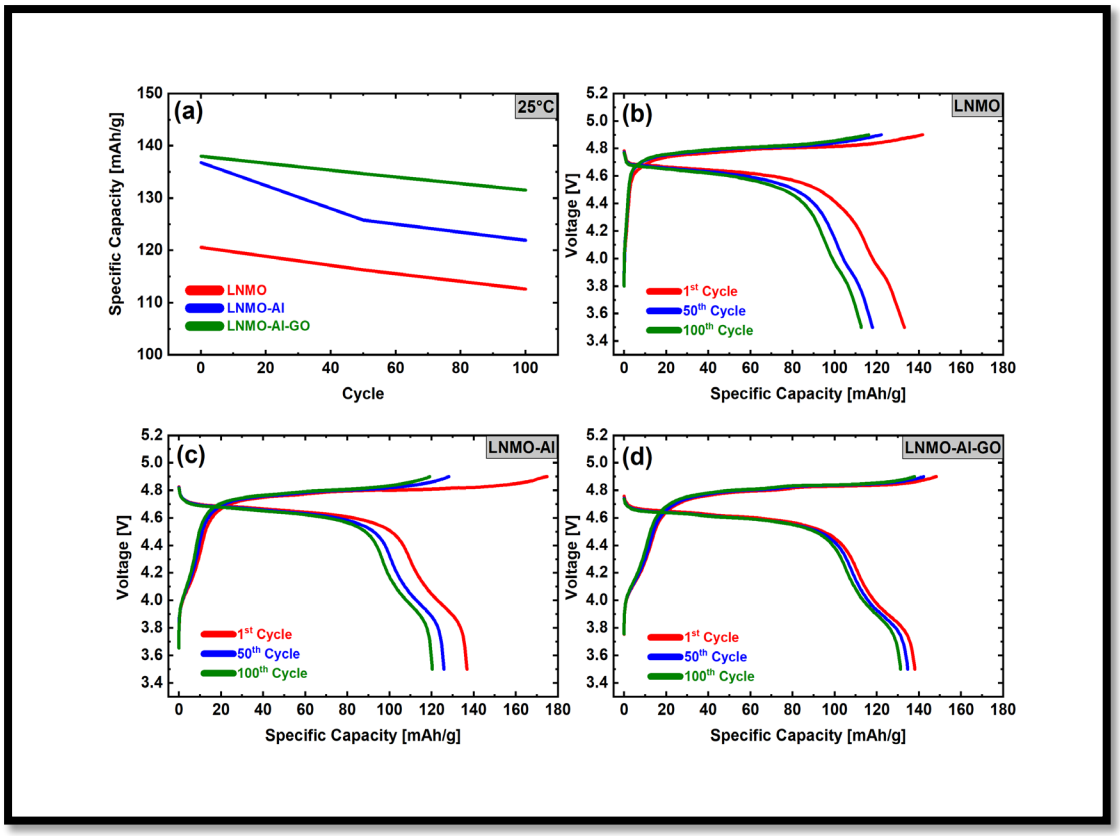

Figure 29: (a) Cycling performance of the synthesized samples at 0.1C and 25°C, Galvanostatic charge/discharge profiles of, (b) Pristine $LiMn_{1.5}Ni_{0.5}O_4$ (LNMO), (c) Al_2O_3 coated $LiMn_{1.5}Ni_{0.5}O_4$ (LNMO-Al), and (d) Al_2O_3 coated $LiMn_{1.5}Ni_{0.5}O_4$ particles wrapped with graphene (LNMO-Al-GO).

By analysing the energy levels of the redox couples present inside LNMO, the cyclic voltammograms displayed in Figure 30 for the cells are utilized to calculate the lithium intercalation kinetics for LNMO, LNMO-Al, and LNMO-Al-GO. The oxidation of Ni^{2+} to Ni^{4+} causes the significant peaks at 4.7 V, but the lesser current required to oxidize Mn^{3+} to Mn^{4+} causes further peaks around 4.0 V. At 4.0 V, the peak intensity of the manganese redox pair is greater in the pure LNMO cell than in the alumina coated LNMO (LNMO-Al) cell and the graphene wrapped alumina coated LNMO (LNMO-Al-GO). This indicates that the ceramic coating reduces manganese oxidation in some way, lending credibility to the cycle data, as seen by the weak voltage

plateau at 4.0 V in Figure 29 (c-d). In contrast to the pure LNMO cell, the nickel redox pair is more prominent in LNMO-Al and LNMO-Al-GO. Peak-to-peak differentiation in LNMO-Al and LNMO-Al-GO cells is larger, indicating improved lithium intercalation reversibility and quicker kinetics.

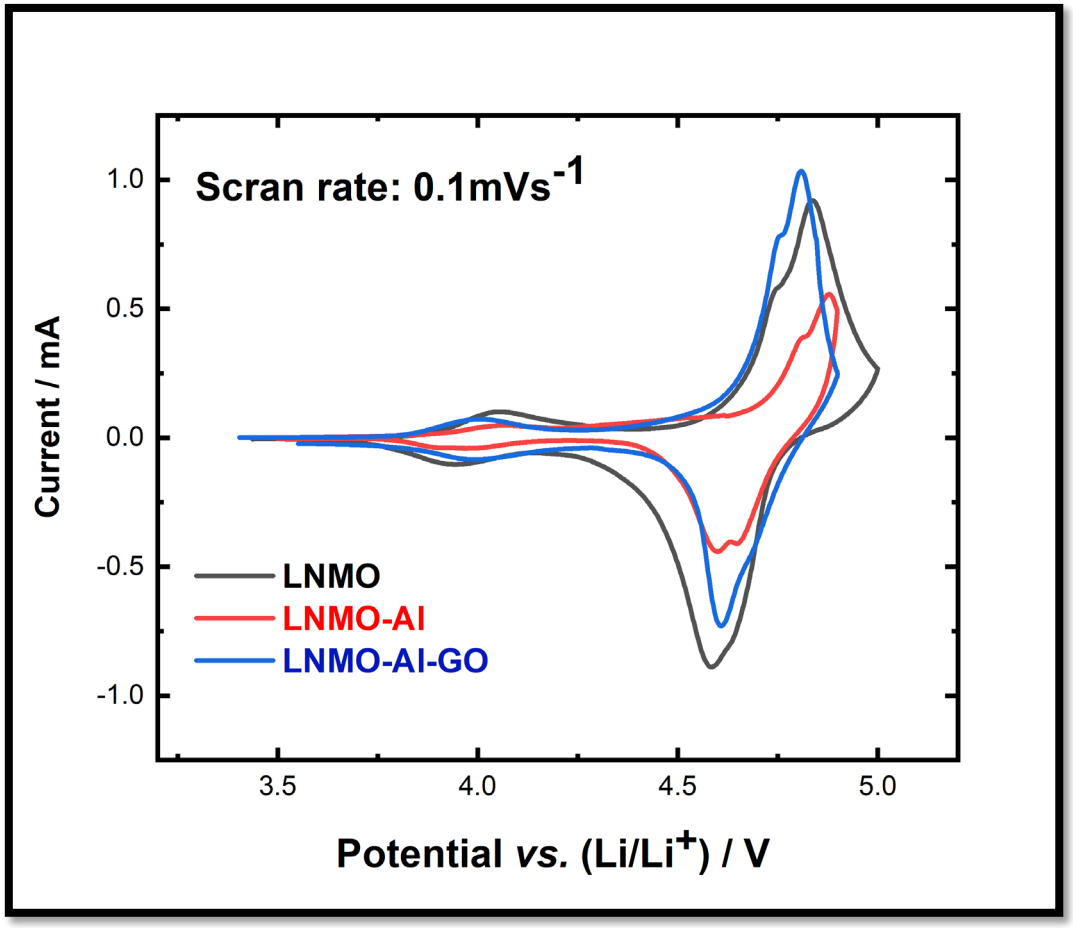

Figure 30: Cyclic Voltammograms of the synthesized samples, at a scan rate of 0.1mV/s.

The constructed cells were charged and discharged at 0.1C, 0.5C, and 1C between 3.5 V and 4.9 V to evaluate their performance at increasing current rates. Diverse capacities are reached, which can be attributed to the various current rates employed and the electrochemical processes that contribute to the cells' degrading performance. The discharge capacity of the LNMO cell decreases dramatically from 136 $mAhg^{-1}$ at 0.1C

to 124 $mAhg^{-1}$ at 1C rate, as shown in Figure 31(a). At 0.1C, the LNMO-Al and LNMO-Al-GO cell discharge capacities are approximately around 134 $mAhg^{-1}$. Moreover, at 1C, LNMO-Al and LNMO-Al-GO cells exhibit a significant decrease in discharge behaviour, with respective discharge capacities of 60.6 and 93.8 $mAhg^{-1}$. The results of the rate capability study suggest that increasing the rate of charge transfer at the cathode-electrolyte interface or lithium-ion transport can restrict the electrochemical performance of the manufactured cells. The results indicate that the ceramic coating and graphene packing does not improve the rate capability of LNMO. Compared to the uncoated LNMO and the cerium coated cells, the LNMO-Al and LNMO-Al-GO cells have inferior discharge characteristics with increased fading during fast discharging.

Galvanostatic intermittent titration (GITT) studies were done to get insight into the electrochemical performance of developed cathode materials. In order to provide sufficient time for possible equilibrium, the cells were cycled through phases separated by rest intervals [203]. Figure 31 (b-d) depicts the quasi-equilibrium curve for the reaction kinetics at C/10. Comparing the GITT curves of the three cells in the nickel redox window indicates a smooth profile of lithium insertion and extraction with polarization spikes. In the LNMO spinel lattice, lithium ions dwell at 8a sites and migrate to the unoccupied octahedral 16c sites. The high polarization of the LNMO sample, which may be attributed to $Ni^{2+/3+}$ and $Ni^{3+/4+}$ redox couples, decreases lithium transport in response to an increase in applied voltage. This behavior is not found in the LNMO-Al and LNMO-Al-GO cells because their profiles are smoother. The small relaxation spikes seen for LNMO-Al and LNMO-Al-GO relative to the LNMO sample imply quicker kinetics with less polarization. The ceramic coated samples possess smooth profiles and demonstrates improved electrochemical performance in addition to full lithium extraction. This low polarization signifies low hindrance of lithium diffusion

from the lattice, during cycling. The lower polarization due to the ceramic coating is possibly the reason for the enhanced cyclability of the alumina coated samples as exhibited in Figure 29. The oxidation peak regions are substantially bigger than the reduction peak regions, corresponding with the asymmetry of oxidation and reduction revealed by the cyclic voltagrams (Figure 30).

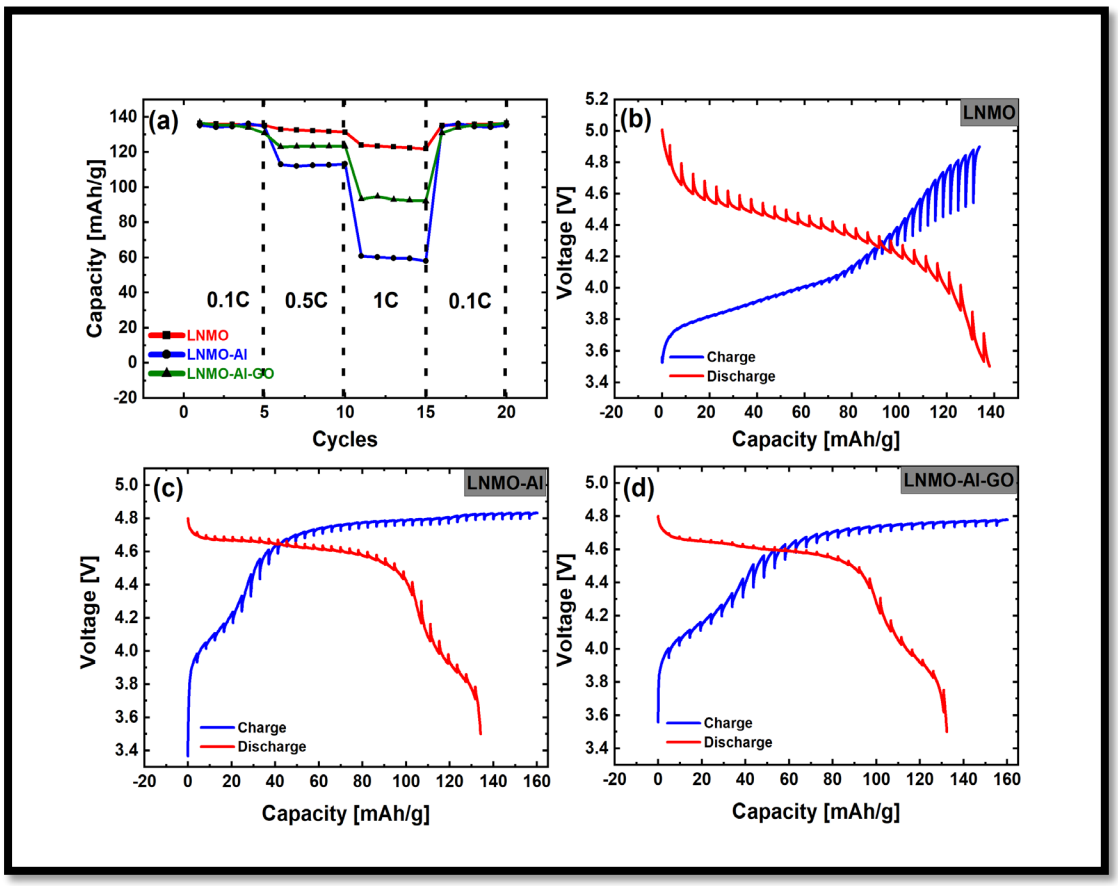

Figure 31: (a) Rate capability of the cells at ambient temperature, and GITT analysis at C/10 rate of (b) LNMO, (c) Alumina coated $LiMn_{1.5}Ni_{0.5}O_4$ (LNMO-Al), and (d) Graphene wrapped-Alumina coated $LiMn_{1.5}Ni_{0.5}O_4$ (LNMO-Al-GO) cells.

DSC was used to determine the thermal stability of the delithiated samples. Figure 32 depicts the DSC thermograms for samples of bare $LiMn_{1.5}Ni_{0.5}O_4$ (LNMO), Al_2O_3-coated $LiMn_{1.5}Ni_{0.5}O_4$ (LNMO-Al), and Al_2O_3-coated $LiMn_{1.5}Ni_{0.5}O_4$ wrapped in

graphene (LNMO-Al-GO) after charging the cells to 4.9V at 0.1C. The pure LNMO sample has an exothermic peak about 256°C, which is consistent with other results [211] in the scientific literature. This peak is mostly due to the interaction between the electrolyte and the charged spinel cathode. At this high working voltage, the oxygen produced by the delithiated LNMO structure oxidizes the electrolyte solvent, resulting in the production of heat [167]. Ceramic coatings are supposed to shields the cathode surface from these exothermic side reactions with the electrolyte, and Figure 32 demonstrates that the LNMO-Al and LNMO-Al-GO cathode samples exhibit significant exothermic activity within the same temperature range. The thermal stability of the alumina coated samples is significantly lower compared to the ceria coated samples. This might be partly due to the consumption of the alumina coating as it acts

as an HF scavenger, or there might be other mechanisms that are not fully understood yet.

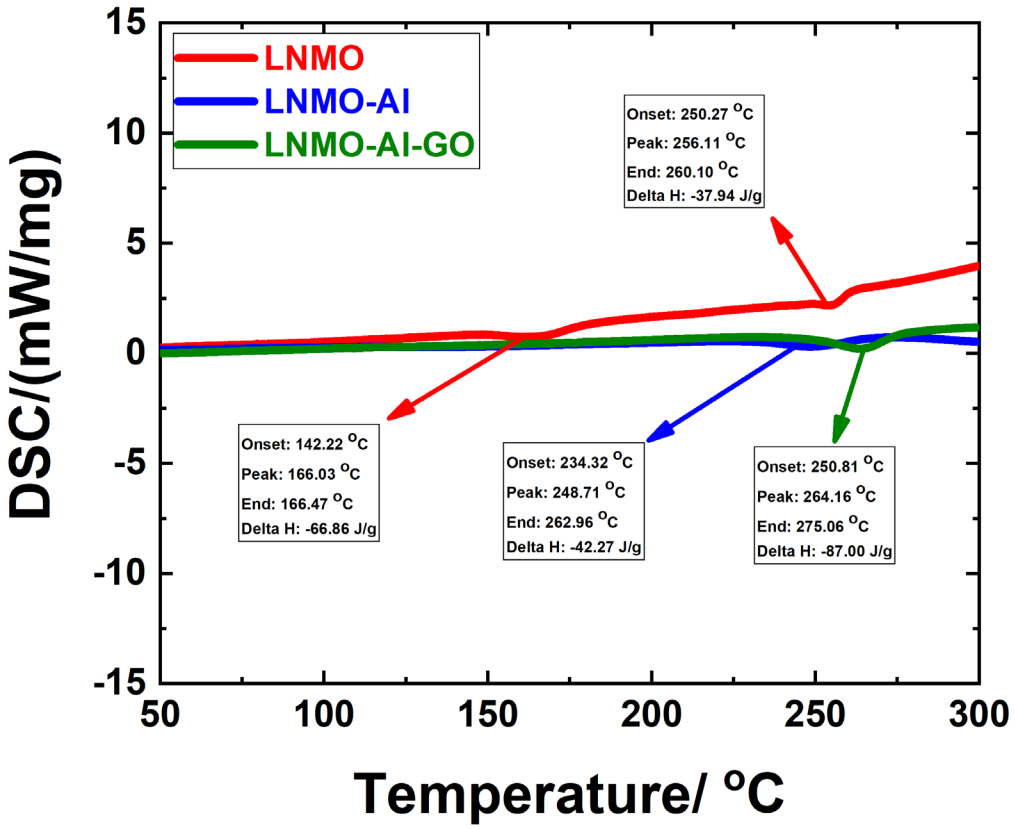

Figure 32: DSC thermogram until 300°C for charged cells (delithiated) equilibrated at 4.9V at 0.1C.

Chapter 5: Conclusion

Lithium-ion batteries are being used extensively in several handheld electronic devices after almost three decades of growth and are still at the forefront of the secondary battery market due to their high demand. To meet the demand for energy storage in recent years, intense research and development efforts have been made in terms of improving capacity, energy density, power density, economics, safety, and environmental impact of LIBs. The shift from utilizing LIBs in computing devices, consumer goods, and communication devices towards automotive vehicles has opened new potential research pathways. A key parameter for research is the improvement in the electrochemical performance of current LIBs in tandem with safety, so they can be securely utilized in automobiles. Another research direction is the expansion of the energy density of the battery to upwards of 200 Wh/kg since anything lower than this would not be competitive in the current market. Lastly, the lifespan of the battery is a critical parameter that is limiting the commercialization of certain battery technologies. The lifespan for a handheld device, typically containing a LIB, has a cycle capacity of 500 cycles that lasts for a couple of years. To incorporate such batteries within a vehicle, an operating standard of 1,000 to 10,000 cycles must be achieved in order to increase the duration of a vehicle battery to nearly ten years. Such an advancement would make battery-powered vehicles feasible and practical in comparison to a traditional fuel-powered car.

The performance and cost of LIBs are dependent primarily on the type of cathode chemistry utilized within the battery. Over the years, various cathode materials have been commercially utilized and tested yet remain constrained by electrical conductivity limitations, sluggish Li^+ diffusion rates, adverse electrolytic interactions,

poor thermal stability, large volume expansion, and mechanical fragility (See Figure 9). Surface coatings have shown mitigation of these side reactions due to electrolyte breakdown, preserved the structural stability of the cathode material, and enhanced the electrochemical performance. Numerous coating materials, including metal oxides, fluorides, phosphates, carbon materials, polymers, and composites, have been tested to provide better electronic and ionic conductivities, structural stability, and durability at elevated temperatures. Considering these factors, the following recommendations for cathode surface coating approaches can be stated:

1. The choice of coating materials is largely dependent on the cathode type utilized in the battery. Additionally, when using surface coatings, it is critical to examine other variables such as coating material and cathode material synergy, cathode chemistry, coating composition, and coating morphology.
2. The coating synthesis processes should create thin, homogeneous coatings while being economically viable, environmentally friendly, and scalable.
3. Inert materials with low ionic conductivities, such as Al_2O_3, are often utilized as cathode coating materials. To improve LIB performance, the thickness of these coatings should be maintained below 10 nm. Thicker inert coatings onto lithium tend to produce secondary phases, such as ZrO_2 coating transforming into Li_2ZrO_3, resulting in capacity fading and poor cyclability.

The potential advancement in electrochemical performance of LIBs from surface modification techniques will continue to concentrate on seeking coating materials with low cost, controllable processing, and outstanding performance. Progress can also be expedited via a thorough understanding of relevant coating

mechanisms that would result in the development of advanced coating techniques such as *in-situ* coatings. Another important technological challenge that needs to be addressed is cheaply obtaining a nanoscale uniform coating over the cathode surface by utilizing multifunctional coatings through advanced synthesis methods. Also, more combinations of composite coating materials are yet to be developed and tested for specific cathode materials, such as MXene composite coatings, thus providing new research avenues. Future research and development of LIBs will continually require an in-depth understanding of the underlying mechanisms of coatings in tandem with progressive research on relatively new battery technologies like sodium-ion, lithium-sulfur, or lithium-air batteries.

$LiNi_{0.5}Mn_{1.5}O_4$ (Lithium Nickel Manganese Oxide referred to as LNMO) is a promising cathode material for LIBs due to its high voltage and energy density, lower cost, and environmental friendliness. However, LNMO cathodes are presently suffering from poor cyclability and capacity degradation at elevated temperatures. Numerous techniques such as chemical vapor deposition (CVD), atomic layer deposition (ALD), Sol-gel, Radiofrequency magnetron sputtering, etc., have been reviewed in the present work to develop coated LNMO. At the same time, the impact of a wide range of various coating materials (oxides, phosphates, fluorides, conductive polymers, etc.) on the electrochemical performance of LNMO has been presented. Finally, some of the possible future directions and challenges are also outlined to provide a guideline and baseline information to the people who are desirous of exploring the ever demanding and fascinating area of LIBs.

Furthermore, spherical microspheres of phase pure $LiMn_{1.5}Ni_{0.5}O_4$ (LNMO), CeO_2 and Al_2O_3 coated $LiMn_{1.5}Ni_{0.5}O_4$ (LNMO-Ce; LNMO-Al), and CeO_2 or Al_2O_3 coated $LiMn_{1.5}Ni_{0.5}O_4$ wrapped in graphene (LNMO-Ce-GO; LNMO-Al-GO) were produced

using a microwave-assisted chemical co-precipitation process. The inclusion of the ceramic coatings and graphene nanosheet wrapping has significantly improved the cyclability and capacity retention of the LNMO spinel; countering major limitations associated with $LiMn_{1.5}Ni_{0.5}O_4$. The enhanced performance can be accredited to the suppression of the side-reactions occurring between the cathode and the electrolyte due to the ceramic coating and graphene addition. Moreover, the novel approach protects the cathode from HF attack and subsequent manganese dissolution due to the Jahn-Teller distortion, obstructs the development of undesirable SEI layer and increases the lithium-ion transport kinetics.

More importantly, the ceria coated samples provided enhanced electrochemical performance compared to the alumina coated LNMO cells. This might be due to the electrochemically active nature of the ceria compared to the inert nature of alumina. The ceramic coated and graphene wrapped cathodes had a higher cyclability as targeted by this approach, however, the ceria coated LNMO also had excellent rate capability, making it useful to be utilized for high-power applications.

References

(1) Nishi, Y. 2 - Past, Present and Future of Lithium-Ion Batteries: Can New Technologies Open up New Horizons? In *Lithium-Ion Batteries*; Pistoia, G., Ed.; Elsevier: Amsterdam, 2014; pp 21–39. https://doi.org/https://doi.org/10.1016/B978-0-444-59513-3.00002-9.

(2) Tarascon, J.-M.; Armand, M. Issues and Challenges Facing Rechargeable Lithium Batteries. *Nature* **2001**, *414* (6861), 359–367. https://doi.org/10.1038/35104644.

(3) Yi, T.-F.; Mei, J.; Zhu, Y.-R. Key Strategies for Enhancing the Cycling Stability and Rate Capacity of LiNi0.5Mn1.5O4 as High-Voltage Cathode Materials for High Power Lithium-Ion Batteries. *J Power Sources* **2016**, *316*, 85–105. https://doi.org/https://doi.org/10.1016/j.jpowsour.2016.03.070.

(4) Guan, P.; Zhou, L.; Yu, Z.; Sun, Y.; Liu, Y.; Wu, F.; Jiang, Y.; Chu, D. Recent Progress of Surface Coating on Cathode Materials for High-Performance Lithium-Ion Batteries. *Journal of Energy Chemistry* **2020**, *43*, 220–235. https://doi.org/10.1016/j.jechem.2019.08.022.

(5) Chen, F.; Liao, Y.; Li, M.; Huang, J.; Huang, Q.; Li, W. Enhancement in Cycling Stability of LiNi0.5Mn1.5O4/Li Cell under High Temperature in Gel Polymer Electrolyte System by Tris(Trimethylsilyl) Borate Additive. *Solid State Ion* **2018**, *327*, 1–10. https://doi.org/https://doi.org/10.1016/j.ssi.2018.10.011.

(6) Rong, H.; Xu, M.; Xie, B.; Liao, X.; Huang, W.; Xing, L.; Li, W. Tris (Trimethylsilyl) Borate (TMSB) as a Cathode Surface Film Forming Additive for 5V Li/LiNi0.5Mn1.5O4 Li-Ion Cells. *Electrochim Acta* **2014**, *147*, 31–39. https://doi.org/https://doi.org/10.1016/j.electacta.2014.09.105.

(7) Shobana, M. K. Metal Oxide Coated Cathode Materials for Li Ion Batteries – A Review. *J Alloys Compd* **2019**, *802*, 477–487. https://doi.org/10.1016/j.jallcom.2019.06.194.

(8) Li, S.; Zhu, K.; Zhao, D.; Zhao, Q.; Zhang, N. Porous LiMn2O4 with Al2O3 Coating as High-Performance Positive Materials. *Ionics (Kiel)* **2019**, *25* (5), 1991–1998. https://doi.org/10.1007/s11581-018-2643-y.

(9) Zuo, D.; Tian, G.; Li, X.; Chen, D.; Shu, K. Recent Progress in Surface Coating of Cathode Materials for Lithium Ion Secondary Batteries. *J Alloys Compd* **2017**, *706*, 24–40. https://doi.org/10.1016/j.jallcom.2017.02.230.

(10) Axmann, P.; Gabrielli, G.; Wohlfahrt-Mehrens, M. Tailoring High-Voltage and High-Performance LiNi0.5Mn1.5O4 Cathode Material for High Energy Lithium-Ion Batteries. *J Power Sources* **2016**, *301*, 151–159. https://doi.org/10.1016/j.jpowsour.2015.10.010.

(11) Yi, T.-F.; Fang, Z.-K.; Xie, Y.; Zhu, Y.-R.; Zang, L.-Y. Synthesis of LiNi0.5Mn1.5O4 Cathode with Excellent Fast Charge-Discharge Performance for Lithium-Ion Battery. *Electrochim Acta* **2014**, *147*, 250–256. https://doi.org/https://doi.org/10.1016/j.electacta.2014.09.119.

(12) Xu, X.; Deng, S.; Wang, H.; Liu, J.; Yan, H. Research Progress in Improving the Cycling Stability of High-Voltage LiNi0.5Mn1.5O4 Cathode in Lithium-Ion Battery. *Nanomicro Lett* **2017**, *9* (2), 22. https://doi.org/10.1007/s40820-016-0123-3.

(13) Ellis, B. L.; Lee, K. T.; Nazar, L. F. Positive Electrode Materials for Li-Ion and Li-Batteries. *Chemistry of Materials*. 2010. https://doi.org/10.1021/cm902696j.

(14) Li, W.; Cho, Y.-G.; Yao, W.; Li, Y.; Cronk, A.; Shimizu, R.; Schroeder, M. A.; Fu, Y.; Zou, F.; Battaglia, V.; Manthiram, A.; Zhang, M.; Meng, Y. S. Enabling

High Areal Capacity for Co-Free High Voltage Spinel Materials in next-Generation Li-Ion Batteries. *J Power Sources* **2020**, *473*, 228579. https://doi.org/https://doi.org/10.1016/j.jpowsour.2020.228579.

(15) Abeywardana, M. Y.; Laszczynski, N.; Kuenzel, M.; Bresser, D.; Passerini, S.; Lucht, B. Increased Cycling Performance of Li-Ion Batteries by Phosphoric Acid Modified LiNi 0.5 Mn 1.5 O 4 Cathodes in the Presence of LiBOB. *International Journal of Electrochemistry* **2019**, *2019*, 1–7. https://doi.org/10.1155/2019/8636540.

(16) Saravanan, K.; Jarry, A.; Kostecki, R.; Chen, G. A Study of Roomerature LixMn1.5Ni0.5O4 Solid Solutions. *Sci Rep* **2015**, *5* (1), 8027. https://doi.org/10.1038/srep08027.

(17) Amin, R.; Belharouk, I. Part I: Electronic and Ionic Transport Properties of the Ordered and Disordered LiNi0.5Mn1.5O4 Spinel Cathode. *J Power Sources* **2017**, *348*, 311–317. https://doi.org/https://doi.org/10.1016/j.jpowsour.2017.02.071.

(18) Yoon, T.; Park, S.; Mun, J.; Ryu, J. H.; Choi, W.; Kang, Y.-S.; Park, J.-H.; Oh, S. M. Failure Mechanisms of LiNi0.5Mn1.5O4 Electrode at Elevated Temperature. *J Power Sources* **2012**, *215*, 312–316. https://doi.org/https://doi.org/10.1016/j.jpowsour.2012.04.103.

(19) Kebede, M. A.; Yannopoulos, S. N.; Sygellou, L.; Ozoemena, K. I. High-Voltage LiNi 0.5 Mn 1.5 O 4- δ Spinel Material Synthesized by Microwave-Assisted Thermo-Polymerization: Some Insights into the Microwave-Enhancing Physico-Chemistry. *J Electrochem Soc* **2017**, *164* (13), A3259–A3265. https://doi.org/10.1149/2.1471713jes.

(20) Yin, C.; Zhou, H.; Yang, Z.; Li, J. Synthesis and Electrochemical Properties of

LiNi0.5Mn1.5O4 for Li-Ion Batteries by the Metal-Organic Framework Method. *ACS Appl Mater Interfaces* **2018**, *10* (16), 13624–13634. https://doi.org/10.1021/acsami.8b02553.

(21) Amin, R.; Muralidharan, N.; Petla, R. K.; ben Yahia, H.; Jassim Al-Hail, S. A.; Essehli, R.; Daniel, C.; Khaleel, M. A.; Belharouak, I. Research Advances on Cobalt-Free Cathodes for Li-Ion Batteries - The High Voltage LiMn1.5Ni0.5O4 as an Example. *J Power Sources* **2020**, *467*, 228318. https://doi.org/10.1016/J.JPOWSOUR.2020.228318.

(22) Li, S.; Wei, Y.; Wang, P.; Feng, Y.; Liang, W.; Ding, H.; Cui, X. Synergism of Cu and Al Co-Doping on Improvements of Structural Integrity and Electrochemical Performance for LiNi0.5Mn1.5O4. *J Alloys Compd* **2020**, *820*, 153140. https://doi.org/https://doi.org/10.1016/j.jallcom.2019.153140.

(23) Santhanam, R.; Rambabu, B. Research Progress in High Voltage Spinel LiNi0.5Mn1.5O4 Material. *J Power Sources* **2010**, *195* (17), 5442–5451. https://doi.org/10.1016/j.jpowsour.2010.03.067.

(24) Fu, L. J.; Liu, H.; Li, C.; Wu, Y. P.; Rahm, E.; Holze, R.; Wu, H. Q. Surface Modifications of Electrode Materials for Lithium Ion Batteries. *Solid State Sci* **2006**, *8* (2), 113–128. https://doi.org/https://doi.org/10.1016/j.solidstatesciences.2005.10.019.

(25) Hou, Q.; Cao, G.; Wang, P.; Zhao, D.; Cui, X.; Li, S.; Li, C. Carbon Coating Nanostructured-LiNi1/3Co1/3Mn1/3O2 Cathode Material Synthesized by Chemical Vapor Deposition Method for High Performance Lithium-Ion Batteries. *J Alloys Compd* **2018**, *747*, 796–802. https://doi.org/10.1016/J.JALLCOM.2018.03.115.

(26) Zhang, J.; Wang, F.; Shenoy, V. B.; Tang, M.; Lou, J. Towards Controlled

Synthesis of 2D Crystals by Chemical Vapor Deposition (CVD). *Materials Today* **2020**, *40*, 132–139. https://doi.org/https://doi.org/10.1016/j.mattod.2020.06.012.

(27) Nakamura, H.; Kawaguchi, T.; Masuyama, T.; Sakuda, A.; Saito, T.; Kuratani, K.; Ohsaki, S.; Watano, S. Dry Coating of Active Material Particles with Sulfide Solid Electrolytes for an All-Solid-State Lithium Battery. *J Power Sources* **2020**, *448*, 227579. https://doi.org/https://doi.org/10.1016/j.jpowsour.2019.227579.

(28) Nisar, U.; Al-Hail, S. A. J. A.; Petla, R. K.; Shakoor, R. A.; Essehli, R.; Kahraman, R.; AlQaradawi, S. Y.; Kim, D. K.; Belharouak, I.; Amin, M. R. Understanding the Origin of the Ultrahigh Rate Performance of a SiO2-Modified LiNi0.5Mn1.5O4 Cathode for Lithium-Ion Batteries. *ACS Appl Energy Mater* **2019**, *2* (10), 7263–7271. https://doi.org/10.1021/acsaem.9b01211.

(29) Tiurin, O.; Solomatin, N.; Auinat, M.; Ein-Eli, Y. Atomic Layer Deposition (ALD) of Lithium Fluoride (LiF) Protective Film on Li-Ion Battery LiMn1.5Ni0.5O4 Cathode Powder Material. *J Power Sources* **2020**, *448*, 227373. https://doi.org/https://doi.org/10.1016/j.jpowsour.2019.227373.

(30) Kim, C. A.; Choi, H. J.; Lee, J. H.; Yoo, S. Y.; Kim, J. W.; Shim, J. H.; Kang, B. Influence of Surface Modification on Electrochemical Performance of High Voltage Spinel Ordered-LiNi0.5Mn1.5O4 Exposed to 5.3 v for 100 h before and after Surface Modification with ALD Method. *Electrochim Acta* **2015**, *184*, 134–142. https://doi.org/10.1016/j.electacta.2015.10.041.

(31) Chen, L.; Warburton, R. E.; Chen, K.-S.; Libera, J. A.; Johnson, C.; Yang, Z.; Hersam, M. C.; Greeley, J. P.; Elam, J. W. Mechanism for Al2O3 Atomic Layer Deposition on LiMn2O4 from In Situ Measurements and Ab Initio Calculations. *Chem* **2018**, *4* (10), 2418–2435.

https://doi.org/https://doi.org/10.1016/j.chempr.2018.08.006.

(32) Feng, Z.; Rajagopalan, R.; Sun, D.; Tang, Y.; Wang, H. In-Situ Formation of Hybrid Li3PO4-AlPO4-Al(PO3)3 Coating Layer on LiNi0.8Co0.1Mn0.1O2 Cathode with Enhanced Electrochemical Properties for Lithium-Ion Battery. *Chemical Engineering Journal* **2020**, *382*, 122959. https://doi.org/https://doi.org/10.1016/j.cej.2019.122959.

(33) Li, Y.; Lai, F.; Zhang, X.; Wang, H.; Chen, Z.; He, X.; Li, Q. Surface Modification of Sr-Doped LaMnO3 Coating by Spray Drying on Ni-Rich LiNi0.8Mn0.1Co0.1O2 Cathode Material for Lithium-Ion Batteries. *J Taiwan Inst Chem Eng* **2019**, *102*, 225–232. https://doi.org/https://doi.org/10.1016/j.jtice.2019.06.006.

(34) Pan, J.-J.; Chen, B.; Xie, Y.; Ren, N.; Yi, T.-F. V2O5 Modified LiNi0.5Mn1.5O4 as Cathode Material for High-Performance Li-Ion Battery. *Mater Lett* **2019**, *253*, 136–139. https://doi.org/https://doi.org/10.1016/j.matlet.2019.06.062.

(35) Lv, S.; Li, M.; Luo, X.; Cheng, J.; Li, Z. High-Voltage LiNi0.5Mn1.5O4 Thin Film Cathodes Stabilized by LiPON Solid Electrolyte Coating to Enhance Cyclic Stability and Rate Capability. *J Alloys Compd* **2020**, *815*, 151636. https://doi.org/https://doi.org/10.1016/j.jallcom.2019.07.348.

(36) Wu, Y.; Li, M.; Wahyudi, W.; Sheng, G.; Miao, X.; Anthopoulos, T. D.; Huang, K.-W.; Li, Y.; Lai, Z. Performance and Stability Improvement of Layered NCM Lithium-Ion Batteries at High Voltage by a Microporous Al2O3 Sol–Gel Coating. *ACS Omega* **2019**, *4* (9), 13972–13980. https://doi.org/10.1021/acsomega.9b01706.

(37) Chudzik, K.; Lis, M.; Świętosławski, M.; Bakierska, M.; Gajewska, M.; Molenda, M. Improving the Performance of Sulphur Doped LiMn2O4 by

Carbon Coating. *J Power Sources* **2019**, *434*, 226725. https://doi.org/https://doi.org/10.1016/j.jpowsour.2019.226725.

(38) Modan, E.; A.G., P. Advantages and Disadvantages of Chemical Methods in the Elaboration of Nanomaterials. **2020**, *43*. https://doi.org/10.35219/mms.2020.1.08.

(39) Ma, G. Three Common Preparation Methods of Hydroxyapatite. *IOP Conf Ser Mater Sci Eng* **2019**, *688*, 33057. https://doi.org/10.1088/1757-899x/688/3/033057.

(40) Zhao, G.; Lin, Y.; Zhu, W.; Yang, W.; Huang, Z. Enhanced Electrochemical Performances of LiNi0.5Mn1.5O4 by Surface Modification with Cu Nanoparticles. *Journal of Mining and Metallurgy, Section B: Metallurgy* **2017**, *53* (1), 61–66. https://doi.org/10.2298/JMMB150906021Z.

(41) Arrebola, J.; Caballero, A.; Herna\'n, L.; Morales, J.; Castello\'n, E. R.; Barrado, J. R. R. Effects of Coating with Gold on the Performance of Nanosized {LiNi}[Sub 0.5]Mn[Sub 1.5]O[Sub 4] for Lithium Batteries. *J Electrochem Soc* **2007**, *154* (3), A178. https://doi.org/10.1149/1.2426799.

(42) He, Z.-Q.; Xiong, L.-Z.; Liang, K.; Lu, B. Preparation and Electrochemical Performances of LiNi0.5Mn1.5O4/Ag Composite. *Zhongguo Youse Jinshu Xuebao/Chinese Journal of Nonferrous Metals* **2010**, *20* (4), 801–806.

(43) Wu, J.; Han, C.; Wu, H.; Liu, H.; Zhang, Y.; Lu, C. Nanocoating of Ce-Tannic Acid Metal-Organic Coordination Complex : For Lithium-Ion Batteries. **2019**, 3031–3040.

(44) Xu, Y.-H.; Zhao, S.-X.; Deng, Y.-F.; Deng, H.; Nan, C.-W. Improved Electrochemical Performance of 5 V Spinel LiNi0.5Mn1.5O4 Microspheres by F-Doping and Li4SiO4 Coating. *Journal of Materiomics* **2016**, *2* (3), 265–272.

https://doi.org/https://doi.org/10.1016/j.jmat.2016.04.005.

(45) Hao, X.; Bartlett, B. M. Improving the Electrochemical Stability of the High-Voltage Li-Ion Battery Cathode LiNi0.5Mn1.5O4by Titanate-Based Surface Modification. *J Electrochem Soc* **2013**, *160* (5), A3162–A3170. https://doi.org/10.1149/2.025305jes.

(46) Cho, H.-M.; Chen, M. V.; MacRae, A. C.; Meng, Y. S. Effect of Surface Modification on Nano-Structured LiNi0. 5Mn1. 5O4 Spinel Materials. *ACS Appl Mater Interfaces* **2015**, *7* (30), 16231–16239.

(47) Tao, S.; Kong, F.; Wu, C.; Su, X.; Xiang, T.; Chen, S.; Hou, H.; Zhang, L.; Fang, Y.; Wang, Z.; Chu, W.; Qian, B.; Song, L. Nanoscale TiO2 Membrane Coating Spinel LiNi0.5Mn1.5O4 Cathode Material for Advanced Lithium-Ion Batteries. *J Alloys Compd* **2017**, *705*, 413–419. https://doi.org/https://doi.org/10.1016/j.jallcom.2017.02.139.

(48) Qian, C.; Ai-Jia, W.; Wen, L.; Li-Hui, Z.; Zhen-Fa, L. Effects of TiO2 Coating on Electrochemical Performance of LiNi0.5Mn1.5O4 Cathode Materials. *Journal of Chemical Engineering of Chinese Universities* **2019**, *33* (3), 715–723. https://doi.org/http://dx.doi.org/10.3969/j.issn.1003-9015.2019.03.027.

(49) Cho, S.; Kim, S.; Kim, W.; Kim, S. Study on Electrochemical Performance of Various Oxides-Coated LiNi0.5Mn1.5O4 Cathode for Lithium Ion Battery. *Electronic Materials Letters* **2019**, *15* (4), 481–492. https://doi.org/10.1007/s13391-019-00129-8.

(50) Alva, G.; Kim, C.; Yi, T.; Cook, J. B.; Xu, L.; Nolis, G. M.; Cabana, J. Surface Chemistry Consequences of Mg-Based Coatings on LiNi0.5Mn1.5O4 Electrode Materials upon Operation at High Voltage. *The Journal of Physical Chemistry C* **2014**, *118* (20), 10596–10605. https://doi.org/10.1021/jp5003148.

(51) Luo, X.; Ben, L. Effect of MgO and Ta2O5 Co-Coatings on Electrochemical Performance of High-Voltage Spinel LiNi0.5Mn1.5O4 Cathode Material. *J Alloys Compd* **2019**, *810*, 151951. https://doi.org/https://doi.org/10.1016/j.jallcom.2019.151951.

(52) Arrebola, J. C.; Caballero, A.; Hernán, L.; Morales, J. Re-Examining the Effect of ZnO on Nanosized 5V LiNi0.5Mn1.5O4 Spinel: An Effective Procedure for Enhancing Its Rate Capability at Room and High Temperatures. *J Power Sources* **2010**, *195* (13), 4278–4284. https://doi.org/https://doi.org/10.1016/j.jpowsour.2010.01.004.

(53) Sun, Y.-K.; Hong, K.-J.; Prakash, J.; Amine, K. Electrochemical Performance of Nano-Sized ZnO-Coated LiNi0.5Mn1.5O4 Spinel as 5 V Materials at Elevated Temperatures. *Electrochem commun* **2002**, *4* (4), 344–348. https://doi.org/https://doi.org/10.1016/S1388-2481(02)00277-1.

(54) Brutti, S.; Greco, G.; Reale, P.; Panero, S. Insights about the Irreversible Capacity of LiNi0.5Mn1.5O4 Cathode Materials in Lithium Batteries. *Electrochim Acta* **2013**, *106*, 483–493. https://doi.org/https://doi.org/10.1016/j.electacta.2013.05.111.

(55) Sun, H.; Xia, B.; Liu, W.; Fang, G.; Wu, J.; Wang, H.; Zhang, R.; Kaneko, S.; Zheng, J.; Wang, H.; Li, D. Significant Improvement in Performances of LiNi0.5Mn1.5O4 through Surface Modification with High Ordered Al-Doped ZnO Electro-Conductive Layer. *Appl Surf Sci* **2015**, *331*, 309–314. https://doi.org/https://doi.org/10.1016/j.apsusc.2015.01.120.

(56) Alcántara, R.; Jaraba, M.; Lavela, P.; Tirado, J. L. X-Ray Diffraction and Electrochemical Impedance Spectroscopy Study of Zinc Coated LiNi0.5Mn1.5O4 Electrodes. *Journal of Electroanalytical Chemistry* **2004**, *566*

(1), 187–192. https://doi.org/https://doi.org/10.1016/j.jelechem.2003.11.025.

(57) Ben, L.; Yu, H.; Wu, Y.; Chen, B.; Zhao, W.; Huang, X. Ta2O5 Coating as an HF Barrier for Improving the Electrochemical Cycling Performance of High-Voltage Spinel LiNi0.5Mn1.5O4 at Elevated Temperatures. *ACS Appl Energy Mater* **2018**, *1* (10), 5589–5598. https://doi.org/10.1021/acsaem.8b01139.

(58) Lee, Y.; Kim, T. Y.; Kim, D.-W.; Lee, J. K.; Choi, W. Coating of Spinel LiNi0.5Mn1.5O4 Cathodes with SnO2 by an Electron Cyclotron Resonance Metal–Organic Chemical Vapor Deposition Method for High-Voltage Applications in Lithium Ion Batteries. *Journal of Electroanalytical Chemistry* **2015**, *736*, 16–21. https://doi.org/https://doi.org/10.1016/j.jelechem.2014.10.022.

(59) Ma, F.; Geng, F.; Yuan, A.; Xu, J. Facile Synthesis and Characterization of a SnO2-Modified LiNi0.5Mn1.5O4 High-Voltage Cathode Material with Superior Electrochemical Performance for Lithium Ion Batteries. *Phys. Chem. Chem. Phys.* **2017**, *19* (15), 9983–9991. https://doi.org/10.1039/C7CP00943G.

(60) Yi, T.-F.; Han, X.; Chen, B.; Zhu, Y.-R.; Xie, Y. Porous Sphere-like LiNi0.5Mn1.5O4-CeO2 Composite with High Cycling Stability as Cathode Material for Lithium-Ion Battery. *J Alloys Compd* **2017**, *703*, 103–113. https://doi.org/10.1016/j.jallcom.2017.01.342.

(61) Lu, C.; Wu, H.; Zhang, Y.; Liu, H.; Chen, B.; Wu, N.; Wang, S. Cerium Fluoride Coated Layered Oxide Li1.2Mn0.54Ni0.13Co0.13O2 as Cathode Materials with Improved Electrochemical Performance for Lithium Ion Batteries. *J Power Sources* **2014**, *267*, 682–691. https://doi.org/https://doi.org/10.1016/j.jpowsour.2014.05.122.

(62) Wei, A.; Li, W.; Zhang, L.; Liu, Z. Improved Electrochemical Performance of 5

V Spinel LiNi $_{0.5}$ Mn $_{1.5}$ O $_{4}$ by La $_{2}$ O $_{3}$ Surface Coating for Li-Ion Batteries. *MATEC Web of Conferences* **2018**, *175*, 01030. https://doi.org/10.1051/matecconf/201817501030.

(63) Gao, J.; Yuan, T.; Luo, S.; Ruan, J.; Sun, H.; Yang, J.; Zheng, S. Boosting Lithium Ion Storage of Lithium Nickel Manganese Oxide via Conformally Interfacial Nanocoating. *J Colloid Interface Sci* **2020**, *570*, 153–162. https://doi.org/https://doi.org/10.1016/j.jcis.2020.02.112.

(64) Deng, M.; Zhang, D.; Shao, Y.; He, X.; Yasmin, A.; Chen, C. Improving Interfacial Electrochemistry of LiNi0. 5Mn1. 5O4 Cathode Coated by Mn3O4. *Chinese Journal of Chemical Physics* **2020**, *33* (4), 485–490.

(65) Wang, J.; Yao, S.; Lin, W.; Wu, B.; He, X.; Li, J.; Zhao, J. Improving the Electrochemical Properties of High-Voltage Lithium Nickel Manganese Oxide by Surface Coating with Vanadium Oxides for Lithium Ion Batteries. *J Power Sources* **2015**, *280*, 114–124. https://doi.org/https://doi.org/10.1016/j.jpowsour.2015.01.087.

(66) Wang, G.; Wen, W.; Chen, S.; Yu, R.; Wang, X.; Yang, X. Improving the Electrochemical Performances of Spherical LiNi0.5Mn1.5O4 by Fe2O3 Surface Coating for Lithium-Ion Batteries. *Electrochim Acta* **2016**, *212*, 791–799. https://doi.org/https://doi.org/10.1016/j.electacta.2016.07.025.

(67) Li, X.; Guo, W.; Liu, Y.; He, W.; Xiao, Z. Spinel LiNi0.5Mn1.5O4 as Superior Electrode Materials for Lithium-Ion Batteries: Ionic Liquid Assisted Synthesis and the Effect of CuO Coating. *Electrochim Acta* **2014**, *116*, 278–283. https://doi.org/https://doi.org/10.1016/j.electacta.2013.11.055.

(68) Guo, J.; Li, Y.; Chen, Y.; Deng, S.; Zhu, J.; Wang, S.; Zhang, J.; Chang, S.; Zhang, D.; Xi, X. Stable Interface Co3O4-Coated LiNi0.5Mn1.5O4 for Lithium-

Ion Batteries. *J Alloys Compd* **2019**, *811*, 152031. https://doi.org/https://doi.org/10.1016/j.jallcom.2019.152031.

(69) Deng, M.-M.; Tang, Z.-F.; Shao, Y.; He, X.-D.; Wen, Z.-Y.; Chen, C.-H. Enhancing the Electrochemical Performances of LiNi0.5Mn1.5O4 by Co3O4 Surface Coating. *J Alloys Compd* **2018**, *762*, 163–170. https://doi.org/https://doi.org/10.1016/j.jallcom.2018.05.245.

(70) Xue, Y.; Zheng, L.-L.; Wang, J.; Zhou, J.-G.; Yu, F.-D.; Zhou, G.-J.; Wang, Z.-B. Improving Electrochemical Performance of High-Voltage Spinel LiNi0.5Mn1.5O4 Cathode by Cobalt Surface Modification. *ACS Appl Energy Mater* **2019**, *2* (4), 2982–2989. https://doi.org/10.1021/acsaem.9b00564.

(71) Li, Y.; Guo, J.; Chen, Y.; Deng, S.; Zhu, J.; Cao, G.; Lei, T.; Zhang, J.; Wang, S.; Chang, S. Phase Transition Regulation and Cd-O/Cd-F Compounds Multi-Effect Modification Synergistically Act on LiNi0.5Mn1.5O4 Cathode. *Ionics (Kiel)* **2020**, *26* (4), 1681–1693. https://doi.org/10.1007/s11581-019-03257-1.

(72) Song, J.; Han, X.; Gaskell, K. J.; Xu, K.; Lee, S. B.; Hu, L. Enhanced Electrochemical Stability of High-Voltage LiNi0.5Mn1.5O4 Cathode by Surface Modification Using Atomic Layer Deposition. *Journal of Nanoparticle Research* **2014**, *16* (11), 2745. https://doi.org/10.1007/s11051-014-2745-z.

(73) Fang, X.; Ge, M.; Rong, J.; Che, Y.; Aroonyadet, N.; Wang, X.; Liu, Y.; Zhang, A.; Zhou, C. Ultrathin Surface Modification by Atomic Layer Deposition on High Voltage Cathode LiNi 0.5 Mn 1.5 O 4 for Lithium Ion Batteries. *Energy Technology* **2014**, *2* (2), 159–165. https://doi.org/10.1002/ente.201300102.

(74) Kim, J. W.; Kim, D. H.; Oh, D. Y.; Lee, H.; Kim, J. H.; Lee, J. H.; Jung, Y. S. Surface Chemistry of LiNi0.5Mn1.5O4 Particles Coated by Al2O3 Using Atomic Layer Deposition for Lithium-Ion Batteries. *J Power Sources* **2015**, *274*,

1254–1262. https://doi.org/https://doi.org/10.1016/j.jpowsour.2014.10.207.

(75) Wang, Y.; Peng, Q.; Yang, G.; Yang, Z.; Zhang, L.; Long, H.; Huang, Y.; Lu, P. High-Stability 5V Spinel LiNi0.5Mn1.5O4 Sputtered Thin Film Electrodes by Modifying with Aluminium Oxide. *Electrochim Acta* **2014**, *136*, 450–456. https://doi.org/https://doi.org/10.1016/j.electacta.2014.04.184.

(76) Sun, P.; Ma, Y.; Zhai, T.; Li, H. High Performance LiNi0.5Mn1.5O4 Cathode by Al-Coating and Al3+-Doping through a Physical Vapor Deposition Method. *Electrochim Acta* **2016**, *191*, 237–246. https://doi.org/https://doi.org/10.1016/j.electacta.2016.01.087.

(77) Chang, Q.; Wei, A.; Li, W.; Bai, X.; Zhang, L.; He, R.; Liu, Z. Structural and Electrochemical Characteristics of Al2O3-Modified LiNi0.5Mn1.5O4 Cathode Materials for Lithium-Ion Batteries. *Ceram Int* **2019**, *45* (4), 5100–5110. https://doi.org/https://doi.org/10.1016/j.ceramint.2018.11.213.

(78) Kim, C. A.; Choi, H. J.; Lee, J. H.; Yoo, S. Y.; Kim, J. W.; Shim, J. H.; Kang, B. Influence of Surface Modification on Electrochemical Performance of High Voltage Spinel Ordered-LiNi<inf>0.5</Inf>Mn<inf>1.5</Inf>O<inf>4</Inf> Exposed to 5.3 v for 100 h before and after Surface Modification with ALD Method. *Electrochim Acta* **2015**, *184*, 134–142. https://doi.org/10.1016/j.electacta.2015.10.041.

(79) Fang, X.; Lin, F.; Nordlund, D.; Mecklenburg, M.; Ge, M.; Rong, J.; Zhang, A.; Shen, C.; Liu, Y.; Cao, Y.; Doeff, M. M.; Zhou, C. Atomic Insights into the Enhanced Surface Stability in High Voltage Cathode Materials by Ultrathin Coating. *Adv Funct Mater* **2017**, *27* (7), 1602873. https://doi.org/https://doi.org/10.1002/adfm.201602873.

(80) Song, C.; Lu, J.; Liu, Y.; Yuan, Q.; Yang, J.; He, H.; Liu, D.; Wang, Q. Enhanced

Electrochemical Performance of Spinel LiNi0.5Mn1.5O4 for Li-Ion Batteries with Moderate Mn3+ Concentration and Nanosized Thin Al2O3 Coating. *Journal of Materials Science: Materials in Electronics* **2020**, *31* (6), 4815–4821. https://doi.org/10.1007/s10854-020-03043-0.

(81) Mereacre, V.; Bohn, N.; Müller, M.; Indris, S.; Bergfeldt, T.; Binder, J. R. Improved Performance of High-Voltage Li-Ion Batteries Using a Novel Chemically Activated Coating Process. *Mater Res Bull* **2021**, *134*. https://doi.org/10.1016/j.materresbull.2020.111095.

(82) Li, C.; Zhang, H. P.; Fu, L. J.; Liu, H.; Wu, Y. P.; Rahm, E.; Holze, R.; Wu, H. Q. Cathode Materials Modified by Surface Coating for Lithium Ion Batteries. *Electrochim Acta* **2006**, *51* (19), 3872–3883. https://doi.org/10.1016/j.electacta.2005.11.015.

(83) Wu, H. M.; Belharouak, I.; Abouimrane, A.; Sun, Y.-K.; Amine, K. Surface Modification of LiNi0.5Mn1.5O4 by ZrP2O7 and ZrO2 for Lithium-Ion Batteries. *J Power Sources* **2010**, *195* (9), 2909–2913. https://doi.org/https://doi.org/10.1016/j.jpowsour.2009.11.029.

(84) Nisar, U.; Amin, R.; Essehli, R.; Shakoor, R. A.; Kahraman, R.; Kim, D. K.; Khaleel, M. A.; Belharouak, I. Extreme Fast Charging Characteristics of Zirconia Modified LiNi0.5Mn1.5O4 Cathode for Lithium Ion Batteries. *J Power Sources* **2018**, *396*, 774–781. https://doi.org/https://doi.org/10.1016/j.jpowsour.2018.06.065.

(85) Fan, Y.; Wang, J.; Tang, Z.; He, W.; Zhang, J. Effects of the Nanostructured SiO2 Coating on the Performance of LiNi0.5Mn1.5O4 Cathode Materials for High-Voltage Li-Ion Batteries. *Electrochim Acta* **2007**, *52* (11), 3870–3875. https://doi.org/https://doi.org/10.1016/j.electacta.2006.10.063.

(86) Pang, W. K.; Lin, H.-F.; Peterson, V. K.; Lu, C.-Z.; Liu, C.-E.; Liao, S.-C.; Chen, J.-M. Enhanced Rate-Capability and Cycling-Stability of 5 V SiO2- and Polyimide-Coated Cation Ordered LiNi0.5Mn1.5O4 Lithium-Ion Battery Positive Electrodes. *The Journal of Physical Chemistry C* **2017**, *121* (7), 3680–3689. https://doi.org/10.1021/acs.jpcc.6b10743.

(87) Wen, W.; Yang, X.; Wang, X.; Shu, L. G. H. Improved Electrochemical Performance of the Spherical LiNi 0.5 Mn 1.5 O 4 Particles Modified by Nano-Y 2 O 3 Coating. *Journal of Solid State Electrochemistry* **2015**, *19* (4), 1235–1246.

(88) Jung, S. H.; Kim, D. H.; Brüner, P.; Lee, H.; Hah, H. J.; Kim, S. K.; Jung, Y. S. Extremely Conductive RuO2-Coated LiNi0.5Mn1.5O4 for Lithium-Ion Batteries. *Electrochim Acta* **2017**, *232*, 236–243. https://doi.org/https://doi.org/10.1016/j.electacta.2017.02.109.

(89) Pang, Q.; Fu, Q.; Wang, Y.; Zhang, Y.; Zou, B.; Du, F.; Chen, G.; Wei, Y. Improved Electrochemical Properties of Spinel LiNi0.5Mn1.5O4 Cathode Materials by Surface Modification with RuO2 Nanoparticles. *Electrochim Acta* **2015**, *152*, 240–248. https://doi.org/https://doi.org/10.1016/j.electacta.2014.11.142.

(90) Singhal, R.; Tomar, M. S.; Burgos, J. G.; Katiyar, R. S. Electrochemical Performance of ZnO-Coated LiMn1.5Ni0.5O4 Cathode Material. *J Power Sources* **2008**, *183* (1), 334–338. https://doi.org/https://doi.org/10.1016/j.jpowsour.2008.05.014.

(91) Wang, J.; Yao, S.; Yu, Y.; Fu, T.; Zhang, P.; Zhao, J. Improving the Stability Properties of 5V Lithium Nickel Manganese Oxide Spinel by Surface Coating with Cobalt Aluminum Oxides for Lithium Ion Batteries. *Electrochim Acta*

2016, *208*, 310–317. https://doi.org/https://doi.org/10.1016/j.electacta.2016.05.021.

(92) Wang, A.-M.; Bai, N. Improved Electrochemical Cycling Performance of High-Voltage Spinel LiNi 0.5 Mn 1.5 O 4 Cathode Materials by Coating with Spinel MgAl 2 O 4. *Solid State Ion* **2019**, *336*, 19–25. https://doi.org/10.1016/j.ssi.2019.03.013.

(93) Lee, Y.; Mun, J.; Kim, D.-W.; Lee, J. K.; Choi, W. Surface Modification of LiNi0.5Mn1.5O4 Cathodes with ZnAl2O4 by a Sol-Gel Method for Lithium Ion Batteries. *Electrochim Acta* **2014**, *115*, 326–331. https://doi.org/10.1016/j.electacta.2013.10.127.

(94) Goodenough, J. B.; Kim, Y. Challenges for Rechargeable Li Batteries. *Chemistry of materials* **2010**, *22* (3), 587–603.

(95) Konishi, H.; Suzuki, K.; Taminato, S.; Kim, K.; Zheng, Y.; Kim, S.; Lim, J.; Hirayama, M.; Son, J.-Y.; Cui, Y.; Kanno, R. Effect of Surface Li3PO4 Coating on LiNi0.5Mn1.5O4 Epitaxial Thin Film Electrodes Synthesized by Pulsed Laser Deposition. *J Power Sources* **2014**, *269*, 293–298. https://doi.org/https://doi.org/10.1016/j.jpowsour.2014.05.052.

(96) Yubuchi, S.; Ito, Y.; Matsuyama, T.; Hayashi, A.; Tatsumisago, M. 5V Class LiNi0.5Mn1.5O4 Positive Electrode Coated with Li3PO4 Thin Film for All-Solid-State Batteries Using Sulfide Solid Electrolyte. *Solid State Ion* **2016**, *285*, 79–82. https://doi.org/https://doi.org/10.1016/j.ssi.2015.08.001.

(97) Ren, N.; Lu, S.-G. Li3Po4 Surface Modification to Improve Performance of LiNi0.5Mn1.5O4 Cathode Material. *Chinese Journal of Inorganic Chemistry* **2017**, *32* (3), 499–507. https://doi.org/10.11862/CJIC.2016.068.

(98) Yi, T.-F.; Li, Y.-M.; Li, X.-Y.; Pan, J.-J.; Zhang, Q.; Zhu, Y.-R. Enhanced

Electrochemical Property of FePO4-Coated LiNi0.5Mn1.5O4 as Cathode Materials for Li-Ion Battery. *Sci Bull (Beijing)* **2017**, *62* (14), 1004–1010. https://doi.org/https://doi.org/10.1016/j.scib.2017.07.003.

(99) Xiao, B.; Liu, J.; Sun, Q.; Wang, B.; Banis, M. N.; Zhao, D.; Wang, Z.; Li, R.; Cui, X.; Sham, T.-K.; Sun, X. Unravelling the Role of Electrochemically Active FePO4 Coating by Atomic Layer Deposition for Increased High-Voltage Stability of LiNi0.5Mn1.5O4 Cathode Material. *Advanced Science* **2015**, *2* (5), 1500022. https://doi.org/https://doi.org/10.1002/advs.201500022.

(100) Zhang, D.; Hu, L.-L.; Sun, Y.-G.; Piao, J.-Y.; Tao, X.-S.; Xu, Y.-S.; Cao, A.-M.; Wan, L.-J. Construction of Uniform Transition-Metal Phosphate Nanoshells and Their Potential for Improving Li-Ion Battery Performance. *J. Mater. Chem. A* **2018**, *6* (19), 8992–8999. https://doi.org/10.1039/C8TA01320A.

(101) Kuenzel, M.; Kim, G.-T.; Zarrabeitia, M.; Lin, S. D.; Schuer, A. R.; Geiger, D.; Kaiser, U.; Bresser, D.; Passerini, S. Crystal Engineering of TMPOx-Coated LiNi0.5Mn1.5O4 Cathodes for High-Performance Lithium-Ion Batteries. *Materials Today* **2020**, *39*, 127–136. https://doi.org/https://doi.org/10.1016/j.mattod.2020.04.003.

(102) Xu, T.; Li, Y.; Wang, D.; Wu, M.; Pan, D.; Zhao, H.; Bai, Y. Enhanced Electrochemical Performance of LiNi0.5Mn1.5O4 Cathode Material by YPO4 Surface Modification. *ACS Sustain Chem Eng* **2018**, *6* (5), 5818–5825. https://doi.org/10.1021/acssuschemeng.7b03935.

(103) Liu, D.; Bai, Y.; Zhao, S.; Zhang, W. Improved Cycling Performance of 5 V Spinel LiMn1.5Ni0.5O4 by Amorphous FePO4 Coating. *J Power Sources* **2012**, *219*, 333–338. https://doi.org/https://doi.org/10.1016/j.jpowsour.2012.07.058.

(104) Deng, S.; Xiao, B.; Wang, B.; Li, X.; Kaliyappan, K.; Zhao, Y.; Lushington, A.;

Li, R.; Sham, T.-K.; Wang, H.; Sun, X. New Insight into Atomic-Scale Engineering of Electrode Surface for Long-Life and Safe High Voltage Lithium Ion Cathodes. *Nano Energy* **2017**, *38*, 19–27. https://doi.org/https://doi.org/10.1016/j.nanoen.2017.05.007.

(105) Piao, J.-Y.; Liu, X.-C.; Wu, J.; Yang, W.; Wei, Z.; Ma, J.; Duan, S.-Y.; Lin, X.-J.; Xu, Y.-S.; Cao, A.-M.; Wan, L.-J. Construction of Uniform Cobalt-Based Nanoshells and Its Potential for Improving Li-Ion Battery Performance. *ACS Appl Mater Interfaces* **2018**, *10* (27), 22896–22901. https://doi.org/10.1021/acsami.8b08528.

(106) Liu, J.; Cheng, Y.; Fan, Q.; Zhang, L.; Liu, L.; Ke, X.; Wang, N.; Shi, Z.; Guo, Z. Tri-Functional Coating to Enhance the Capacity Retention of LiNi0.5Mn1.5O4 for High Power Lithium Ion Battery. *Mater Lett* **2018**, *214*, 68–71. https://doi.org/https://doi.org/10.1016/j.matlet.2017.11.046.

(107) Yu, C.; Dong, L.; Zhang, Y.; Du, K.; Gao, M.; Zhao, H.; Bai, Y. Promoting Electrochemical Performances of LiNi0.5Mn1.5O4 Cathode via YF3 Surface Coating. *Solid State Ion* **2020**, *357*, 115464. https://doi.org/https://doi.org/10.1016/j.ssi.2020.115464.

(108) Li, J.; Zhang, Y.; Li, J.; Wang, L.; He, X.; Gao, J. AlF 3 Coating of LiNi 0.5 Mn 1.5 O 4 for High-Performance Li-Ion Batteries. *Ionics (Kiel)* **2011**, *17* (8), 671.

(109) Wu, Q.; Yin, Y.; Sun, S.; Zhang, X.; Wan, N.; Bai, Y. Novel AlF3 Surface Modified Spinel LiMn1.5Ni0.5O4 for Lithium-Ion Batteries: Performance Characterization and Mechanism Exploration. *Electrochim Acta* **2015**, *158*, 73–80. https://doi.org/https://doi.org/10.1016/j.electacta.2015.01.145.

(110) Wu, Q.; Zhang, X.; Sun, S.; Wan, N.; Pan, D.; Bai, Y.; Zhu, H.; Hu, Y. S.; Dai, S. Improved Electrochemical Performance of Spinel LiMn1.5Ni0.5O4 through

MgF2 Nano-Coating. *Nanoscale* **2015**, *7* (38), 15609–15617. https://doi.org/10.1039/c5nr03564c.

(111) Ke, X.; Zhao, Z.; Liu, J.; Shi, Z.; Li, Y.; Zhang, L.; Zhang, H.; Chen, Y.; Guo, Z.; Wu, Q.; Liu, L. Improvement in Capacity Retention of Cathode Material for High Power Density Lithium Ion Batteries: The Route of Surface Coating. *Appl Energy* **2017**, *194*, 540–548. https://doi.org/https://doi.org/10.1016/j.apenergy.2016.09.040.

(112) Chu, C.-T.; Mondal, A.; Kosova, N. v; Lin, J.-Y. Improved High-Temperature Cyclability of AlF3 Modified Spinel LiNi0.5Mn1.5O4 Cathode for Lithium-Ion Batteries. *Appl Surf Sci* **2020**, *530*, 147169. https://doi.org/https://doi.org/10.1016/j.apsusc.2020.147169.

(113) Li, Y.; Zhang, Q.; Xu, T.; Wang, D.; Pan, D.; Zhao, H.; Bai, Y. LaF3 Nanolayer Surface Modified Spinel LiNi0.5Mn1.5O4 Cathode Material for Advanced Lithium-Ion Batteries. *Ceram Int* **2018**, *44* (4), 4058–4066. https://doi.org/https://doi.org/10.1016/j.ceramint.2017.11.203.

(114) Li, Y.; Wang, D.; Xu, T.; Wu, M.; Pan, D.; Zhao, H.; Bai, Y. Stabilized Structural and Electrochemical Properties of LiNi0.5Mn1.5O4 via ZrF4 Nanolayer Modification for Li-Ion Batteries. *Solid State Ion* **2018**, *324*, 7–12. https://doi.org/https://doi.org/10.1016/j.ssi.2018.06.001.

(115) Wu, Q.; Zhang, X.; Sun, S.; Wan, N.; Pan, D.; Bai, Y.; Zhu, H.; Hu, Y. S.; Dai, S. Improved Electrochemical Performance of Spinel LiMn1.5Ni0.5O4 through MgF2 Nano-Coating. *Nanoscale* **2015**, *7* (38), 15609–15617. https://doi.org/10.1039/C5NR03564C.

(116) Lin, Y.; Yang, Y.; Yu, R.; Lai, H.; Huang, Z. Enhanced Electrochemical Performances of LiNi0.5Mn1.5O4 by Surface Modification with

Superconducting YBa2Cu3O7. *J Power Sources* **2014**, *259*, 188–194. https://doi.org/https://doi.org/10.1016/j.jpowsour.2014.02.093.

(117) Monaco, S.; de Giorgio, F.; da Col, L.; Riché, M.; Arbizzani, C.; Mastragostino, M. Electrochemical Performance of LiNi0.5Mn1.5O4 Composite Electrodes Featuring Carbons and Reduced Graphene Oxide. *J Power Sources* **2015**, *278*, 733–740. https://doi.org/https://doi.org/10.1016/j.jpowsour.2014.12.099.

(118) Xiong, L.; Long, Q.; Wang, Y.; Xiang, Y.; Wu, X.; He, Z. Sandwich-Structured Graphene Sheets@LiNi0.5Mn1.5O4@graphene Sheets Composites as Cathode Materials for Lithium Ion Batteries with High Rate Performance. *Ceram Int* **2016**, *42* (12), 14141–14147. https://doi.org/https://doi.org/10.1016/j.ceramint.2016.06.030.

(119) Yang, T.; Zhang, N.; Lang, Y.; Sun, K. Enhanced Rate Performance of Carbon-Coated LiNi0.5Mn1.5O4 Cathode Material for Lithium Ion Batteries. *Electrochim Acta* **2011**, *56* (11), 4058–4064. https://doi.org/https://doi.org/10.1016/j.electacta.2010.12.109.

(120) Fang, X.; Ge, M.; Rong, J.; Zhou, C. Graphene-Oxide-Coated LiNi0.5Mn1.5O4 as High Voltage Cathode for Lithium Ion Batteries with High Energy Density and Long Cycle Life. *J. Mater. Chem. A* **2013**, *1* (12), 4083–4088. https://doi.org/10.1039/C3TA01534C.

(121) Jia, G.; Jiao, C.; Xue, W.; Zheng, S.; Wang, J. Improvement in Electrochemical Performance of Calcined LiNi0.5Mn1.5O4/GO. *Solid State Ion* **2016**, *292*, 15–21. https://doi.org/https://doi.org/10.1016/j.ssi.2016.05.003.

(122) Wang, H.; Shi, Z.; Li, J.; Yang, S.; Ren, R.; Cui, J.; Xiao, J.; Zhang, B. Direct Carbon Coating at High Temperature on LiNi0.5Mn1.5O4 Cathode: Unexpected Influence on Crystal Structure and Electrochemical Performances. *J Power*

Sources **2015**, *288*, 206–213. https://doi.org/https://doi.org/10.1016/j.jpowsour.2015.04.137.

(123) Hwang, T.; Lee, J. K.; Mun, J.; Choi, W. Surface-Modified Carbon Nanotube Coating on High-Voltage LiNi0.5Mn1.5O4 Cathodes for Lithium Ion Batteries. *J Power Sources* **2016**, *322*, 40–48. https://doi.org/https://doi.org/10.1016/j.jpowsour.2016.04.118.

(124) Gao, C.; Liu, H.; Bi, S.; Fan, S.; Meng, X.; Li, Q.; Luo, C. Insight into the Effect of Graphene Coating on Cycling Stability of LiNi0.5Mn1.5O4: Integration of Structure-Stability and Surface-Stability. *Journal of Materiomics* **2020**, *6* (4), 712–722. https://doi.org/10.1016/j.jmat.2020.05.010.

(125) Li, F.; Xu, Z.; Sun, Q.; Hong, D.; Xu, C.-Y.; Wang, Y.; Fang, H.-T. Electrophoretically Deposited P-Phenylene Diamine Reduced Graphene Oxide Ultrathin Film on LiNi0.5Mn1.5O4 Cathode to Improve the Cycle Performance. *ACS Appl Mater Interfaces* **2019**, *11* (39), 35667–35674. https://doi.org/10.1021/acsami.9b10024.

(126) Lin, W.; Wang, J.; Zhou, R.; Wu, B.; Zhao, J. Improving the Electrochemical Performance of LiNi0. 5Mn1. 5O4 Cathode Materials by Surface Coating with Cyclized Polyacrylonitrile for Lithium-Ion Batteries. *Int. J. Electrochem. Sci* **2017**, *12*, 12047–12059.

(127) Cho, J.-H.; Park, J.-H.; Lee, M.-H.; Song, H.-K.; Lee, S.-Y. A Polymer Electrolyte-Skinned Active Material Strategy toward High-Voltage Lithium Ion Batteries: A Polyimide-Coated LiNi0.5Mn1.5O4 Spinel Cathode Material Case. *Energy Environ. Sci.* **2012**, *5* (5), 7124–7131. https://doi.org/10.1039/C2EE03389E.

(128) Gao, X.-W.; Deng, Y.-F.; Wexler, D.; Chen, G.-H.; Chou, S.-L.; Liu, H.-K.; Shi,

Z.-C.; Wang, J.-Z. Improving the Electrochemical Performance of the LiNi 0.5 Mn 1.5 O 4 Spinel by Polypyrrole Coating as a Cathode Material for the Lithium-Ion Battery. *J Mater Chem A Mater* **2015**, *3* (1), 404–411.

(129) Lin, H.; Huang, W.; Rong, H.; Mai, S.; Hu, J.; Xing, L.; Xu, M.; Li, W. Improving Cyclic Stability and Rate Capability of LiNi0.5Mn1.5O4 Cathode via Protective Film and Conductive Polymer Formed from Thiophene. *Journal of Solid State Electrochemistry* **2015**, *19*. https://doi.org/10.1007/s10008-014-2717-3.

(130) Dong, H.; Zhang, Y.; Zhang, S.; Tang, P.; Xiao, X.; Ma, M.; Zhang, H.; Yin, Y.; Wang, D.; Yang, S. Improved High Temperature Performance of a Spinel LiNi0.5Mn1.5O4 Cathode for High-Voltage Lithium-Ion Batteries by Surface Modification of a Flexible Conductive Nanolayer. *ACS Omega* **2019**, *4* (1), 185–194. https://doi.org/10.1021/acsomega.8b02571.

(131) Liu, Z.; Hu, P.; Ma, J.; Qin, B.; Zhang, Z.; Mou, C.; Yao, Y.; Cui, G. Conformal Poly(Ethyl α-Cyanoacrylate) Nano-Coating for Improving the Interface Stability of LiNi0.5Mn1.5O4. *Electrochim Acta* **2017**, *236*, 221–227. https://doi.org/https://doi.org/10.1016/j.electacta.2017.03.168.

(132) Liu, J.; Chen, Y.; Xu, J.; Sun, W.; Zheng, C.; Li, Y. Effectively Enhanced Structural Stability and Electrochemical Properties of LiNi 0.5 Mn 1.5 O 4 Cathode Materials via Poly-(3, 4-Ethylenedioxythiophene)-in Situ Coated for High Voltage Li-Ion Batteries. *RSC Adv* **2019**, *9* (6), 3081–3091.

(133) Kwon, Y.; Lee, Y.; Kim, S.-O.; Kim, H.-S.; Kim, K. J.; Byun, D.; Choi, W. Conducting Polymer Coating on a High-Voltage Cathode Based on Soft Chemistry Approach toward Improving Battery Performance. *ACS Appl Mater Interfaces* **2018**, *10* (35), 29457–29466.

(134) Zheng, X.; Liu, W.; Qu, Q.; Shi, Q.; Zheng, H.; Huang, Y. Effectively Stabilizing 5 V Spinel LiNi0.5Mn1.5O4 Cathode in Organic Electrolyte by Polyvinylidene Fluoride Coating. *Appl Surf Sci* **2018**, *455*, 349–356. https://doi.org/https://doi.org/10.1016/j.apsusc.2018.05.151.

(135) Zhang, Q.; Mei, J.; Wang, X.; Tang, F.; Fan, W.; Lu, W. High Performance Spinel LiNi0.5Mn1.5O4 Cathode Material by Lithium Polyacrylate Coating for Lithium Ion Battery. *Electrochim Acta* **2014**, *143*, 265–271. https://doi.org/https://doi.org/10.1016/j.electacta.2014.08.030.

(136) Deng, Y.; Mou, J.; Wu, H.; Jiang, N.; Zheng, Q.; Lam, K. H.; Xu, C.; Lin, D. A Superior Li2SiO3-Composited LiNi0.5Mn1.5O4 Cathode for High-Voltage and High-Performance Lithium-Ion Batteries. *Electrochim Acta* **2017**, *235*, 19–31. https://doi.org/https://doi.org/10.1016/j.electacta.2017.03.066.

(137) Deng, Y.; He, L.; Ren, J.; Zheng, Q.; Xu, C.; Lin, D. Reinforcing Cycling Stability and Rate Capability of LiNi0.5Mn1.5O4 Cathode by Dual-Modification of Coating and Doping of a Fast-Ion Conductor. *Mater Res Bull* **2018**, *100*, 333–344. https://doi.org/https://doi.org/10.1016/j.materresbull.2017.12.050.

(138) Chong, J.; Xun, S.; Song, X.; Liu, G.; Battaglia, V. S. Surface Stabilized LiNi0.5Mn1.5O4 Cathode Materials with High-Rate Capability and Long Cycle Life for Lithium Ion Batteries. *Nano Energy* **2013**, *2* (2), 283–293. https://doi.org/https://doi.org/10.1016/j.nanoen.2012.09.013.

(139) Zhao, G.; Lin, Y.; Zhou, T.; Lin, Y.; Huang, Y.; Huang, Z. Enhanced Rate and High-Temperature Performance of La0.7Sr0.3MnO3-Coated LiNi0.5Mn1.5O4 Cathode Materials for Lithium Ion Battery. *J Power Sources* **2012**, *215*, 63–68. https://doi.org/https://doi.org/10.1016/j.jpowsour.2012.04.090.

(140) Zhang, J.; Sun, G.; Han, Y.; Yu, F.; Qin, X.; Shao, G.; Wang, Z. Boosted Electrochemical Performance of LiNi0.5Mn1.5O4 via Synergistic Modification of Li+-Conductive Li2ZrO3 Coating Layer and Superficial Zr-Doping. *Electrochim Acta* **2020**, *343*, 136105. https://doi.org/https://doi.org/10.1016/j.electacta.2020.136105.

(141) Wang, J.; Nie, P.; Jiang, J.; Wu, Y.; Fu, R.; Xu, G.; Zhang, Y.; Dou, H.; Zhang, X. High-Voltage Li2SiO3−LiNi0.5Mn1.5O4 Hollow Spheres Prepared through In Situ Aerosol Spray Pyrolysis towards High-Energy Li-Ion Batteries. *ChemElectroChem* **2018**, *5* (8), 1212–1218. https://doi.org/https://doi.org/10.1002/celc.201701305.

(142) Zhu, R.; Zhang, S.; Guo, Q.; Zhou, Y.; Li, J.; Wang, P.; Gong, Z. More than Just a Protection Layer: Inducing Chemical Interaction between Li3BO3 and LiNi0·5Mn1·5O4 to Achieve Stable High-Rate Cycling Cathode Materials. *Electrochim Acta* **2020**, *342*, 136074. https://doi.org/https://doi.org/10.1016/j.electacta.2020.136074.

(143) Park, J. S.; Meng, X.; Elam, J. W.; Hao, S.; Wolverton, C.; Kim, C.; Cabana, J. Ultrathin Lithium-Ion Conducting Coatings for Increased Interfacial Stability in High Voltage Lithium-Ion Batteries. *Chemistry of Materials* **2014**, *26* (10), 3128–3134. https://doi.org/10.1021/cm500512n.

(144) Li, L.; Zhao, R.; Pan, D.; Yi, S.; Gao, L.; He, G.; Zhao, H.; Yu, C.; Bai, Y. Constructing Tri-Functional Modification for Spinel LiNi0.5Mn1.5O4 via Fast Ion Conductor. *J Power Sources* **2020**, *450*, 227677. https://doi.org/https://doi.org/10.1016/j.jpowsour.2019.227677.

(145) Zhu, Y.-R.; Yi, T.-F.; Li, X.-Y.; Xie, Y.; Luo, S. Improved Rate Performance of LiNi0.5Mn1.5O4 as Cathode of Lithium-Ion Battery by Li0.33La0.56TiO3

Coating. *Mater Lett* **2019**, *239*, 56–58. https://doi.org/https://doi.org/10.1016/j.matlet.2018.12.070.

(146) Deng, Y.-F.; Zhao, S.-X.; Xu, Y.-H.; Nan, C.-W. Effect of Temperature of Li2O–Al2O3–TiO2–P2O5 Solid-State Electrolyte Coating Process on the Performance of LiNi0.5Mn1.5O4 Cathode Materials. *J Power Sources* **2015**, *296*, 261–267. https://doi.org/https://doi.org/10.1016/j.jpowsour.2015.07.017.

(147) Bi, K.; Zhao, S.-X.; Huang, C.; Nan, C.-W. Improving Low-Temperature Performance of Spinel LiNi0.5Mn1.5O4 Electrode and LiNi0.5Mn1.5O4/Li4Ti5O12 Full-Cell by Coating Solid-State Electrolyte Li-Al-Ti-P-O. *J Power Sources* **2018**, *389*, 240–248. https://doi.org/https://doi.org/10.1016/j.jpowsour.2018.03.071.

(148) Chae, J. S.; Yoon, S.-B.; Yoon, W.-S.; Kang, Y.-M.; Park, S.-M.; Lee, J.-W.; Roh, K. C. Enhanced High-Temperature Cycling of Li2O–2B2O3-Coated Spinel-Structured LiNi0.5Mn1.5O4 Cathode Material for Application to Lithium-Ion Batteries. *J Alloys Compd* **2014**, *601*, 217–222. https://doi.org/https://doi.org/10.1016/j.jallcom.2014.02.154.

(149) Du, C.; Yang, M.; Liu, J.; Sun, S.; Tang, Z.; Qu, D.; Zhang, X. Surface Modification of a LiNi0.5Mn1.5O4 Cathode with Lithium Boron Oxide Glass for Lithium-Ion Batteries. *RSC Adv.* **2015**, *5* (71), 57293–57299. https://doi.org/10.1039/C5RA06271C.

(150) Deng, Y.; Mou, J.; He, L.; Xie, F.; Zheng, Q.; Xu, C.; Lin, D. A Core-Shell Structured LiNi0.5Mn1.5O4@LiCoO2 Cathode Material with Superior Rate Capability and Cycling Performance. *Dalton Transactions* **2018**, *47* (2), 367–375. https://doi.org/10.1039/c7dt03963h.

(151) Jang, W. H.; Kim, M. C.; Lee, S. N.; Ahn, J. Y.; Aravindan, V.; Lee, Y. S.

Enhanced Elevated Temperature Performance of LiFePO4 Modified Spinel LiNi0.5Mn1.5O4 Cathode. *J Alloys Compd* **2014**, *612*, 51–55. https://doi.org/https://doi.org/10.1016/j.jallcom.2014.05.149.

(152) Yi, T.-F.; Jiang, L.-J.; Shu, J.; Yue, C.-B.; Zhu, R.-S.; Qiao, H.-B. Recent Development and Application of Li4Ti5O12 as Anode Material of Lithium Ion Battery. *Journal of Physics and Chemistry of Solids* **2010**, *71* (9), 1236–1242. https://doi.org/https://doi.org/10.1016/j.jpcs.2010.05.001.

(153) Zhu, Y.-R.; Yi, T.-F.; Zhu, R.-S.; Zhou, A.-N. Increased Cycling Stability of Li4Ti5O12-Coated LiMn1.5Ni0.5O4 as Cathode Material for Lithium-Ion Batteries. *Ceram Int* **2013**, *39* (3), 3087–3094. https://doi.org/https://doi.org/10.1016/j.ceramint.2012.09.088.

(154) Zhao, J.; Liu, Y.; He, Y.; Lu, K. Li4Ti5O12 Epitaxial Coating on LiNi0.5Mn1.5O4 Surface for Improving the Electrochemical Performance through Solvothermal-Assisted Processing. *J Alloys Compd* **2019**, *779*, 978–984. https://doi.org/https://doi.org/10.1016/j.jallcom.2018.11.152.

(155) Wu, Q.; Xue, K.; Zhang, X.; Xie, X.; Wang, H.; Zhang, J.; Li, Q. Enhanced Cyclic Stability at Elevated Temperature of Spinel LiNi0.5Mn1.5O4 by Li4Ti5O12 Coating as Cathode Material for High Voltage Lithium Ion Batteries. *Ceram Int* **2019**, *45* (4), 5072–5079. https://doi.org/https://doi.org/10.1016/j.ceramint.2018.11.209.

(156) Mou, J.; Deng, Y.; Song, Z.; Zheng, Q.; Lam, K. H.; Lin, D. Excellent Rate Capability and Cycling Stability in Li+-Conductive Li2SnO3-Coated LiNi0.5Mn1.5O4 Cathode Materials for Lithium-Ion Batteries. *Dalton Trans.* **2018**, *47* (20), 7020–7028. https://doi.org/10.1039/C8DT00014J.

(157) Deng, H.; Nie, P.; Luo, H.; Zhang, Y.; Wang, J.; Zhang, X. Highly Enhanced

Lithium Storage Capability of LiNi0.5Mn1.5O4 by Coating with Li2TiO3 for Li-Ion Batteries. *J. Mater. Chem. A* **2014**, *2* (43), 18256–18262. https://doi.org/10.1039/C4TA03802A.

(158) Gellert, M.; Gries, K. I.; Sann, J.; Pfeifer, E.; Volz, K.; Roling, B. Impedance Spectroscopic Study of the Charge Transfer Resistance at the Interface between a LiNi0.5Mn1.5O4 High-Voltage Cathode Film and a LiNbO3 Coating Film. *Solid State Ion* **2016**, *287*, 8–12. https://doi.org/https://doi.org/10.1016/j.ssi.2016.01.031.

(159) Kim, H.; Byun, D.; Chang, W.; Jung, H.-G.; Choi, W. A Nano-LiNbO3 Coating Layer and Diffusion-Induced Surface Control towards High-Performance 5 V Spinel Cathodes for Rechargeable Batteries. *J. Mater. Chem. A* **2017**, *5* (47), 25077–25089. https://doi.org/10.1039/C7TA07898F.

(160) Yang, X.; Yang, T.; Liang, S.; Wu, X.; Zhang, H. Modification of LiNi0.5Mn1.5O4 High Potential Cathode from the Inner Lattice to the Outer Surface with Cr3+-Doping and Li+-Conductor Coating. *J. Mater. Chem. A* **2014**, *2* (27), 10359–10364. https://doi.org/10.1039/C4TA00974F.

(161) Wu, D.; Li, W.; Tegus, O.; Yang, Y.; Tian, X.; Bator, S. Solid Electrolyte Li1. 4Al0. 4Ti1. 6 (PO4) 3 as Coating for High Voltage Spinel LiNi0. 5Mn1. 5O4 Cathode Material. *Int. J. Electrochem. Sci* **2020**, *15*, 3715–3728.

(162) Liu, Y.; Lu, Z.; Deng, C.; Ding, J.; Xu, Y.; Lu, X.; Yang, G. A Novel LiCoPO 4-Coated Core–Shell Structure for Spinel LiNi 0.5 Mn 1.5 O 4 as a High-Performance Cathode Material for Lithium-Ion Batteries. *J Mater Chem A Mater* **2017**, *5* (3), 996–1004.

(163) Duan, J.; Liu, Y.; Tang, X.; Li, J.; Guo, J.; Zeng, M.; Wang, L. Improve Electrochemical Performance of Spinel LiNi0.5Mn1.5O4 via Surface Modified

by Li1.2Ni0.2Mn0.6O2 Layered Materials. *Journal of Materials Science: Materials in Electronics* **2020**, *31* (5), 4336–4344. https://doi.org/10.1007/s10854-020-02991-x.

(164) Liu, D.; Trottier, J.; Charest, P.; Fréchette, J.; Guerfi, A.; Mauger, A.; Julien, C. M.; Zaghib, K. Effect of Nano LiFePO4 Coating on LiMn1.5Ni0.5O4 5V Cathode for Lithium Ion Batteries. *J Power Sources* **2012**, *204*, 127–132. https://doi.org/https://doi.org/10.1016/j.jpowsour.2011.11.059.

(165) Mou, J.; Wu, H.; Deng, Y.; Zhou, L.; Zheng, Q.; Liao, J.; Lin, D. BiFeO3-Coated Spinel LiNi0.5Mn1.5O4 with Improved Electrochemical Performance as Cathode Materials for Lithium-Ion Batteries. *Journal of Solid State Electrochemistry* **2017**, *21* (10), 2849–2858. https://doi.org/10.1007/s10008-017-3608-1.

(166) Mou, J.; Deng, Y.; He, L.; Zheng, Q.; Jiang, N.; Lin, D. Critical Roles of Semi-Conductive LaFeO3 Coating in Enhancing Cycling Stability and Rate Capability of 5 V LiNi0.5Mn1.5O4 Cathode Materials. *Electrochim Acta* **2018**, *260*, 101–111. https://doi.org/https://doi.org/10.1016/j.electacta.2017.11.059.

(167) Kim, H.; Byun, D.; Chang, W.; Jung, H. G.; Choi, W. A Nano-LiNbO3 Coating Layer and Diffusion-Induced Surface Control towards High-Performance 5 V Spinel Cathodes for Rechargeable Batteries. *J Mater Chem A Mater* **2017**, *5* (47), 25077–25089. https://doi.org/10.1039/C7TA07898F.

(168) Li, L.; Zhao, R.; Xu, T.; Wang, D.; Pan, D.; Zhang, K.; Yu, C.; Lu, X.; He, G.; Bai, Y. Stabilizing a High-Voltage LiNi 0.5 Mn 1.5 O 4 Cathode towards All Solid State Batteries: A Li-Al-Ti-P-O Solid Electrolyte Nano-Shell with a Host Material. *Nanoscale* **2019**, *11* (18), 8967–8977. https://doi.org/10.1039/C9NR01655D.

(169) Lee, K.; Yang, G. J.; Kim, H.; Kim, T.; Lee, S. S.; Choi, S.-Y.; Choi, S.; Kim, Y. Composite Coating of Li2O–2B2O3 and Carbon as Multi-Conductive Electron/Li-Ion Channel on the Surface of LiNi0.5Mn1.5O4 Cathode. *J Power Sources* **2017**, *365*, 249–256. https://doi.org/https://doi.org/10.1016/j.jpowsour.2017.08.080.

(170) Han, Y.; Xue, Y.; Xia, Y.-F.; Zhang, J.-N.; Yu, F.-D.; Gu, D.-M.; Wang, Z.-B. Design of Synergistic-Coated Layer of La2O3/Al2O3 in LiNi0.5Mn1.5O4 Cathode for Enhanced Cycling Stability and Rate Capability. *Ionics (Kiel)* **2019**, *25* (6), 2459–2468. https://doi.org/10.1007/s11581-018-2714-0.

(171) Deng, S.; Wang, B.; Yuan, Y.; Li, X.; Sun, Q.; Doyle-Davis, K.; Banis, M. N.; Liang, J.; Zhao, Y.; Li, J.; Li, R.; Sham, T.-K.; Shahbazian-Yassar, R.; Wang, H.; Cai, M.; Lu, J.; Sun, X. Manipulation of an Ionic and Electronic Conductive Interface for Highly-Stable High-Voltage Cathodes. *Nano Energy* **2019**, *65*, 103988. https://doi.org/https://doi.org/10.1016/j.nanoen.2019.103988.

(172) Qiao, Z.; Sha, O.; Tang, Z.; Yan, J.; Wang, S.; Liu, H.; Xu, Q.; Su, Y. Surface Modification of LiNi0.5Mn1.5O4 by LiCoO2/Co3O4 Composite for Lithium-Ion Batteries. *Mater Lett* **2012**, *87*, 176–179. https://doi.org/https://doi.org/10.1016/j.matlet.2012.07.110.

(173) Shu, Y.; Xie, Y.; Yan, W.; Meng, S.; Sun, D.; Jin, Y.; Xiang, L. Tuning the Ratio of Al2O3 to LiAlO2 in the Composite Coating Layer for High Performance LiNi0.5Mn1.5O4 Materials. *Ceram Int* **2020**, *46* (10, Part A), 14840–14846. https://doi.org/https://doi.org/10.1016/j.ceramint.2020.03.009.

(174) Li, X.; Zhang, Y.; Li, W.; Qiao, Y.; Shang, H.; Ge, W.; Qu, M.; Fan, W.; Xie, Z. The Synergetic Effect of LiMg0.5Mn1.5O4 Coating and Mg2+ Doping on Improving Electrochemical Performances of High-Voltage LiNi0.5Mn1.5O4 by

Sol-Gel Self-Combustion Method. *ChemistrySelect* **2020**, *5* (8), 2593–2601. https://doi.org/https://doi.org/10.1002/slct.201904719.

(175) Zettsu, N.; Kida, S.; Uchida, S.; Teshima, K. Sub-2 Nm Thick Fluoroalkylsilane Self-Assembled Monolayer-Coated High Voltage Spinel Crystals as Promising Cathode Materials for Lithium Ion Batteries. *Sci Rep* **2016**, *6* (1), 31999. https://doi.org/10.1038/srep31999.

(176) Chae, S.; Soon, J.; Jeong, H.; jin Lee, T.; Ryu, J. H.; Oh, S. M. Passivating Film Artificially Built on LiNi0.5Mn1.5O4 by Molecular Layer Deposition of (Pentafluorophenylpropyl)Trimethoxysilane. *J Power Sources* **2018**, *392*, 159–167. https://doi.org/https://doi.org/10.1016/j.jpowsour.2018.04.091.

(177) Wei, L.; Tao, J.; Yang, Y.; Fan, X.; Ran, X.; Li, J.; Lin, Y.; Huang, Z. Surface Sulfidization of Spinel LiNi0.5Mn1.5O4 Cathode Material for Enhanced Electrochemical Performance in Lithium-Ion Batteries. *Chemical Engineering Journal* **2020**, *384*, 123268. https://doi.org/https://doi.org/10.1016/j.cej.2019.123268.

(178) Yao, J.; Wu, F.; Qiu, X.; Li, N.; Su, Y. Effect of CeO2-Coating on the Electrochemical Performances of LiFePO4/C Cathode Material. *Electrochim Acta* **2011**, *56* (16), 5587–5592. https://doi.org/https://doi.org/10.1016/j.electacta.2011.03.141.

(179) Patel, R. L.; Park, J.; Liang, X. Ionic and Electronic Conductivities of Atomic Layer Deposition Thin Film Coated Lithium Ion Battery Cathode Particles. *RSC Adv* **2016**, *6* (101), 98768–98776. https://doi.org/10.1039/C6RA20829K.

(180) Yang, X.; Huang, Y.; Wang, X.; Jia, D.; Pang, W. K.; Guo, Z.; Tang, X. High Rate Capability Core–Shell Lithium Titanate@ceria Nanosphere Anode Material Synthesized by One-Pot Co-Precipitation for Lithium-Ion Batteries. *J*

Power Sources **2014**, *257*, 280–285. https://doi.org/10.1016/J.JPOWSOUR.2014.02.005.

(181) Yuan, W.; Zhang, H. Z.; Liu, Q.; Li, G. R.; Gao, X. P. Surface Modification of Li(Li0.17Ni0.2Co0.05Mn0.58)O2 with CeO2 as Cathode Material for Li-Ion Batteries. *Electrochim Acta* **2014**, *135*, 199–207. https://doi.org/10.1016/J.ELECTACTA.2014.04.181.

(182) Wu, F.; Wang, M.; Su, Y.; Bao, L.; Chen, S. Surface of LiCo1/3Ni1/3Mn1/3O2 Modified by CeO2-Coating. *Electrochim Acta* **2009**, *54* (27), 6803–6807. https://doi.org/10.1016/J.ELECTACTA.2009.06.075.

(183) Ha, H.-W.; Yun, N. J.; Kim, K. Improvement of Electrochemical Stability of LiMn2O4 by CeO2 Coating for Lithium-Ion Batteries. *Electrochim Acta* **2007**, *52* (9), 3236–3241. https://doi.org/https://doi.org/10.1016/j.electacta.2006.09.066.

(184) Patel, R. L.; Xie, H.; Park, J.; Yaghoobnejad Asl, H.; Choudhury, A.; Liang, X.; Patel, R. L.; Liang, X.; Xie, H.; Park, J.; Asl, H. Y.; Choudhury, A. Significant Capacity and Cycle-Life Improvement of Lithium-Ion Batteries through Ultrathin Conductive Film Stabilized Cathode Particles. *Adv Mater Interfaces* **2015**, *2* (8), 1500046. https://doi.org/10.1002/ADMI.201500046.

(185) Patel, R. L.; Palaparty, S. A.; Liang, X. Ultrathin Conductive CeO 2 Coating for Significant Improvement in Electrochemical Performance of LiMn 1.5 Ni 0.5 O 4 Cathode Materials . *J Electrochem Soc* **2017**, *164* (1), A6236–A6243. https://doi.org/10.1149/2.0371701jes.

(186) Mo, M.; Chen, H.; Hong, X.; Hui, K. S.; Ye, C.; Lai, K. Hydrothermal Synthesis of Reduced Graphene Oxide-LiNi0.5Mn1.5O4 Composites as 5 V Cathode Materials for Li-Ion Batteries. *J Mater Sci* **2017**, *52* (5), 2858–2867.

https://doi.org/10.1007/S10853-016-0579-Z/FIGURES/7.

(187) Kucinskis, G.; Bajars, G.; Kleperis, J. Graphene in Lithium Ion Battery Cathode Materials: A Review. *J Power Sources* **2013**, *240*, 66–79. https://doi.org/10.1016/j.jpowsour.2013.03.160.

(188) Zhao, X.; Hayner, C. M.; Kung, H. H. Self-Assembled Lithium Manganese Oxide Nanoparticles on Carbon Nanotube or Graphene as High-Performance Cathode Material for Lithium-Ion Batteries. *J Mater Chem* **2011**, *21* (43), 17297–17303. https://doi.org/10.1039/c1jm12373d.

(189) Chen, L.; Li, D.; Zheng, X.; Chen, L.; Zhang, Y.; Liang, Z.; Feng, J.; Si, P.; Lou, J.; Ci, L. Integrated Nanocomposite of LiMn2O4/Graphene/Carbon Nanotubes with Pseudocapacitive Properties as Superior Cathode for Aqueous Hybrid Capacitors. *Journal of Electroanalytical Chemistry* **2019**, *842* (January), 74–81. https://doi.org/10.1016/j.jelechem.2019.04.056.

(190) Ding, Y.; Jiang, Y.; Xu, F.; Yin, J.; Ren, H.; Zhuo, Q.; Long, Z.; Zhang, P. Preparation of Nano-Structured LiFePO4/Graphene Composites by Co-Precipitation Method. *Electrochem commun* **2010**, *12* (1), 10–13. https://doi.org/10.1016/j.elecom.2009.10.023.

(191) Jan, S. S.; Nurgul, S.; Shi, X.; Xia, H.; Pang, H. Improvement of Electrochemical Performance of LiNi0.8Co0.1Mn0.1O2 Cathode Material by Graphene Nanosheets Modification. *Electrochim Acta* **2014**, *149*, 86–93. https://doi.org/10.1016/J.ELECTACTA.2014.10.093.

(192) Gao, C.; Liu, H.; Bi, S.; Fan, S.; Liu, Q.; Li, H.; Cao, L.; Luo, C. Insight into the High-Temperature Cycling Stability of a Micro-Nanostructured LiNi0.5Mn1.5O4/Graphene Composite Cathode for High-Voltage Lithium-Ion Batteries. *Journal of Physical Chemistry C* **2020**, *124* (35), 18847–18858.

https://doi.org/10.1021/ACS.JPCC.0C02933/SUPPL_FILE/JP0C02933_SI_001.PDF.

(193) Tang, X.; Jan, S. S.; Qian, Y.; Xia, H.; Ni, J.; Savilov, S. v.; Aldoshin, S. M. Graphene Wrapped Ordered LiNi0.5Mn1.5O4 Nanorods as Promising Cathode Material for Lithium-Ion Batteries. *Scientific Reports 2015 5:1* **2015**, *5* (1), 1–10. https://doi.org/10.1038/srep11958.

(194) Chen, J.; Huang, Z.; Zeng, W.; Cao, F.; Ma, J.; Tian, W.; Mu, S. Synthesis, Modification, and Lithium-Storage Properties of Spinel LiNi0.5Mn1.5O4. *ChemElectroChem*. Wiley-VCH Verlag February 12, 2021, pp 608–624. https://doi.org/10.1002/celc.202001414.

(195) Li, Y.; Wang, J.; Zhou, Z.; Yao, Q.; Wang, Z.; Zhou, H.; Deng, J. LiNi 0.5 Mn 1.5 O 4 Porous Micro-Cubes Synthesized by a Facile Oxalic Acid Co-Precipitation Method as Cathode Materials for Lithium-Ion Batteries. *Int J Electrochem Sci* **2019**, *14* (3), 2822–2832. https://doi.org/10.20964/2019.03.56.

(196) Jafta, C. J.; Mathe, M. K.; Manyala, N.; Roos, W. D.; Ozoemena, K. I. Microwave-Assisted Synthesis of High-Voltage Nanostructured LiNi0.5Mn1.5O4 Spinel: Tuning the Mn3+ Content and Electrochemical Performance. *ACS Appl. Mater. Interfaces* **2013**, *5* (15), 7592–7598. https://doi.org/10.1021/am401894t.

(197) Xiao, Y.; Xiang, W.; Zhang, J.; Zhu, Y.; Guo, X. Synthesis of Spinel LiNi0.5Mn1.5O4 as Advanced Cathode via a Modified Oxalate Co-Precipitation Method. *Ionics (Kiel)* **2016**, *22* (8), 1361–1368. https://doi.org/10.1007/s11581-016-1659-4.

(198) Bak, S. M.; Nam, K. W.; Lee, C. W.; Kim, K. H.; Jung, H. C.; Yang, X. Q.; Kim, K. B. Spinel LiMn2O4/Reduced Graphene Oxide Hybrid for High Rate Lithium

Ion Batteries. *J Mater Chem* **2011**, *21* (43), 17309–17315. https://doi.org/10.1039/c1jm13741g.

(199) Alvarez-Galvan, C.; Trunschke, A.; Falcon, H.; Sanchez-Sanchez, M.; Campos-Martin, J. M.; Schlögl, R.; Fierro, J. L. G. Microwave-Assisted Coprecipitation Synthesis of LaCoO3 Nanoparticles and Their Catalytic Activity for Syngas Production by Partial Oxidation of Methane. *Front Energy Res* **2018**, *6* (APR), 1–11. https://doi.org/10.3389/fenrg.2018.00018.

(200) Dong Peng, Z.; Bing Cao, Y.; Rong Hu, G.; Du, K.; Guang Gao, X.; Wei Xiao, Z. Microwave Synthesis of Li2FeSiO4 Cathode Materials for Lithium-Ion Batteries. *Chinese Chemical Letters* **2009**, *20* (8), 1000–1004. https://doi.org/10.1016/J.CCLET.2009.03.051.

(201) Liu, S.; Yan, P.; Li, H.; Zhang, X.; Sun, W. One-Step Microwave Synthesis of Micro/Nanoscale LiFePO4/Graphene Cathode With High Performance for Lithium-Ion Batteries. *Front Chem* **2020**, *8*, 104. https://doi.org/10.3389/FCHEM.2020.00104/BIBTEX.

(202) Zhang, M.; Wang, J.; Xia, Y.; Liu, Z. Microwave Synthesis of Spherical Spinel LiNi 0.5Mn 1.5O 4 as Cathode Material for Lithium-Ion Batteries. *J Alloys Compd* **2012**, *518*, 68–73. https://doi.org/10.1016/j.jallcom.2011.12.128.

(203) Tariq, H. A.; Abraham, J. J.; Quddus, A. A.; AlQaradawi, S.; Kahraman, R.; Shakoor, R. A. Graphene Wrapped Y2O3 Coated LiNi0.5Mn1.5O4 Quasi-Spheres as Novel Cathode Materials for Lithium-Ion Batteries. *Journal of Materials Research and Technology* **2021**, *14*, 1377–1389. https://doi.org/10.1016/J.JMRT.2021.07.038.

(204) Zong, B.; Deng, Z.; Yan, S.; Lang, Y.; Gong, J.; Guo, J.; Wang, L.; Liang, G. Effects of Si Doping on Structural and Electrochemical Performance of

LiNi0.5Mn1.5O4 Cathode Materials for Lithium-Ion Batteries. *Powder Technol* **2020**, *364*, 725–737. https://doi.org/10.1016/J.POWTEC.2020.02.033.

(205) Radzi, Z. I.; Kufian, M. Z.; Balakrishan, V.; Pandey, A. K.; Zainal Abidin, Z. H.; Sheikh Raihan, S. R.; Abd Rahim, N.; Subramaniam, R. Improved Cycling Stability of V2O5 Modified Spinel LiMn2O4 Cathode at High Cut-off Voltage for Lithium-Ion Batteries. *Int J Appl Ceram Technol* **2022**. https://doi.org/10.1111/IJAC.14033.

(206) Lin, H. B.; Hu, J. N.; Rong, H. B.; Zhang, Y. M.; Mai, S. W.; Xing, L. D.; Xu, M. Q.; Li, X. P.; Li, W. S. Porous LiMn 2 O 4 Cubes Architectured with Single-Crystalline Nanoparticles and Exhibiting Excellent Cyclic Stability and Rate Capability as the Cathode of a Lithium Ion Battery. **2014**. https://doi.org/10.1039/c4ta01474j.

(207) Wei, Y.; Nam, K. W.; Kim, K. B.; Chen, G. Spectroscopic Studies of the Structural Properties of Ni Substituted Spinel LiMn2O4. *Solid State Ion* **2006**, *177* (1–2), 29–35. https://doi.org/10.1016/J.SSI.2005.10.015.

(208) Al-Hail, S. A. J. A.; Amin, M. R.; Petla, R. K.; Nisar, U.; Essehli, R.; Ahzi, S.; Belharouak, I. Understanding the Nature of Capacity Decay and Interface Properties in Li//LiNi0.5Mn1.5O4Cells by Cycling Aging and Titration Techniques. *ACS Appl Energy Mater* **2020**, *3* (7), 6400–6407. https://doi.org/10.1021/ACSAEM.0C00614/SUPPL_FILE/AE0C00614_SI_001.PDF.

(209) Nisar, U.; Muralidharan, N.; Essehli, R.; Amin, R.; Belharouak, I. Valuation of Surface Coatings in High-Energy Density Lithium-Ion Battery Cathode Materials. *Energy Storage Mater* **2021**, *38*, 309–328. https://doi.org/10.1016/j.ensm.2021.03.015.

(210) Zhang, H.; Wang, D.; Shen, C. In-Situ EC-AFM and Ex-Situ XPS Characterization to Investigate the Mechanism of SEI Formation in Highly Concentrated Aqueous Electrolyte for Li-Ion Batteries. *Appl Surf Sci* **2020**, *507*, 145059. https://doi.org/10.1016/J.APSUSC.2019.145059.

(211) Li, L.; Zhao, R.; Xu, T.; Wang, D.; Pan, D.; Zhang, K.; Yu, C.; Lu, X.; He, G.; Bai, Y. Stabilizing a High-Voltage LiNi0.5Mn1.5O4 Cathode towards All Solid State Batteries: A Li–Al–Ti–P–O Solid Electrolyte Nano-Shell with a Host Material. *Nanoscale* **2019**, *11* (18), 8967–8977. https://doi.org/10.1039/C9NR01655D.

(212) Yu, X.; Yu, W. A.; Manthiram, A. Advances and Prospects of High-Voltage Spinel Cathodes for Lithium-Based Batteries. *Small Methods* **2021**, *5* (5). https://doi.org/10.1002/SMTD.202001196.

(213) Kunduraci, M.; Amatucci, G. G. Synthesis and Characterization of Nanostructured 4.7 V LixMn1. 5Ni0.5O4 Spinels for High-Power Lithium-Ion Batteries. *J. Electrochem. Soc.* **2006**, *153* (7), A1345–A1352. https://doi.org/10.1149/1.2198110.

(214) Kunduraci, M.; Al-Sharab, J. F.; Amatucci, G. G. High-Power Nanostructured LiMn2-XNixO4 High-Voltage Lithium-Ion Battery Electrode Materials: Electrochemical Impact of Electronic Conductivity and Morphology. *Chem. Mater.* **2006**, *18* (15), 3585–3592. https://doi.org/10.1021/cm060729s.

(215) Wang, L.; Li, H.; Huang, X.; Baudrin, E. A Comparative Study of Fd-3m and P4332 "LiNi0.5Mn1.5O4." *Solid State Ion* **2011**, *193* (1), 32–38. https://doi.org/10.1016/J.SSI.2011.04.007.

(216) Kim, J.-H.; Huq, A.; Chi, M.; Pieczonka, N. P. W.; Lee, E.; Bridges, C. A.; Tessema, M. M.; Manthiram, A.; Persson, K. A.; Powell, B. R. Integrated Nano-

Domains of Disordered and Ordered Spinel Phases in LiNi 0.5 Mn 1.5 O 4 for Li-Ion Batteries. **2014**. https://doi.org/10.1021/cm501203r.

(217) Amdouni, N.; Zaghib, K.; Gendron, F.; Mauger, A.; Julien, C. M. Structure and Insertion Properties of Disordered and Ordered LiNi 0.5Mn1.5O4 Spinels Prepared by Wet Chemistry. *Ionics (Kiel)* **2006**, *12* (2), 117–126. https://doi.org/10.1007/s11581-006-0021-7.

(218) Xue, Y.; Wang, Z.; Zheng, L.; Yu, F.; Liu, B.; Zhang, Y.; Ke, K. Investigation on Preparation and Performance of Spinel LiNi0.5Mn1.5O4 with Different Microstructures for Lithium-Ion Batteries. *Scientific Reports 2015 5:1* **2015**, *5* (1), 1–11. https://doi.org/10.1038/srep13299.

(219) Xiao, Y.; Zhu, Y.; Gao, T.; Zhong, B.; Guo, X. LiNi0.5Mn1.5O4 Hollow Nano-Micro Hierarchical Microspheres as Advanced Cathode for Lithium Ion Batteries. *Ionics (Kiel)* **2017**, *23* (1), 27–34. https://doi.org/10.1007/S11581-016-1804-0/FIGURES/12.